UNIVERSITY "ROMA TRE"

DOCTORAL THESIS

Brain Waves for Biometric User Recognition

Author:
Daria LA ROCCA

Supervisor:
Prof. Patrizio CAMPISI

A thesis submitted in fulfilment of the requirements
for the degree of Doctor of Philosophy

in the

Biometric Systems and Multimedia Forensics Laboratory
Department of Engineering, Section of Applied Electronics

"Were the ends of a person already explicit, there would be no room for development, for growth, for life; and consequently there would be no personality."

Charles Sanders Peirce

UNIVERSITY "ROME TRE"

Abstract

Department of Engineering, Section of Applied Electronics

Doctor of Philosophy

Brain Waves for Biometric User Recognition

by Daria LA ROCCA

Brain signals are being investigated within the medical field for more than a century to study brain diseases like epilepsy, spinal cord injuries, Alzheimer, Parkinson, schizophrenia, and stroke among the others. They are also used as the basis of brain computer interface and brain machine interface with assistance, rehabilitative and entertainment applications. Despite the broad interest in clinical applications, the use of brain signals sensed by means of electroencephalogram has been only recently investigated by the scientific community as a biometric characteristic, and the use of brain waves for the purpose of automatic people recognition is only at an embryonic stage. However, brain signals present some peculiarities, not shared by the most commonly used biometrics, like face, iris, and fingerprints, concerning secretness, privacy compliance, robustness against spoofing attacks, possibility to perform continuous identification, intrinsic liveness detection, and universality. Moreover since 70s there is evidence that EEG signals are genetically influenced and that they carry personality correlates. These peculiarities make the use of brain signals appealing. On the other hand there are many challenges related to the use of brain signals which need to be properly addressed in order to deploy biometric systems based on brain activity in real life applications. Among these challenges, the definition of the brain response elicitation protocol and the convenience of the acquisition process should be addressed, to cite a few.

In this work of doctoral thesis the aforementioned issues are further developed. The first chapters provide a comprehensive and critical review of state of the art methods for electroencephalogram based automatic user recognition that have been proposed in literature so far, also pointing out neurophysiological evidences related to the performed claims. The methods implemented and the experiments carried on within the present work are reported and detailed in the next chapters, together with the results obtained from the analysis of data.

Sommario

I sistemi biometrici per il riconoscimento di utenti hanno come scopo l'autenticazione o l'identificazione di un individuo sulla base di caratteristiche fisiologiche o comportamentali che risultino distintive, difficili da alterare o da simulare. Tra i parametri più frequentemente presi in esame per l'analisi e la realizzazione di sistemi biometrici che permettano il riconoscimento affidabile degli individui i più comuni sono: impronte digitali, geometria della mano e del volto, conformazione della retina o dell'iride, timbro e tonalità di voce, andatura. Questi tratti biometrici rappresentano tutti caratteristiche dell'individuo esposte sulla superficie del corpo, o osservabili dall'esterno, e sono descrtittivi di come egli appare o si comporta. Alternativamente le caratteristiche indicate come cognitive biometrics, tra cui l'EEG, descrivono come l'individuo sente o pensa. Infatti, la sensibilità agli stimoli esterni e l'organizzazione delle funzioni cerebrali durante specifici task risultano essere proprietà tipiche di ogni soggetto, provenienti dalla combinazione di fattori genetici, psicofisiologici, ambientali e culturali. Questi aspetti risultano di grande interesse dal punto di vista della sicurezza dei sistemi biometrici rispetto agli attacchi di impostori, in grado di rubare o falsificare la maggiorparte dei parametri comunemente usati, osservabili dall'esterno sulla superficie del corpo.

L'attività di ricerca oggetto del presente lavoro di tesi di dottorato riguarda lo studio delle particolari caratteristiche funzionali nel cervello del particolare individuo, con lo scopo di estrarre le invarianze nei pattern di attività elettrica cerebrale tipica di ogni soggetto per il riconoscimento automatico sicuro di utenti.

Lo studio dell'attività elettrica cerebrale risale all'inizio del secolo scorso, quando il fisiologo e psichiatra Hens Berger registrò il primo elettroencefalogramma (EEG). Da allora questa tecnica di brain imaging é stata ampliamente sviluppata grazie al suo vasto impiego soprattutto in campo medico per la diagnosi e il supporto al trattamento delle lesioni alla spina dorsale, ictus e malattie neurologiche tra cui epilessia, malattia di Alzheimer, schizofrenia e malattia di Parkinson. Il segnale EEG rappresenta anche l'elemento di base nei sistemi di interfaccia cervello-computer e più in generale cervello-macchina, che hanno come scopo permettere la comunicazione con l'ambiente esterno e il controllo di dispositivi remoti attraverso l'interpretazione dell'attività elettrica cerebrale.

L'interesse mostrato negli ultimi decenni per l'utilizzo dell'EEG nel riconoscimento biometrico di utenti si basa sugli importanti vantaggi che esso presenta rispetto ai tratti biometrici tradizionalmente utilizzati come impronte digitali, iride e volto, in termini di sicurezza e privacy. A tale riguardo, nel corso del presente lavoro di tesi è stato realizzato uno studio sugli aspetti di sicurezza, rispetto agli attacchi esterni, relativi all'utilizzo del segnale EEG in sistemi biometrici per il riconoscimento di individui. Tali proprietà sono indispensabili per l'applicazione

di qualsiasi sistema di riconoscimento biometrico in scenari reali. Inoltre, sin dagli anni '70 è nota la dipendenza di alcune caratteristiche dell'EEG da fattori genetici, che contribuiscono a determinare i caratteri distintivi del segnale di un individuo. Nonostante tali evidenze solo recentemente il segnale EEG è stato studiato nel contesto della biometria per estrarre informazione distintiva a scopo di riconoscimento.

Sebbene si osservi un crescente interesse per lo studio delle caratteristiche distintive dell'EEG, diverse sono le difficoltà da superare. In primo luogo è necessario identificare lo stimolo o stato mentale che produca il tratto o la caratteristica funzionale tipica di ogni soggetto, e stabile nel tempo. In questo contesto assume importanza la scelta del numero minimo di elettrodi e la loro configurazione, la ricerca delle invarianze nel tempo per ogni soggetto, e la massimizzazione della varianza tra diversi soggetti. A tale scopo, oltre all'utilizzo delle conoscenze neurifisiologiche sulle caratteristiche del segnale EEG, possono essere esplorati i recenti avanzamenti nel campo delle tecniche di machine learning, per ottenere un'efficiente rappresentazione (feature extraction) e classificazione dei segnali registrati.

La tecnica di brain imaging basata su EEG presenta come svantaggio una particolare sensibilità rispetto al rumore durante il processo di acquisizione. Questo rappresenta il principale problema da affrontare nell'elaborazione numerica, e diversi metodi sono stati proposti ed utilizzati nelle varie applicazioni. Nel caso in cui le componenti spettrali degli artefatti si sovrappongono a quelle del segnale utile è necessario l'utilizzo di tecniche di denoising più raffinate rispetto al filtraggio passa banda, basate ad esempio sulla trasformazione wavelet o sulla principal component analysis. Diverse tecniche di pre-processing finalizzate al denoising sono state utilizzate nel presente lavoro, verificandone l'efficienza relativamente al protocollo sperimentale indagato. Tra queste, la rimozione degli artefatti da movimento oculare e blink attraverso l'analisi delle componenti indipendenti nella condizione di rest ad occhi aperti. Per il miglioramento del rapporto segnale-rumore si è inoltre implementato il filtraggio spaziale common average reference (CAR), che consiste nel sottrarre, istante per istante, al canale di acquisizione di interesse la media spaziale dell'intero set dei canali impiegati. Tale tecnica permette di controllare gli artefatti dovuti a scelte non appropriate degli elettrodi di riferimento, o a variazioni impreviste del potenziale rilevato da questi dovute ad esempio a problemi nel contatto elettrodo-pelle. Allo scopo di eliminare artefatti di natura stocastica facendo emergere invece le componenti di natura (pseudo-)stazionaria è stata utilizzata la tecnica della segmentazione del tracciato EEG seguita da medie d'insieme dei parametri di interesse.

Il successivo lavoro di elaborazione dei segnali EEG si è concentrato sullo studio di particolari approcci di estrazione di feature e di classificazione, con il supporto di tecniche di modellizzazione complessa e analisi statistica dei dati. Lo studio delle influenze genetiche, ambientali e della personalità sull'EEG ha condotto all'indagine del carattere distintivo di aspetti funzionali dell'attività elettrica cerebrale. Nelle analisi realizzate si sono studiati i diversi ritmi cerebrali

componenti l'EEG, che rappresentano oscillazioni con contenuto frequenziale in bande separate, individuando il peso e la distribuzione spaziale di ogni oscillazione nelle diverse regioni cerebrali in relazione al task. Risultati incoraggianti sono stati ottenuti considerando singole sessioni di acquisizione per ogni utente, di cui una partizione è stata utilizzata per l'arruolamento e la rimanente per la fase di riconoscimento, evitando la sovrapposizione dei due dataset. Si è quindi proceduto studiando le caratteristiche di stabilità del segnale EEG, aspetto fondamentale per il suo impiego in biometria.

A tale riguardo, oltre agli studi metodologici, nel corso del presente lavoro è stata condotta una campagna di acquisizione del segnale EEG di soggetti volontari, finalizzata alla raccolta di un dataset da studiare, che contenesse registrazioni longitudinali (multi-sessione). Una tale struttura temporale del dataset è necessaria per lo studio della ripetibilità a breve e lungo termine dei tratti biometrici estratti da EEG, proprietà necessaria per qualsiasi implementazione in un contesto reale, in cui un soggetto arruolato precedentemente nel sistema deve essere riconosciuto in istanti diversi. Un dataset composto da circa 60 soggetti è stato raccolto, considerando 5 registrazioni per ogni soggetto, la prima all'istante t0, la seconda all'istante t0 + 1 settimana, la terza all'istante t0 + 1 mese, la quarta all'istante t0 + 6 mesi e l'ultima all'istante t0 + 12 mesi. Durante le registrazioni è stato richiesto ai soggetti di realizzare diversi task sperimentali. Ogni particolare task sperimentale induce specifiche risposte cerebrali ed evidenzia determinate caratteristiche dell'organizzazione e della coordinazione delle funzioni all'interno del cervello, alcune delle quali risultano particolarmente variabili da soggetto a soggetto. È stata quindi considerata la dipendenza dell'EEG dallo stato mentale del soggetto durante la registrazione e dal particolare compito cognitivo da svolgere allo scopo di individuare condizioni sperimentali appropriate per il riconoscimento.

Il contributo del lavoro svolto consiste nell'aver condotto un'analisi esaustiva, assente in letteratura, dei parametri coinvolti nella soluzione del problema di riconoscimento di utenti basato su EEG, individuando, per i particolari dataset considerati, la combinazione di ritmi cerebrali contenente maggiore informazione distintiva, la migliore configurazione spaziale di elettrodi da impiegare minimizzandone il numero, e la durata temporale dei segmenti di EEG capace di cogliere i caratteri distintivi delle feature da estrarre, compatibilmente con la grandezza dei campioni indagati. Inoltre, attraverso l'implementazione di tecniche di estrazione di feature sono state individuate rappresentazioni distintive del segnale EEG relativo a ciascun utente. Un ulteriore aspetto innovativo è rappresentato dallo studio sistematico del carattere di stabilità e riproducibilità delle feature estratte dal segnale EEG in registrazioni longitudinali, che si sta portando avanti su dataset sempre di maggiori dimensioni, dati i promettenti risultati ottenuti. Data la scarsa disponibilità di materiale contenente registrazioni longitudinali di un gruppo di soggetti statisticamente significativo, si è proceduto a realizzare una campagna di acquisizioni attraverso un dispositivo amplificatore appositamente acquistato, e a studiare adeguati protocolli

di registrazione. Il dataset acquisito è stato oggetto di applicazione di tecniche avanzate di machine learning durante un periodo di formazione e attività di ricerca presso LRI (Laboratoire de Recherche en Informatique, unité mixte de recherche - UMR8623) dell'Université Paris-Sud et du CNRS, Orsay, France. In generale tale attività di ricerca riguarda lo studio statistico della struttura dei segnali EEG relativi a registrazioni longitudinali attraverso un'efficiente rappresentazione dei dati, finalizzato a 1) combinare tecniche di machine learning e signal processing per riconoscimento di soggetti basato su EEG; 2)comprendere la struttura della variabilità del segnale EEG per ogni soggetto rispetto al tempo. I metodi implementati e gli esperimenti condotti nel corso del predente lavoro di ricerca vengono riportati in dettaglio nei seguenti capitoli, contestualmente ai risultati ottenuti attraverso l'analisi dei dati.

Acknowledgements

I wish to thank Professor Patrizio Campisi for his supervision, his careful support, his valuable guidance and advice throughout these years.

My sincere gratitude also goes to Professor Gaetano Scarano for leading me through my education from the Biomedical Engineering course to my Master thesis, which I performed under his supervision.

I thank Fabrizio for his crucial role in my scientific research since its early beginning, and for being to me a constant source of motivation.

Contents

List of Figures

List of Tables

Abbreviations

AF	**A**nterior-**F**rontal
APSG	**A**ntero-**P**osterior **S**pectral **G**radient
AR	**A**uto-**R**egressive
BCI	**B**rain **C**omputer **I**nterface
C	**C**entral
CAR	**C**ommon **A**verage **R**eference
CC	**C**ross-**C**orrelation
CMA-ES	**C**ovariance **M**atrix **A**daptation-**E**volution **S**trategy
CP	**C**entro-**P**arietal
CRR	**C**orrect **R**ecognition **R**ate
CV	**C**ross **V**alidation
DA	**D**iscriminant **A**nalysis
EC	**E**yes **C**losed
EEG	**E**lectro**E**ncephalo **G**raphy
EER	**E**qual **E**rror **R**ate
EO	**E**yes **O**pen
ERD	**E**vent **R**elated **D**e-synchronization
ERP	**E**vent **R**elated **P**otential
ERS	**E**vent **R**elated **S**ynchronization
F	**F**rontal
FAR	**F**alse **A**cceptance **R**ate
FC	**F**ronto-**C**entral
F/G	**F**ocus/**G**iven
F/N	**F**ocus/**N**ew
Fp	**F**ronto-**p**olar

FRR	**F**alse **R**ejection **R**ate
FT	**F**ronto-**T**emporal
FW	**F**ast **W**ave
GAR	**G**enuine **A**cceptance **R**ate
LDA	**L**inear **D**iscriminant **A**nalysis
MI	**M**otor **I**magery
MuIn	**Mu**tual **In**formation
O	**O**ccipital
P	**P**arietal
PO	**P**arieto-**O**ccipital
PS	**P**ower **S**pectrum
PSD	**P**ower **S**pectral **D**ensity
ROI	**R**egion **O**f **I**nterest
SCP	**S**low **C**ortical **P**otential
RS	**R**esting **S**tate
SI	**S**peech **I**magery
SPR	**S**pectral **P**ower **R**atio
SW	**S**low **W**ave
T	**T**emporal
T/G	**T**opic/**G**iven
T/N	**T**opic/**N**ew
TP	**T**emporo-**P**arietal

Symbols

d	Mahalanobis distance between feature values	
i	Generic identity (subject)	
I	Length (number of time samples) of EEG epochs (segments)	
J	Objective function	
$\mathbf{M}$	Miss-classification matrix	
N	Number of identities	
N_{ch}	Number of channels	
N_{FT}	Number of frequency points (samples)	
O_L	overlapping factor between consecutive epochs	
$S_{(\cdot)}$	Acquisition session	
S_r	Sampling frequency	Hz
$S_{x,y}(f)$	Cross-spectrum	$V^2\text{Hz}^{-1}$
$S_{x,x}(f)$	Auto-spectrum	$V^2\text{Hz}^{-1}$
T	Number of EEG epochs	
$x_{i,t}$	EEG waveform after pre-processing	

α	Alpha rhythm
β	Beta rhythm
γ	Gamma rhythm
δ	Delta rhythm
θ	Theta rhythm
μ	Mean value
σ	Standard deviation
τ	Generic EEG epoch
$\chi^{(\cdot)}$	Feature vector

To Emma, Raffaele
and Martina

Chapter 1

EEG systems

In the last decade, an always growing interest towards the use of biological signals, like electroencephalogram (EEG), electrodermal response (EDR), electrocardiogram (ECG), blood pulse volume (BPV), electromyogram (EMG), to cite a few, for the purpose of automatic user recognition is being witnessed. Within this framework the so-called "cognitive biometric" refers to biometric traits which are detected during cognitive and/or emotional brain states. Therefore, while conventional biometric rely on the use of either physiological or behavioral characteristics, that is on some biological characteristics the individual "possesses' or on the "way the individual behaves" respectively, cognitive biometrics are based on the measurement of signals directly or indirectly generated by the "way the individual thinks" as a distinctive characteristic for automatic user recognition. In particular, the evidence that the brain activity carries distinctive information about the individual identity has led to the development of research on cognitive biometrics in last decade.

The study of brain activity during specific mental states is being explored by means of different methodologies in order to extract discriminating features for the purpose of user recognition. Specifically, brain activity can be recorded either by measuring the blood flow in the brain or by measuring the neuron electrical activity. To the first category belong approaches like functional magnetic resonance imaging (fMRI), which measures the concentration of oxygenated and deoxygenated haemoglobin in response to magnetic fields; the near-infrared spectroscopy (NIRS), which measures the concentration of oxygenated and deoxygenated haemoglobin by means of the reflection of infrared light by the brain cortex through the skull; the positron emission tomography (PET), which measures neuron metabolism through the injection of a radioactive substance in the subject. To the second category belong approaches like magneto-encephalography (MEG), which is sensitive to the small magnetic fields induced by the electric currents in the brain, and electroencephalography, which is sensitive to the electrical field generated by the electric currents in the brain.

EEG recordings are acquired with portable and relatively inexpensive devices when compared to the other brain imaging techniques. Specifically, signal amplifiers with high sensitivity and high noise rejection are used to measure the voltage fluctuation on the scalp surface resulting from the electric field generated by the firing of collections of pyramidal neurons of the cortex. For the sake of completeness it is worth mentioning that, in principle, also EEG subdermal needle electrodes can be employed although they are used only in medical applications due to their high invasiveness. The EEG amplitude of a normal subject in the awake state, recorded with scalp electrodes, is in the range $[10, 200]\mu V$ and the most relevant cerebral activity falls in the range of $[0.5, 40]$Hz. The EEG based brain imaging technique presents a limited spatial resolution due to the physical dimension, in the range of several millimeters, of the surface electrodes, usually employed in the acquisition setup, which limits the possible number of the electrodes covering the whole scalp. A limited spatial resolution is also due to the dispersion of the signals, generated by the sources on the cortex, within the head structures before they reach the scalp. On the contrary, EEG techniques have a high temporal resolution, in the range of milliseconds, which allows dynamic studies to understand the underlying mechanisms by means of complex computational methods. In fact, information concerning for instance psycho-physiological state, neurological and neuromuscular health, emotions, memory, the course of concentration, attention, levels of arousal, mental fatigue or workload during special tasks, sensitiveness to external stimulation can be extracted from EEG inspection and manipulation [1]. Such a kind of evidence has led in last decades to use brain signals to convey conscious volition in EEG-based systems, like brain computer interface (BCI) [2], [3], and brain machine interface (BMI) [4], aiming at controlling remote devices by means of the interpretation of the brain electrical activity.

Although some isolated attempts to use EEG to discriminate people have been performed in the past [5], only recently [6], [7] the scientific community has started a more systematic investigation on the use of EEG signals as human distinctive traits which can be potentially used in a biometric system. In fact, the way the brain regions are organized and coordinated during specific cognitive functions or mental states, such as the response to audio or visual stimuli, during real or imagined body movements, imagined speech, resting states, etc., or during emotional states, can provide relevant information about the brain conditions which, in the studies conducted so far, have shown to have some discriminant capabilities among subjects [8], [9], due to both morphological and anatomical traits, and functional plasticity traits.

In this first chapter a characterization of a generic EEG signal acquisition system is given along with a characterization of the brain rhythms. Also, in Section 1.2 the EEG signal acquisition protocols used in biometric oriented applications are described.

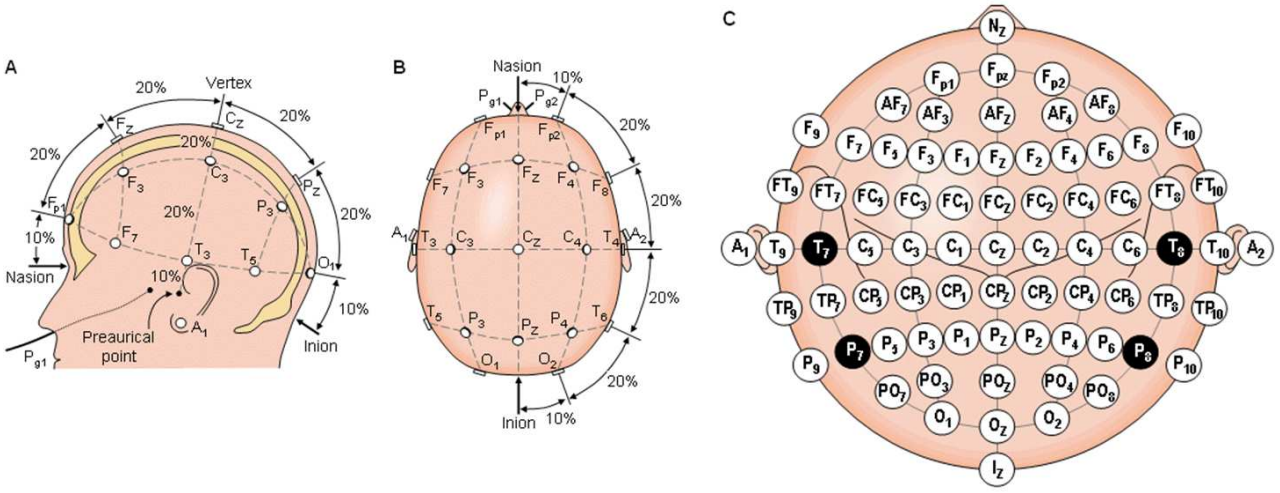

FIGURE 1.1: The 10-20 international standard seen from left (A) and above the head (B). A montage according to an extended 10-20 standard is shown in (C). The letters F, T, C, P and O stand for frontal, temporal, central, parietal, and occipital lobes. Even numbers identify electrodes on the right hemisphere, odd numbers those on the left hemisphere, and "z" (zero) refers to electrodes placed on the midline. (Jaakko Malmivuo and Robert Plonsey, Bioelectromagnetism, Oxford University Press, 1995, WEB version).

1.1 Brain activity sensing: EEG brain rhythms

EEG signals are usually acquired using superficial scalp electrodes, placed according to the 10-20 international standard depicted in Figure 1.1 and recommended by the International Federation of Societies for Electroencephalography and Clinical Neurophysiology. The "10" and "20" refer to the percentage of the distances between the landmark points, namely the inion, the nasion, as shown in Figure 1.1 (a) and (b), used to draw the lines at which intersections the electrodes are positioned. In other words, given the landmark points, the electrodes positioning is made by considering the intersections between lines which are sagittally and coronally drawn at 10 or 20 % of the distances between the inion and nasion. An example of brain waves acquired during a resting state with closed eyes using a 19 channel device with electrodes positioned using the 10-20 international system is shown in Figure 1.2.

Since the early research on EEG analysis, it has been observed that the most relevant cerebral activity, consisting of superimposed oscillations at different frequencies, falls in the range of $[1, 40]$Hz. In general, five main rhythms can be detected from an EEG recording: Delta (δ $[0.5, 4]$Hz), Theta (θ $[4, 8]$Hz), Alpha (α $[8, 14]$Hz), Beta (β $[14, 30]$Hz) and Gamma (γ over 30Hz). In Figure 1.3 examples of $\delta, \theta, \alpha, \beta$, and γ rhythms acquired through the O2 channel using a resting state with closed eyes protocol are depicted.

The amount of activity in different EEG frequency bands can be quantified employing spectral analysis techniques. The contribution of the different rhythms to the EEG depends mainly on

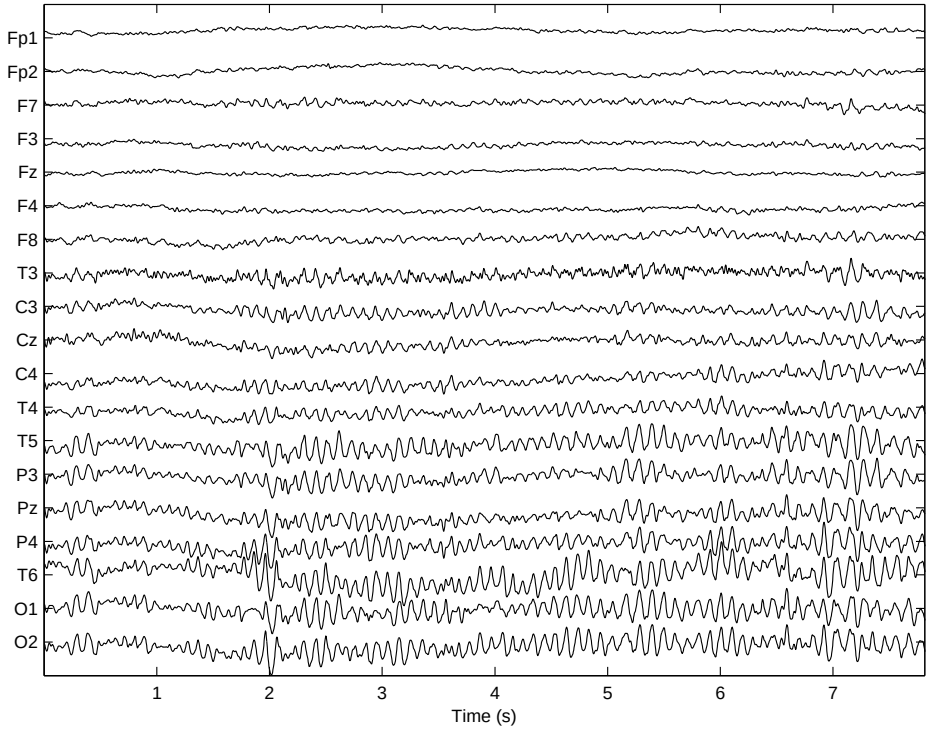

FIGURE 1.2: Example of an electroencephalogram acquired using a 19 channel system using a "rest state with closed eyes" protocol.

the level of alertness, on the age and behavioral state of the subject. Moreover an EEG pattern is influenced by neuro-pathological conditions, metabolic disorders, and drug action. The different brain rhythms or some combination of them become dominant oscillations during specific mental states, which can be induced by the performance of a proper acquisition protocol. Specifically, Delta and Theta frequency bands are considered to represent slow oscillating neural synchronization, or slow wave (SW) activity, while Beta and Gamma bands represent fast wave (FW) activity. Brain oscillations in these frequency bands has been linked to various physiopsychological states and cognitive functions, as reported for instance in [10], [11]and [12]. A more detailed characterization of the subbands is given in the following.

- **Delta** $[0.5, 4]$Hz: Delta rhythm is a predominant oscillatory activity in EEGs recorded during the so called deep or slow wave sleep (SWS). In this stage, Delta waves usually have large amplitudes $(75 - 200\mu V)$ and show strong coherence all over the scalp. In newborns, slow Delta rhythms predominate. An increase in Delta EEG activity during the performance of a mental tasks has shown to be related to an increase in subjects' attention to internal processing [13].

- **Theta** $[4, 8]$Hz: In human scalp EEG, changes in Theta rhythms are very difficult or almost impossible to detect without the help of computational methods. If EEG power in

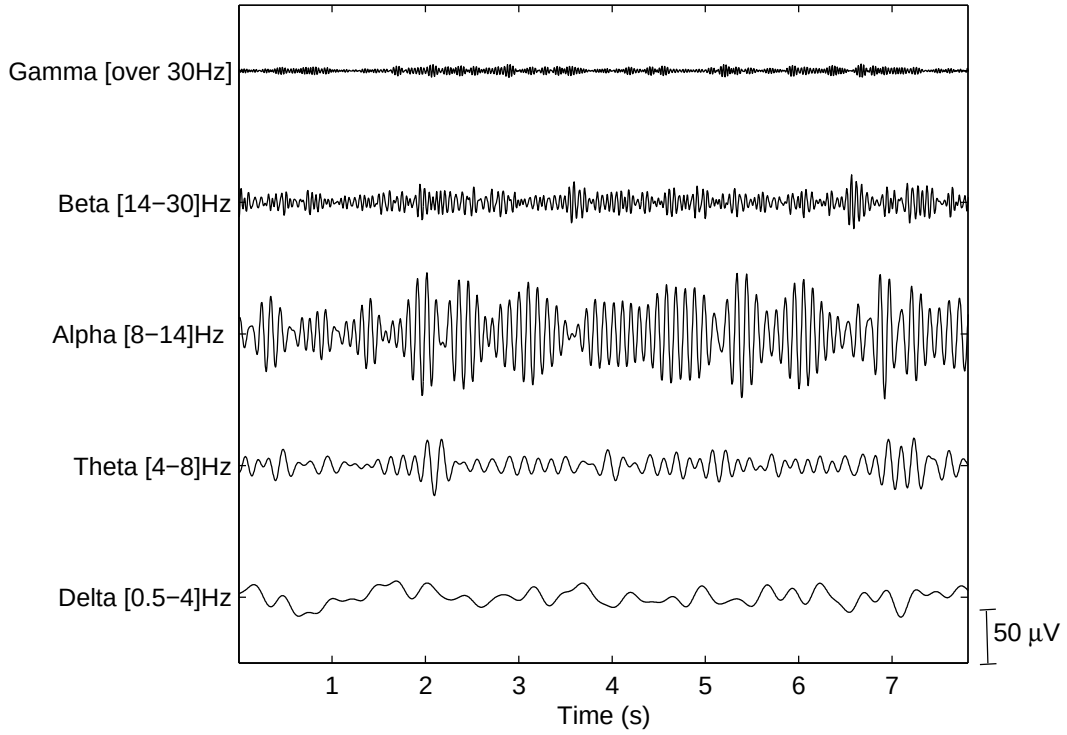

FIGURE 1.3: Examples of Delta, Theta, Alpha, Beta, and Gamma waves acquired through the channel O2 using a "rest state with closed eyes" protocol.

a resting condition is compared with a test condition, Theta power synchronizes, that is an increased Theta activity is observed. In particular Theta band power increases in response to memory demands, selectively reflecting the successful encoding of new information [14].

- **Alpha** $[8, 14]$Hz: The oscillatory Alpha band activity is the most dominant rhythm which emerges in normal subjects, most pronounced in the parieto-occipital region. It is manifested by a peak in spectral analysis. The Alpha brain oscillations may present amplitudes large enough to be clearly seen in raw EEG traces acquired in specific mental states (see Figure 1.3). It is characteristic of a relaxed but wakeful state primarily with closed eyes, and attenuates with eyes opening or mental exertion due to event-related Alpha power desynchronization. These changes in the Alpha band reflect an increase in tonic energetic levels related to increased arousal caused by basic processing of visual information [15]. Moreover there is evidence that attentional and semantic memory demands lead to a selective suppression of Alpha in different subbands and that the well described effects of visual stimulation represent just a special class of sensory-semantic task demand [16]. According to these evidences, the Alpha oscillations play an important role in suppression of processing for inputs in the brain. This confirms the evidence that Theta and Alpha band power are related to each other, although in an *opposite* way.

- **Beta** $[14, 30]$Hz: Phase synchrony in Beta frequency band is enhanced for consciously perceived stimuli [17], and detectable mainly from the involved cortical areas, including somatosensory, frontal, parietal and motor regions, depending on the performed task. Specifically, Beta activity is characteristic for the states of increased alertness and focused attention.

- **Gamma** (over 30Hz): Neuronal synchronization in the Gamma band is considered important for the transient functional integration of neural activity across brain areas, in order to achieve various functions involving active information processing, e.g., recognition of sensory stimuli, and the onset of voluntary movements [18]. Gamma components are difficult to record by scalp electrodes and their frequency usually does not exceed 45Hz. Components up to 100Hz, or even higher, may be registered in electrocorticogram (ECoG).

In general, it can be assumed that the slowest brain rhythms are dominant during an inactive state and the fastest are typical of information processing performance.

In Figure 1.4 the topographic maps related to the main brain rhythms during resting with closed eyes are displayed in false colors. Specifically, the mean value of the power spectral density for each frequency band is reported.

1.2 Acquisition protocols

EEG signals can be acquired through portable devices that sense the electric field generated by the brain while resting or during a variety of cognitive tasks, such as response to audio or visual stimuli, real or imagined body movements, imagined speech, etc. More specifically we refer to "event related potentials" (ERP) as to a small change in the electrical activity of the brain, time-locked to a meaningful externally (exogenous) or internally (endogenous) generated event [19]. ERP signals convey information on changes which occur when similarly oriented pyramidal neurons of both individual and different local networks fire in synchrony. For endogenous ERPs, time-locked to a mental event such as the recognition of a target stimulus, the activity of the cortex reflects functional coordination during neurocognitive information processing [20]. ERPs components can be described in terms of latency time, polarity, and topography. Large individual differences exist for the ERP components, while a certain stability is observed within a subject [21]. Other largely studied brain signals are "slow cortical potentials" (SCPs), also used as control signals in BCI context. They represent slow voltage shifts in EEG, which are involved in the modulation of the excitability level of underlying cortical regions, and in the preparatory allocation of resources for cortical processing [22]. SCPs last from 300 ms to several seconds and can be self-regulated with different purposes using immediate feedback.

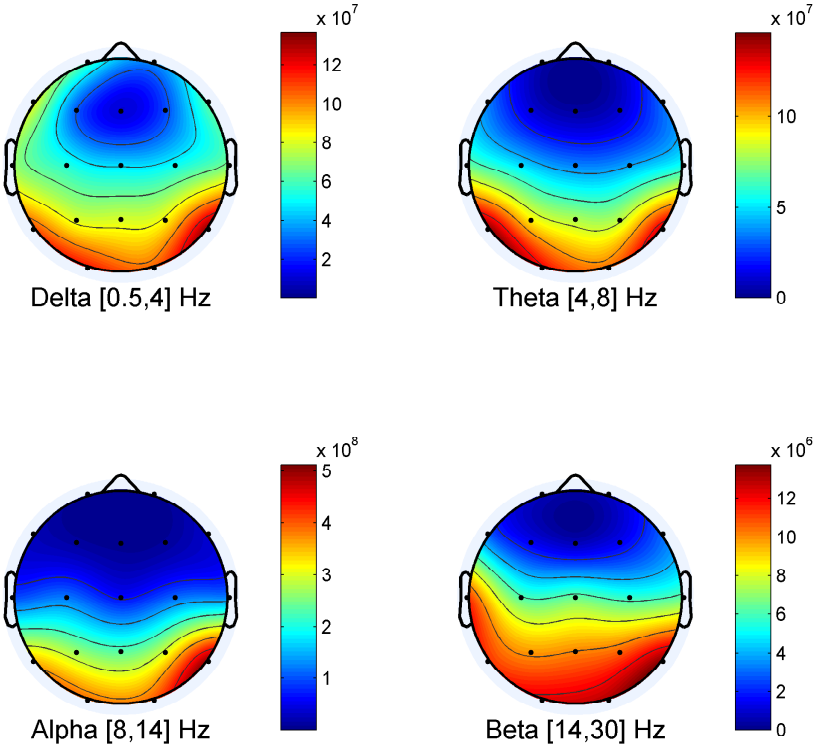

FIGURE 1.4: Topographic maps of rhythms. Each map shows in false colors the spatial distribution on the scalp surface of the related EEG rhythm, for a test subject. The mean value of the power spectral density for each frequency band is reported. Maps for rhythms Delta, Theta, Alpha, and Beta are shown. Each circle represents the top view of a head, where the highest point is the nasion while the lowest is the inion.

EEG signal analysis allows catching the relative timing of neural events during a specific task performance. The physiological phenomena underlying some brain signals have been decoded studying EEG recorded within dedicated acquisition protocols. These protocols are specially designed in order to elicit specific brain responses of interest, with the aim of studying the neural mechanisms of information processing in environmental perception as well as during complex cognitive operations. In this regard several data acquisition protocols have been proposed in the literature specifying the data acquisition conditions, the task definition, and the sensing electrodes configuration related to the neurophysiological function under analysis.

In this Section we describe some acquisition protocols employed in EEG studies. Topographic information on source activation are reported depending on the performed task, and guidelines for efficient scalp electrodes configurations are provided.

1.2.1 Elicitation of brain responses

Since the earliest applications of EEG signals, particular interest has been shown in the study of cerebral activity during a state of rest, due mainly to the simplicity of the acquisition process. Therefore, the resting state (RS) protocol, with eyes closed or open, has been widely studied for different purposes. Within this paradigm, typically, the enrolled subjects are comfortably seated in a chair with both arms resting, in a dimly lit or completely dark room. Generally, external sounds and noise are minimized to favor the relaxed state of the subjects. Participants are asked to perform few minute of resting state with closed eyes (EC) or open eyes (EO), avoiding any focusing or concentration, but keeping awake and alert. Brain activity during resting state without performing any task carries interesting information as contained in EEG specific patterns [23]. Eyes-closed and eyes-open resting conditions are usually employed in EEG research studies for baseline estimates, although they represent different processes related to global arousal and focal activation [24].

Moreover, EEG patterns have shown significant differences, specially related to the spectral analysis, between rest and several cognitive tasks, and even between different cognitive tasks themselves, involving distinct neural systems. In order to infer about the properties of neural activation in the involved brain regions, math, logical and spatial cognitive operations have been considered in the development of suitable acquisition protocols. Changes in activation patterns due to specific components of mental calculation can be observed from the analysis of each frequency band, as they seem to be related to oscillatory activity of different neural networks. In this regard different EEG patterns have been examined by testing healthy subjects in different conditions of mental calculation through properly designed protocols. In these protocols the mental task period is usually preceded by a rest period in order to provide a baseline. During the mental task interval, the subject is asked to solve a problem providing an answer [25]. The features of such kind of brain patterns reflect inter-individual variability due to different abilities, aptitudes, innate mechanisms of habit, brain plasticity, etc.

The most explored protocols involve the elicitation of the above mentioned ERPs. Task-related ERPs, as well as background EEG, are associated to different behavioral and cognitive traits. ERP signals can be elicited within different stimulation/acquisition paradigms involving for instance sensory, cognitive or motor events. Usually, the exogenous eliciting events are repetitively modulated sensory stimuli such as a visual flicker. The so elicited evoked potentials strongly depend on the physical parameters of the stimuli. On the other hand endogenous ERPs depend on internal cognitive events reflecting the way the subject evaluate a stimulus.

A largely studied and employed brain potential is the P300 ERP, especially used in BCI context. The P300 ERP is a positive deflection of the scalp potential which typically occurs around 300

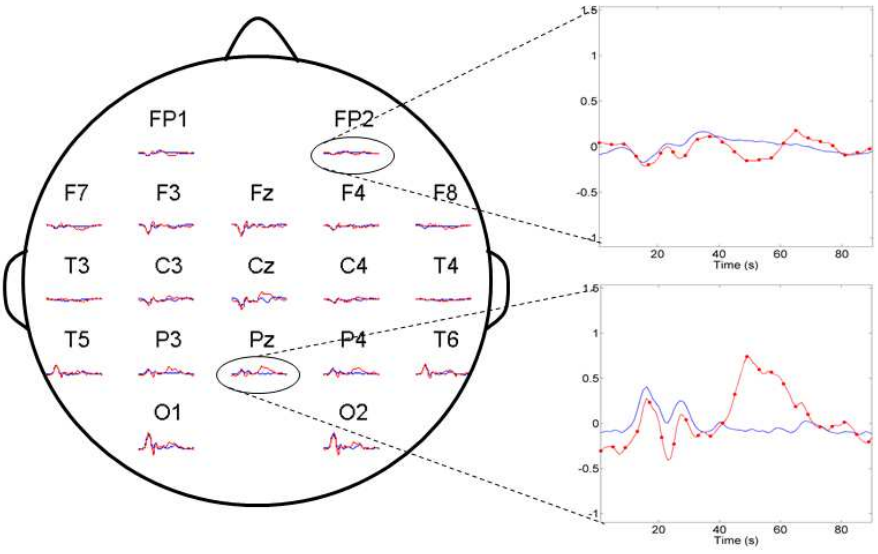

FIGURE 1.5: Topographic distribution of P300 brain potential as elicited through an oddball paradigm, employing a 19 electrodes configuration based on the 10-20 standard. Labels which indicate the related channel are reported on each P300 waveform, obtained averaging the EEG segments time-locked to target stimuli (red lines). Similarly, brain responses related to non-target stimuli are also reported in each subplot (blue lines) as a reference to evaluate the P300 responde.

ms after the onset of a task-relevant stimulus, with a centro-parietal focus [26]. The most effective paradigm for inducing a P300 response is the 'oddball' task. In this paradigm an infrequent but task-relevant stimulus is presented among frequent irrelevant stimuli [27]. Different kind of stimuli can be employed to carry out such paradigm. One example is the well-known P3Speller first designed by Farwell and Donchin for a BCI application[28]. It provides a matrix speller, that is a matrix of characters where rows and columns are randomly flashed while EEG is acquired. The user is asked to focus on the desired symbol detecting every time the corresponding row and column flash. Subsequently the BCI uses the P300 responses to identify the target symbol. The characteristics of the P300 response will change with the type of stimulation, its timing, and with the task difficulty. The P300 individual differences relate to amplitude, latency, waveform and scalp potential distribution [26], and also reflect psychophysiological aspects of individual central nervous system reactivity. Figure 1.5 reports an example of the P300 response for a subject involved in an oddball paradigm, where the presented stimuli are different geometric shapes, and the subject is asked to detect just one specific shape among the others. The topographic distribution of the brain response can be observed, and it could be noticed that the polarity change across the scalp, shown by the P300 wave, depends on the reference electrode. For the particular case shown in the figure a good brain response can be detected in central and parietal electrodes, as a much larger P300 amplitude (red line) related to target stimuli stands out from a baseline measure (blue line) obtained by averaging non-target responses.

Another typically employed ERP stimulation protocol during EEG acquisitions is the elicitation

of Visual Evoked Potentials (VEP), performed in order to analyze the way the brain perceives and processes visual input, to control BCI applications and to support neurological diagnosis. VEPs are evoked potentials that occur in the visual cortex, time-locked to a repeated sensory stimulation related to a subject's visual field. Within VEP protocols no response or cognitive processing by the subject is required. The visual stimulation can consist for instance of checkerboard pattern reversal, flashing black/white images, pattern onset stimuli or photic stimulation (light) [29]. In a typical setup to elicit VEPs a flashing stimulus is displayed either at the center of a screen or through light-emitting diodes (LEDs) in the central visual field, since it causes a greater response amplitude.

Some interesting evidences have been obtained from the analysis of μ and β EEG rhythms recorded over sensorimotor cortex within the so-called motor imagery paradigm. Typically, during each acquisition session, subjects are asked to imagine moving for few seconds when the cue representing the movement instruction appears on a screen. As reported in [30] it has been observed that the patterns of μ and β band desynchronization over sensorimotor cortical areas during motor imagery are similar to those during actual movement. Moreover, principal components analysis on sample average signals has shown marked individual differences in motor-related EEG patterns, topographically and spectrally focused. These evidences support the possibility of effectively controlling μ and β rhythm amplitude through motor imagery and individual training.

More recently, EEG acquisitions have been performed during the so called "speech imagery", aiming at recognizing the neural activities associated with speech production. In some protocols, enrolled subjects are instructed to imagine continuous vowel vocalization for few seconds from the onset of a specific cue which can be an acoustic signal or a task-representative image appearing on a screen [31]. In BCI context this kind of tasks are designed in order to discriminate differences in brain activity during vowel or syllables speech imagery providing a control scheme for communication based on the interpretation of individual speech correlates in EEG.

Furthermore,when using SCPs, the training for their voluntary control can be carried out within an acquisition protocol where a thought-translation device provides a feedback cursor on a screen, whose position constantly reflects the voltage shifts. Typically [32] the subjects are asked to move a cursor which appears at the center or at the periphery of a screen toward a target, by modulating their brain electrical activity. A preparatory phase in which the cursor remains stationary on the screen is followed by an active phase in which it moves in a direction, either horizontal or vertical, with constant speed, and in the perpendicular one according to the user's SCP amplitude.

A tree summarizing the EEG signals elicitation approaches described above is given in Figure 1.6.

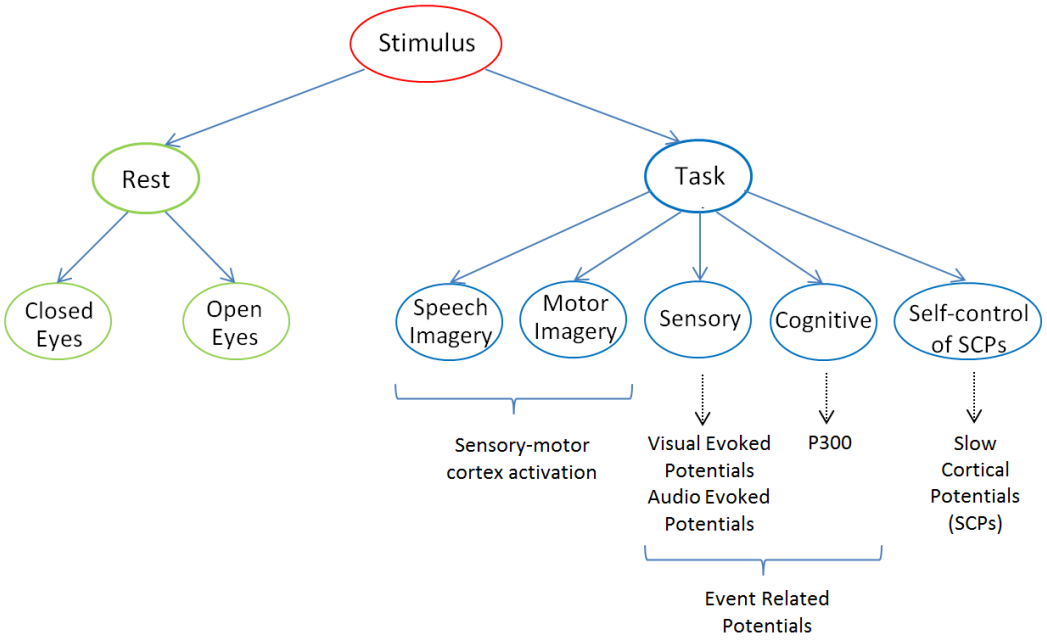

FIGURE 1.6: EEG signals elicitation approaches.

Several acquisition protocols have also been designed for emotion recognition purpose, which consists in the detection of changes in the brain electrical activity related to distinct emotions which are elicited by a specific stimulation content like images, sounds, words, scenes, videos, etc. In this regard it is important to consider that different stimuli influence individual emotional state, so that different subjects with personal emotional experiences show distinct responses to the same stimulus. Emotional activities of the brain causes different distributions of characteristic EEG waves. In several works EEG data are collected from subjects during the projection of movie clips or pictures. In [33] features from EEG signals are used for discriminate among three different emotions, happiness, disgust, and fear, artificially elicited while watching two commercial movie clips for each emotion. In [34] authors employed a specially designed acquisition protocol for the classification of six emotions evoked by visual inputs consisting of pictures with emotion-related facial expressions. The functional properties of the system formed by mirror neurons, which plays a fundamental role in emotion induction related to action imitation [35], are considered within this protocol. In the proposed experiment, pictures showing people expressing the six basic emotions, namely happiness, surprise, anger, fear, disgust and sadness are subsequently and randomly projected (10 pictures per emotion), separated by black and counting down frames allowing subjects to relax during intervals between stimuli.

In [36] an acquisition protocol for arousal monitoring has been also proposed. Authors evaluated EEG signals acquired during the simulation of a security surveillance system. Different stimuli representing x-ray images of luggage objects were displayed on a screen and users are required to perform a choice task to distinguish dangerous from harmless objects. Users had to quickly respond to stimuli presented in blocks of many trials, so that a fading level of arousal

was expected. These kind of EEG acquisition protocols have a high relevance within the framework of reducing risk of errors or accidents when dealing with sensitive tasks, and can also provide monitoring of individual mental activity for purpose of continuous authentication in high security contexts.

The experimental setups described above represent an overview of acquisition protocols commonly employed when investigating brain functioning with different purposes, such as the evaluation of brain activity patterns for applications like diagnosis and device control. Some of the aforementioned paradigms are also employed in biometrics for user recognition as detailed in the following, while some others have some potentials which have not been explored within the biometric framework.

1.2.2 Scalp electrodes configurations

The spatial distribution of brain activations as reflected in scalp EEG signals strongly depends either on the mental state of the subject or on the performed task during the acquisition session. For each designed protocol it can be identified a suitable electrode configuration in terms of number of sensors, their placement on the scalp as well as their density, according to the aim of the analysis, selecting a subset of channels in the 10-20 extended system shown in Figure 1.1. A specific minimal set of electrodes selected considering neurophysiological evidences and optimization criteria is generally employed in each experimental setup. Usually, the reduction of data dimension due to a selection of electrodes helps in improving the effectiveness of the data analysis.

As previously pointed out in Section 1.1, in the closed eyes resting condition the predominant Alpha oscillations can be detected especially in the parieto-occipital region of the scalp. They reflect the default mechanisms of synchronization of cortical neurons activity [11]. Therefore a description of the ability of the central nervous system to transmit signals to and from the cerebral cortex can be carried out focusing on signals from parieto-occipital electrodes. On the other hand, a widespread reduction in activity is commonly observed turning to open eyes resting conditions, wich reflects neuronal Alpha desynchronization. Further topographic changes occurring across frequency bands can be detected considering a full-scalp montage in the analysis of open eyes resting state.

Furthermore, various configurations can be employed for the effective detection of different EEG activation patterns during the performance of different mental calculation tasks. Some significant differences between mental calculation tasks, related to change in power between task and rest conditions, have been observed in the δ and β bands in the frontal lobe, reflecting different selective processes during focusing on relevant information [25], depending on the complexity of the task and the specific cognitive function involved. In general an increase of

Delta, Theta and Beta activity in frontal leads during subject's internal concentration has been observed. This is in accordance with the evidence that among the various functions of the human brain directing and allocating brain resources are governed by the frontal lobe. In particular decision making, reasoning and complex calculation require the integration of multiple processes, specific of each task. It results in differences of frontal lobe activity between tasks, reflecting activation of different neural networks. Therefore frontal leads can be effectively employed for the analysis of such specific functions.

More specific electrodes configurations are commonly employed in the analysis of brain responses. In particular, several studies in literature addressed the effectiveness of different electrode configurations used to detect the P300 brain response. A trade off between user friendly solutions employing few electrodes and accuracy in terms of correct classification of brain responses is needed for the suitability of such P300-based systems. Good results have been obtained in [37] employing only eight electrodes from the midline and the parietal region of the scalp, namely Fz, Cz, Pz, Oz, PO7, PO8, P3, P4, as pictorially shown in Figure 1.7 (a). Thereby accuracy improvement has been obtained removing redundant information from contiguous time points which would reduce the generality of the analysis.

A different smaller subset of the electrodes montage is considered when studying VEP signals related to specific kind of visual attention stimulation as detailed in Section 1.2.1. In these cases typically EEG signals are recorded from electrodes located in the posterior region of the scalp, mostly over the left and right hemispheres of the primary visual cortex. Indeed either periodic or transient brain responses to stimulation involving the visual system can be detected just considering electrodes O1 and O2 within the 10-20 international system [38].

Also in the analysis of rhythm topographies during motor imagery protocols, a subset of the extended 10-20 international system is often employed, considering sensors placed over the sensory-motor cortical area, namely FC3, FC1, FCz, FC2, FC4, C5, C3, C1, Cz, C2, C4, C6, CP3, CP1, CPz, CP2, CP4 as shown in Figure 1.7 (b). In fact it has been repeatedly shown that both movement and motor imagery are accompanied by desynchronization in μ and β bands over the centro-lateral side of the scalp, showing hemispheric asymmetries for specific conditions and frequency ranges [30]. Results showed marked individual-specific traits regarding topographic and spectral effects of movement and motor imagery, also indicating that movement, imagery and bands are dissociated in terms of individual differences. Signals from motor cortex are also employed for the performance of speech imagery protocols. In has been shown that neural activation detected over medial and posterior regions occur during imaginary lip movement and vocalization of vowels [31] or their mental repetition. The electrodes that are distant from the active regions may not provide relevant information. Therefore, a more effective analysis of EEG features during speech imagery could be obtained discarding them.

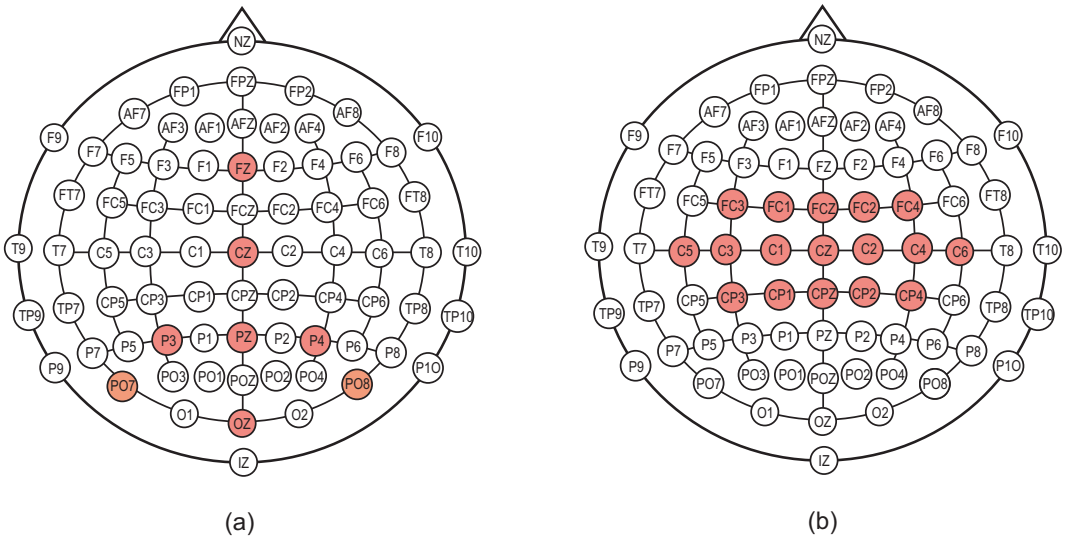

FIGURE 1.7: Electrodes placement for a P300 based system: an example (a). Electrodes placement for a motor imagery based system: an example (b).

Moreover, effective negative and positive SCP shifts can be controlled selecting the best performing channel. In this regard, in [32] it is shown that self-regulation skills differ between subjects, but that the Cz derivation could be generally used for an effective SCP feedback learning. Interestingly, in that study it was shown that many subjects generated a maximal SCP differentiation at other, often neighboring, electrodes than Cz.

On the other hand, the evaluation of the most effective electrodes placement for purposes of mental state monitoring or emotion recognition strongly depends on the task the enrolled subject is involved in. In [36] it is observed how occipital channels account strongest for the detection of mental state differences reflected in Alpha activity during a visual surveillance task. Interestingly, it is there pointed out that accordingly changes of Alpha activity depend on visual processes.

To sum up, in the above mentioned studies, it has been shown that depending on the given goal, the selection of electrodes based on neurophysiological considerations brings to higher performance systems.

Chapter 2

EEG biometrics

This chapter will focus on the level of understanding that is been achieved about the use of EEG signals as biometric identifier.

Specifically, we cover and discuss the several issues which need to be taken into account to design an EEG based recognition framework, and to perform a fair comparison among the existing systems in terms of usability and recognition performance. A comprehensive though critical review of the methodologies dealing with EEG biometrics proposed in the existing literature is presented to effectively crystallize the state of the art, and to systematically identify the most important issues to address in the research agenda on EEG biometrics. The correlation between the recognition capabilities of the state of the art approaches and neurophysiological evidences, can help to identify the distinctive elements in the brain functions and organization. The different modeling approaches suitable for the several scenarios considered to elicit brain responses are reviewed and evaluated according to the specific application. In particular we compare the existing EEG based biometric systems with respect to the employed acquisition protocols in terms of cognitive task, the number of electrodes and their spatial configuration, the feature extraction algorithm and the features' physical and functional significance, the classification algorithms and their effectiveness in clustering the observations. Whenever possible, also a physiological interpretation of the extracted features is provided by correlating them to the anatomical and functional distinctive aspects describing the organization of the brain structures during specific mental tasks.

2.1 EEG signals as biometric identifiers

In [5], back in 1980, the basis for automatic people recognition using EEG signals where posed. However, only in the last decade the study of EEG based recognition systems has received a

significant development. EEG signals present some peculiarities, which are not shared by the most commonly used biometrics, like face, iris, and fingerprints, and that make the investigation on the use of EEG signal as biometric identifier not a mere academic exercise but an analysis with potential dramatic effects on the design of the next generation biometric systems, namely the cognitive based systems.

Specifically, brain signals, as a result of a cognitive process, are not exposed like face, iris, and fingerprints, therefore they are more privacy compliant than other biometrics since they are "secret" by their nature. In fact they are not left on objects like fingerprints, and it is impossible to capture them at a distance while this is possible for face or iris. Moreover, being EEG signals the result of ionic current flows within the neurons of the cortex, EEG biometric are robust against spoofing attacks at the sensor since an attacker should be able to acquire them at a distance which is not feasible at the present state of technology. Furthermore, being brain signals the result of a cognitive process, they cannot be synthetically generated and fed to a sensor to spoof it, like when using gummy fingers for fingerprints. Therefore the problem of liveness detection, which needs to be addressed when using conventional biometrics, is naturally overcome without the need to resort to specifically designed sensors. On the other hand the use of brain signals poses new challenges. In fact being the brain continuously and spontaneously active, there is a background electrical activity upon which the signals of interest, which come from the firing of specific collections of neurons responding accordingly to a variety of cognitive tasks, are superimposed. Part of this difficulty is the understanding of the brain areas where the response originates. These findings would drive an optimal or sub-optimal choice about the number of electrodes to use and their location. Furthermore, due to the weakness of the signal detected on the scalp while generated on the cortex, the EEG acquisition process results very sensitive to endogenous and exsogenous noise, that is artefacts generated by physiological processes and by external sources respectively. Therefore, the basic mechanisms which are behind the physiological process of brain signal generation, the signal stability in time, the acquisition protocols, the optimal sensors location depending on the employed acquisition protocol, the amount of the discriminative information, as well its frequency localization, need a much deeper understanding.

In this Section the different characteristics of a biometric identifier, namely *universality*, *uniqueness*, *permanence*, *collactability*, *performance*, *acceptability*, and *circumvention*, are detailed with respect to EEG biometrics. It is worth pointing out that the analysis that follows has different depth levels for the different desired characteristics, since EEG biometrics is still at its infancy and an exhaustive analysis of the aforementioned issues referred to EEG biometrics is still missing in literature. Nevertheless, in the following we draw some considerations, which, in same cases, have been borrowed from physiological studies on EEG signals made for clinical applications and that can be applied to the field of EEG biometrics.

2.1.1 Universality

Each person should have that characteristic

The level of universality of brain signals is very high. In fact people with no degenerative pathological conditions affecting the brain, can make use of EEG biometrics. Therefore it can be seen as an enabling technology which could allow to overcome physical disabilities preventing the use of biometrics like fingerprint or iris.

2.1.2 Permanence

The characteristic should be sufficiently invariant, with respect to the matching criterion, over a period of time

The issue of the reproducibility of EEG biometrics in different acquisition sessions, in other words the intra-individual EEG stability, has been object of scientific investigation within the neurophysiology field in the past [39], [40], [41]. In fact, also in clinical applications, it would be desirable not to have significant variations of an individual EEG pattern when no alterations, due for example to new pathological conditions, occur. In the clinical field these studies are known as "test-retest reliability" or as "longitudinal" studies. Of course the aforementioned issue is strictly dependent on the features which are extracted to summarize the EEG and on their reliability. It is worth pointing out that a significant effort has been done for the test-retest reliability analysis of EEG in resting conditions as well as, in the recent years, when performing cognitive and sensory tasks.

In [8] eight-channel recordings for a set of 47 healthy subjects under conditions of rest and perceptual stimuli have been acquired. The power spectra in the range $[8, 13]$Hz, α subband, were evaluated and an analysis of variance was done in order to determine their dispersion characteristic. The performed analysis has revealed that EEG spectra are more distinctive in the eyes closed resting state with a significantly strong Alpha rhythm, while performing a task would somehow normalize the Alpha activity thus reducing the inter-individual difference.

In [9] both the intra-individual and the inter-individual reproducibility of EEG parameters have been analyzed for a group of 12 healthy people, mainly women, in open eyes resting condition. Parameters related to the amplitude profiles in the different frequency bands were considered in this analysis. Results showed that for all the considered characteristics, their variance among different individuals was greater than among different measurements for the same individual over a period of two-three months. It appeared that Alpha activity is the most powerful indicator of the inter-individual differences, whereas Delta and Theta indicators have smaller inter-individual variances.

In [42] eight-channel signals for a set of 26 healthy children, with an age between 10 and 13 years, under conditions of rest with closed eyes, were acquired to study test-retest reliability considering two EEG recordings 10 months apart from each other. Power spectrum related features were used and different rhythms were examined. In summary the Alpha rhythm manifested a good reliability in the test-retest framework for the considered features, whereas the Delta band was found less reliable.

In [43] test-retest reliability was investigated for a set of 19 healthy adults whose EEG was recorded using 15 electrodes, F3, F4, F8, T3, T4, T5, T6, O1, O2, P3, P4, C3, C4, and Cz, considering acquisition sessions separated by 12-16 weeks intervals. The employed elicitation protocol consisted in instructing the subjects to listen to randomly reproduced tones with closed eyes, and in asking them to respond to the stimulus by pressing as quickly as possible one of two switches, depending on the played tone's level, high or low. Spectral analysis was done, and peak Alpha frequency and median frequency resulted as the most stable spectral features. It was also experimented that the electrodes montage affects the test-retest reliability.

In [44] 45 healthy subjects were tested in an interval of 25-62 months in order to infer about the intra-individual variability. Features such as the absolute and relative power, the median and peak frequency, the entropy, etc. where used. It was shown that Alpha peak frequency and median frequency are stable characteristics for the period under investigation, in the sense that their intra-individual variation was less significant than the inter-individual variations.

Test-retest reliability has been considered also in [45], where a closed eyes protocol has been used to acquire signals from a sample of 20 people during two EEG recording sessions at a mean distance of 15 months. The authors resorted to rely on power spectra which, when a closed eyes protocol is implemented, are dominated by a peak in the Alpha subband. Specifically, the amplitude and the frequency of the peak as well as the shape of the power spectra were taken into account, and a set of three electrodes, namely AFz, Cz, and Pz, from the median sites was chosen among 60. The test-retest reliability was verified by implementing a recognition system, which proved that the considered features guarantee high performance across the two considered period of time.

It is worth pointing out that although a significant effort has been done mainly for the test-retest EEG reliability analysis in resting state, some attempts to analyze other tasks have been performed as well. In [46] the reliability of EEG signals recorded during cognitive tasks, specifically a working memory task and a psychomotor vigilance task, were investigated on a set of 21 healthy adults. The inter-session time was on average 7 days and the power spectra of Theta at Fz and Pz, and the slow and fast Alpha spectra at Pz were examined. Both considered tasks showed a high reliability within and among sessions. In [47] the test-retest reliability of a working memory task has been analyzed using the same acquisition conditions, that is electrodes' type, time span between the two acquisition sessions, features, and validation strategy

as in [45]. The intra-individual stability was found higher with respect to the inter-individual variation, and the recognition rate was found comparable to that obtained in resting state with closed eyes in [45].

Despite the effort that has been done in the neurophysiology field, the repeatability issue of EEG biometrics has not received the necessary attention from researchers in the biometric scientific community. Nevertheless, its understanding is propaedeutic towards the deployment of EEG biometrics in real life. Few sporadic and non exhaustive analysis have been given in the biometric literature so far. In [48] the session-to-session variability was tested on a dataset composed of 6 subjects performing imagined speech. The entire set of 128 channels was used to extract features, and results show a decreasing performance when considering sessions temporally apart. In [49] the problem of repeatability over time of EEG biometrics, for the same user, has been specifically addressed. A simple "resting state" protocol has been employed to acquire a database of nine people on two different sessions separated in time from 1 to 3 weeks, depending on the user. Although the dimension of the database employed is contained, [49] represents the first systematic analysis on the repeatability issue in EEG biometrics. Simulations have been performed by considering different sets of electrodes both with respect to their positioning and number. In summary, the analysis has shown that a significant degree of repeatability over the considered interval can be achieved with a proper number of electrodes, their adequate positioning, and by considering appropriate subband related to the employed acquisition protocol.

However a more exhaustive analysis involving a relevant number of sessions over a significant period of time as well as different acquisition protocols is still needed. In fact, a lack of systematic and extensive studies on the issue does not allow to infer about the repeatability of genetic and individual-specific EEG traits over time, also due to difficulties in obtain longitudinal recordings from the same group of subjects.

2.1.3 Performance

The use of the characteristic must ensure good performance

Promising recognition rates have been achieved. A detailed analysis of the recognition performance of state-of-the-art EEG-based biometric systems is given in Section 2.2. In the presented works performance is expressed using different figures of merit like the genuine authentication rate (GAR), the false acceptance rate (FAR), the false rejection rate (FRR), the half total error rate (HTER=(FAR+FRR)/2) and the equal error rate (EER), that is the HTER evaluated when FAR=FRR.

2.1.4 Collectability

The characteristic should be quantitatively measurable with some practical device

Collectability of EEG signals, is dependent on many factors like the number of electrodes to be used, the need to use conductive paste to lower the skin impedance to acceptable levels, and the acquisition time needed to be able to collect relevant information for the recognition process. All these issues can limit the collectability of EEG biometrics. However, recent advances have shown that interesting performance can be achieved also limiting the number of used electrodes thus making the signal collection more manageable as detailed in Section 2.2. Moreover, the latest technological developments have shown that the aforementioned issues can be mitigated as clarified in Section 2.3.

2.1.5 Acceptability

The public should have no strong objection to the measuring/collection of the characteristic

Acquisition of EEG signals may present some drawbacks in terms of user acceptability being related to brain activity thus potentially evoking ancestral worries related to "mind reading" and emotion analysis from the data controller. This may generate a sense of discomfort in the users. Also privacy issues can be seen as an obstacle towards the acceptability of EEG based biometric applications in real life due to the potentiality to detect existing pathologies or disposition towards pathologies, as possible also for other biometrics. This could potentially lead to discrimination and undermine the human dignity. However, no specific studies on the acceptability issue of EEG signals biometrics have been performed yet.

2.1.6 Circumvention

The characteristic should be robust to attacks

Brain signals, as a result of cognitive processes, are not exposed biometrics like face, iris, and fingerprints. Therefore, as internal traits, they are less prone to spoofing attacks than other external biometrics, since they are "secret" by their nature, being impossible to capture them furtively at a distance, while this is possible for face and iris, which can then be synthetically generated. Besides, EEG biometrics cannot be acquired in absence of the user, since they are not left on objects like it might happen with fingerprints, that can be used at a later time in order to spoof the employed acquisition sensor. This is virtually impossible with brain signals since they are the result of ionic current flows within the neurons of the brain in response to a specific task or during a specific mental state. Therefore, an attacker should be able to synthetically

generate resulting EEG waveforms and feed them to a sensor to spoof it, like with the use of gummy fingers for fingerprints. Hence, the problem of liveness detection, which needs to be addressed when using conventional biometrics, is naturally overcome without the need to resort to specifically designed sensors. A study on possible countermeasures to specific attacks to EEG-based biometric systems is provided in [50].

2.1.7 Uniqueness

Any two persons should be different in terms of the characteristic

The uniqueness of EEG signals is a complex issue which has several facets to consider and that has never captured so far the necessary attention within the biometric community. Nevertheless, some early studies in neurophysiology, see for example [8], [51], [52], have demonstrated that EEG is a highly individual characteristic. In [53] a variance analysis of Alpha waves in a closed eyes condition showed a significant level of individuality. In [54] the same conclusions were drawn for the open eyes condition. Of course the level of individuality is also related to the specific acquisition protocol, subband analyzed and to the extracted features. Moreover, it is worth pointing out that the uniqueness and the permanence issues can be considered as two facets of the same medal, being related to the intra-individual and inter-individual distances, and that these distances get some meanings when related to each other. Therefore works that address one issue need to consider also the other one, as evident in the analysis on the *permanence* carried out in Section 2.1.2.

Heritability and personality factors also play an important role in characterizing an individual's EEG. In the following we focus on the dependance of EEG signals on heritability and personality factors, and report some results found in the field of neurophysiology which can help to have a better understanding of the uniqueness issue within the biometric framework. Specifically the heritability and the personality issues are considered in detail in Sections 2.1.7.1 and 2.1.7.2 respectively.

2.1.7.1 Heritability of EEG variants

In neuroscience, the influence of hereditary factors on individual differences in central nervous system functioning has been addressed by using electroencephalography as neurophysiological investigation technique among the others. Therefore we rely on those findings in order to infer about the heritability of EEG signals which is an important element to be considered when dealing with biometric based recognition.

In the early seventies it emerged that some aspects of the ongoing brain activity during resting state is hereditarily determined, that is it carries genetic information [55]. Automatic classification of genetic EEG variants was first performed in [56], where spectral analysis was used. More recent studies have confirmed that both genetic factors and shared and non-shared environmental influences, affect important traits of neurophysiological functions, as well as anatomical features of the brain and of the related structures around, like for instance the skull thickness. An interesting study on genetic determination of inter-individual variability of brain functioning assessed through EEG features evaluation was performed in [57]. In that work the relative power values in each frequency band were analyzed as features, extracted from EEG recording acquired from a group of 213 adolescent twins, while resting with closed eyes. Univariate genetic model fitting was used to estimate the degree of heritability of EEG power spectrum features, considering the variations of the observed data as decomposed into genetic and environmental variances. In general, the results of the univariate analysis showed that ongoing activity in monozygotic twins is significantly similar for all frequency bands and areas, mainly because of the additive genetic influence tested through model fitting. In particular for most EEG rhythms the variance of power related features explained by genetic factors resulted high at all brain regions, except for power features in the Delta band, where lower heritability was found at frontal regions. Also multivariate modeling was used in [57] in order to estimate the contribution of genetic and environmental factors to the covariance of EEG power features related to different brain regions, to evaluate if same genes were expressed in the different brain areas and hemispheres. Only the dominant Alpha power related features were considered for multivariate modeling. From this analysis it could be concluded that there are no hemispheric differences in genetic heritability of power features, and that the same genes influences Alpha power related features at all brain regions. In [58] 1038 adolescent twins were recruited and asked to perform 4 minutes of resting state with closed eyes. Data were analyzed through multivariate genetic, still partitioning the total variance into the contributions due to additive and non-additive genetic factors and to the contribution due to non-genetic factors, including both common and non-common environmental influences, and measurement errors. Results confirmed that EEG is a high heritable trait and that common genetic factors influence all bands in both hemisphere, especially at occipital sites. Also band-specific effects were observed more influential at frontal sites. Authors interpreted the common factors as due to basic structural features such as skull thickness, or reflecting neural genetic properties affecting EEG features across all frequency spectrum. On the other hand band-specific influences seem to be related to the higher functional and structural complexity of anterior than posterior regions, confirmed by neuro-anatomical evidences.

Task performances other than resting state have been considered to investigate inheritance aspects in cognitive functions such as attention, focusing, memory or general cognitive processing. Specifically heritability has been suggested to affect individual variations of ERPs characteristic features. The P300 brain response elicited within oddball paradigm is commonly considered to

reflect attention to incoming stimulus information when memory representation of environment is updated [59]. Both the amplitude and latency of the P300 component vary as a function of task parameters and demand and exhibit broad individual variability as well as good temporal stability. The type of task demand is considered to influence the relationship between the P300 response features and the individual cognitive ability, supposed to be biologically based. Several family studies have shown significant heritability of P300 characteristic waveform. In particular in [60] authors studied the genetic influences on individual differences in the amplitude and latency of P300 responses, elicited within a so-called delayed-response working memory task, where subjects are asked to remember for short time the spatial location on a screen of target stimuli briefly presented. 708 siblings from 354 families were recruited for this study; maximum likelihood (ML) analysis of the individual observations together with Cholesky decomposition were used in order to perform a preliminary statistical analysis and to infer about heritability of the P300 waveform. The analysis aimed at distinguishing three sources of variance for P300 amplitude and latency: additive genes, shared and non-shared environmental influences. Also, the detection of common and specific genetic influences across sites (frontal, central and parietal regions) was addressed. Results showed a significant influence of genetic factors on P300 amplitude, while just suggesting the same influence on the latency. Findings from the application of multivariate genetic models indicated that common genes influence P300 amplitude at frontal, central and parietal regions. From the analysis of genetic expression in frontal region P300 response, authors suggested that specific and common genetic factors influence functionally distinctive cognitive processes, not in contrast with the evidence that there are more neural generators of P300. A comparison with results of other studies on the same issue suggests that the heritability of P300 amplitude is not influenced by task difficulty, so that a low level cognitive process genetically mediated could be involved in the P300 elicitation. On the contrary the genetically controlled processes influencing P300 latency involve speed in allocation of attentional resources for the processing of new stimuli, showing heritability only when the task is cognitively demanding. The studies cited above, among others, have provided strong evidence for heritability of spontaneous EEG and ERPs.

Moreover there is evidence that ERP amplitude is positively correlated with EEG spectral power, especially for low frequency bands, suggesting commonality of genetic factors influencing variability of spontaneous EEG rhythms and ERPs. In [61] EEG signals from 213 pairs of twins were analyzed by performing multivariate genetic analysis of P300 amplitude and EEG spectral power in different frequency bands. ERPs signals were acquired during the performance of a visual oddball task, and resting EEG was subsequently recorded with eyes closed. Results demonstrated that genetic influences on EEG power spectrum, especially in the Delta range, also affect the determination of the P300 amplitude. Authors observed that this is in accordance with the evidence that ERPs are the result of the synchronization of spontaneous EEG oscillations elicited by a kind of stimulus onsets. Moreover the high heritability of lower frequency EEG

activity is in agreement with the finding that a strong genetic correlation between ongoing EEG power measures and P300 amplitude is observed in the Delta band, suggesting variation in P300 amplitude to be the effect of heritable individual differences in EEG spectral power.

All the aspects discussed above lead to the observation that, although the EEG is influenced by psychophysiological factors and depends on the particular cognitive demand, genetic and environmental factors contribute to provide some unique features of the EEG signals acquired during a given mental state, assumed to be individual-specific.

2.1.7.2 EEG personality correlates

Personality definition and analysis is a broad topic of research itself. Roughly speaking, personality reflects the combination of emotional and attitudinal traits of an individual, which define a specific profile of each human being, which is influenced by different factors like genetics, biology, and environment. Several research studies on healthy subject have reported evidence that relationships between observed properties of brain activity and personality profiles exist. Some highlights are given in the following.

Personality, among the others, affects the way an individual responds to exogenous stimuli and this is reflected in EEG activation patterns. In [62] the association between arousal indices, measured through EEG, and extroversion is examined. Extroverts are expected to show more rhythmic low-arousal EEG activity than introverts. Emotional imagery was employed as experimental condition, and the related degree of brain activation was considered to reflect sensitiveness underlying personality traits. Participants were asked to perform emotional imagery for three conditions: pleasant, neutral, and unpleasant. Different datasets were considered to test replicability of results, which showed higher levels of slow activity in the Theta band for the impulsive subjects in all conditions. It is important to point out that extraversion, which is a secondary trait, is a combination of the primary traits impulsivity and sociability. Moreover broadly distributed Theta activity, especially in the posterior region of the head, seems to reflect low arousal levels. These evidences support the initial assumption.

Affective disposition linked to extroversion and neuroticism has also been related to frontal asymmetry of cortical activation. In this regard, anterior EEG asymmetry in resting conditions has been investigated considering the functional relation with the Behavioral Inhibition System (BIS) and the Behavioral Approach System (BAS), postulated in [63], which are neural systems reflecting the emotional response to positive or negative affects respectively. In [64] it has been speculated that each anterior brain hemisphere is functionally involved in one of these two neural systems. Therefore individual differences of asymmetrical anterior activity have been supposed to reflect different affective styles influenced by sensitivity of individual's BIS and BAS systems. Several studies on healthy subjects have shown the relationship between

affective style and anterior EEG asymmetry as observed in cortical activation patterns while experimenting emotions [65] or resting [66], and significant reliability and test-retest stability along time were observed.

The studies mentioned above support the evidence that different cortical areas participate in different functional processes. Furthermore, different frequency oscillations are involved in the integration of different kind of brain activity. The specificity of such functional processes and integration activity with respect to personality has been investigated. Individual specific time-varying patterns of the distribution of the EEG spectral power across the different scalp regions have been considered in order to study within- and between-subjects differences in brain functioning. In this regard spatial EEG asymmetries other than anterior patterns have been analyzed in order to understand their link with personality traits. In [67] some findings are given concerning the relationship linking Alpha and Theta activity gradient between frontal and posterior sites, with the sensitivity of the BIS and BAS emotion-based neural systems introduced above responsible for behavior regulation. In the experimental setup, images of facial expressions from a public database were presented sequentially and evaluated by participants during the EEG recording. Some correlation between personality variables, related to extroversion and neuroticism, and individual differences of the Antero-Posterior Spectral Power Gradient (APSPG) values was observed in all frequency bands. Specifically higher behavioral inhibition and lower sociability have been related to relatively higher oscillatory activity in frontal than in posterior regions, which could be explained by electrophysiological correlates of higher vigilance and emotional tension in introvert subjects. Disinhibited and sociable individuals showed opposite APSPG patterns. These empirical evidences together with results of source localization analysis, have been corroborated by theoretical considerations linking brain oscillations with emotion perception and processing mechanisms involving cingulate cortex. The analysis of the so called EEG microstates provides evidence of such relationships, revealing differences in cognitive styles and dispositions. EEG microstates describes rapid spontaneous reorganization of large scale neuronal activity, resulting from the integration of incoming information. For multichannel recordings, given the observed change of functional state at very high time resolution, EEG microstates represent quasi-stable configurations in the sequence of momentary potential maps, which display the topographic distribution of brain potentials ([68]). Different compositions of microstate classes reflect different processing strategies. In [69] differences between belivers and skeptics were addressed. The microstate syntax allowed the interpretation of cognitive processes typical of each personality group. Significant differences in lateralization of brain activity were observed, resulting in group-specific shifted gravity center of activity in specific frequency bands. Several other experimental evidences support the idea that individual characteristics of the EEG describing mental activation patterns reflect personality correlates.

Paper	Protocol	DB	Channels	Features	Classifier	Performance	sessions
Poulos et al. [70]	EC	4	1 (O2)	α spectrum	NN	GAR=80%-100% CRR=80%-95%	-
Poulos et al. [71]	EC	4	1 (O2)	AR (8th-12ve)	NN	GAR=72%-84%	-
Riera et al. [72]	EC	51	2 (FP1, FP2)	AR (100th)&DFT MuIn&COH.&CC	DA	EER=3.4%	4
Su et al. [73]	EC	40	1 (FP1)	PDS	k-NN	CRR=97.5%	2
Campisi et al. [74]	EC	48	3 (T7,Cz,T8)	AR	Poly. regr.	CRR=96.98%	1
La Rocca et al. [75]	EC	45	2, 3, 5	AR	Poly. regr.	CRR=98.73%	1
La Rocca et al. [49]	EC/EO	9	3, 5	AR	MMSE	CRR=100%	2
Abdullah et al. [76]	EC/EO	10	4	AR	NN	CRR=97%	5
Paranjape et al. [77]	EO	40	1 (P4)	AR (3rd-21st)	DA	GAR=49%-82%	1
Das et al. [78]	VEP	20	20 O	LDA	KNN	CRR=94%	1
Palaniappan and Mandic [79]	VEP	102	61	MUSIC	Elman NN	GAR=98.12%	1
Palaniappan [80]	VEP	20	61	SPR	BP NN	CRR=99.15%	1
Palaniappan [81]	Mental tasks	5	6 P	AR, PS, synch., entropy	Manhattan dist.	FRR==1.5-0% FAR=0%	5
Marcel and Millán [82]	MI	9	8 CP	GMM	MAP	HTER=8.1%-12.3%	3
	Word gen.	9	8 CP	GMM	MAP	HTER=12.1%	1
He and Wang [83]	Motion tasks	7	17	AR (7th) on ICA	NB	HTER=4.1%	1
Brigham and Vijaya Kumar [48]	SI	6	128	Burg's AR (2nd)	SVM.	GAR=99.76%	4
	VEP	120	64	Burg's AR (4th)	SVM	GAR=98.96%	1

TABLE 2.1: Overview of state of the art contributions using EEG signals as a biometrics.

2.2 EEG signal based recognition systems. State of the art

The use of brain activity as user identifier is suggested by its general role in controlling the functioning of the whole body, the cognitive processing and the response to external stimuli. In this regard memory mechanisms (experience), personality correlates and anatomo-physiological factors contribute generating individual specific traits.

Some promising results have been obtained employing different EEG acquisition protocols, involving both resting conditions with closed or open eyes, response to specific stimuli, like visual stimuli, and execution of real or imagined body movements.

Since the recognition performance of a biometric system in general, and of an EEG based system in particular, depends on a proper selection of the acquisition protocol, of the extracted features, and of the classification algorithm, in this Section the aforementioned issues will be considered to compare the state of the art EEG based biometric systems. Databases structures will also be taken into account.

2.2.1 Protocols

Some mental tasks are more appropriate to be performed for person recognition than others being intrinsically able to highlight distinctive traits of individuals. The analysis conducted

hereafter aims at pointing out which aspects of cognitive and mental functions are worth to be further investigated to effectively recognize users.

Several studies investigate EEG traits during brain ongoing activity (Section 1.2.1) for user recognition, which does not require any mental task at all. Specifically, in [70] a closed eyes in resting condition protocol was employed to acquire data using the O2 channel from the occipital region of the head (see Figure 1.1 for electrodes positioning on the scalp). The α rhythm, predominant in the parieto-occipital region during rest as discussed in Section 1.1, was obtained and overlapping subbands are individually considered for feature extraction. The tests performed were aimed at verifying four *authorized* users against a single class of *non-authorized* users, and at identifying them. The obtained classification scores in terms of genuine acceptance rate (GAR) ranged between 80% and 100% depending on the individual, the frequency band, and the test performed, while the correct recognition rate (CRR) related to the identification tests ranged between 80% and 96%. In general, different frequency bands showed to be more performant for different individuals. The same protocol was tested in [71]. A different analysis of the same rest EEG signals, briefly described in the next Section, yield to a GAR ranging from 72% to 84%. In [77] the EEG activity was recorded from 40 subjects while resting both with open eyes (EO) and with closed eyes (EC). Although eight sensors were employed for the acquisition, only the signals acquired using the channel P4, from the parietal region of the head, were considered in the study. An analysis was performed for user identification in the EO condition and GAR ranging from 49% to 82% depending on the modeling parameters was obtained. In [72] a closed eyes resting condition was used to acquire EEG signals from 51 subjects using two forehead electrodes (FP1 and FP2). Through discriminant analysis the best achieved result was an EER=3.4%. In [73] the influence of the diet and circadian effects on the identification performance was investigated. In the considered protocol, segments of 5 minutes EEG signals, acquired by an FP1 electrode, were recorded during rest with closed eyes. Signals were acquired on two separate days (sessions) in which subjects assumed water and coffee respectively. In each session, 6 EEG runs were recorded. A database of 40 subjects was collected. The classification accuracy achieved for subject identification was of 97.5%. In the same study an implementation of the Covert Warning (CW) concept to enhance the security of the EEG-based biometric system was presented. Muscle signals from clenching the teeth, shown to produce robust signals, were used to send the covert message. 24 volunteers were enrolled and performed 3 minutes of resting with closed eyes, while clenching the teeth 3 times. Authors showed that CW messages were detected perfectly, while a small amount of decrease in the identification performance with respect to the scenario without CW was observed. Abdullah et al. [76] collected signals from 10 subjects in 5 different sessions over two weeks, using 8 electrodes to obtain bipolar signals at C3, P3, C4, P4. In each session subjects performed resting state with closed eyes and open eyes, repeating each task in 5 runs of 30 seconds. Different spatial arrangements were evaluated in order to identify users using a suitable electrodes configuration. Best performance of

CRR=97% was obtained employing all 4 channels in the closed eyes condition, while configurations in the right hemisphere (C4, C4-P4) produced the highest CRR compared to the other arrangements relying on an equal number of electrodes. Such result was in accordance with the significant role of the right hemisphere, involved in processes like imagination, creativity and feeling, which are dominant during resting. This supports the idea that brain activity detected in the right hemisphere shows distinctive information during rest. Brain ongoing activity in EC condition was investigated in [74] for user identification. EEG signals were recorded from 48 subjects employing 56 scalp electrodes. An analysis on suitable scalp configurations was carried out considering different sets of symmetrically placed electrodes. Signals filtered in the range $[0, 33]$Hz were analyzed, and a best CRR=96.98% was obtained considering channels T7, Cz, T8. In [75] signals from 45 subjects in EC resting conditions, acquired through 56 electrodes, were analyzed. Signals were filtered in order to extract the main brain rhythms related to the resting condition ($\delta, \theta, \alpha, \beta$), so that the different frequency bands were individually analyzed, as well as combined together. Different channel configurations were considered to perform user identification and a best CRR=98.73% was obtained from a set of 3 parieto-occipital channels. A comparison between EC and EO condition for user identification was carried out in [49] on a smaller dataset. Longitudinal recordings allowed addressing the repeatability of EEG features, which is a very important issue for the application of biometric systems in real life scenarios. A perfect identification of users enrolled in a previous acquisition session was obtained for the EC condition considering the subband $[0.5, 30]$Hz and a set of 3 electrodes placed in the posterior part of the head. An extensive analysis was here performed in order to find the most appropriate set of parameters involved in the signal processing.

Other studies on EEG biometrics address the analysis of brain activity recorded during the performance of different tasks, involving real or imagined motion, imagined speech, response to visual stimuli and mental calculation. In particular in [83] data were acquired meanwhile 7 subjects performed motion related tasks. It consisted of the interaction with a virtual environment by blocking virtual target balls rapidly approaching the subject. Each subject performed five runs in one acquisition session. Seventeen channels have been employed, clustered into 5 groups according to their physical position. Specifically, the regions right fronto-polar, left fronto-polar, central, right parieto-occipital and left parieto-occipital were individually considered for feature extraction. A HTER=4.1% was achieved, averaging over all subjects and runs, and employing all acquisition channels. Marcel et al. [82] proposed a person authentication system based on EEG recorded during imagination tasks, such as imagination of left and right hand movements, as well as during the generation of words beginning with the same random letter. The employed dataset was composed of 9 enrolled subjects and eight centro-parietal recording channels, specifically C3, Cz, C4, CP1, CP2, P3, Pz, and P4, most of them from the sensory-motor region of the scalp (Section 1.2.2). Each subject performed three recording

sessions on different days, and four 4-minute runs per session, where the three tasks were sequentially proposed each lasting 15 seconds. The signals were preprocessed by retaining the band 8-30 Hz, which contain μ, β and γ rhythms involved in the activation of the primary sensory-motor area during movement and imagination movement (Section 1.2.2). A surface Laplacian (SL) spatial filter was also applied for a better representation of the local sources below the electrodes. HTER performance of 6.6% was achieved for left hand task considering 3 subjects and runs of the first day, while HTER ranging from 19.3% to 36.2% was obtained for the same task considering training/validation and evaluation on different days. Best results ranging from HTER=8.1% to HTER=12.3% were achieved for the evaluation sets of days 2 and 3, respectively, performing incremental learning. Authors showed that the left hand task was the best suited on the database under analysis for person authentication and that using training data over different days improved performance. Brigham et al. [48] proposed a subject identification system relying on two different EEG datasets. One contained VEP responses to visual stimuli, and was collected through 64 channels while showing black and white images of objects to 120 subjects with a number of trials per subject ranging from 30 to 120. The other one contained imagined speech EEG data collected using 128 channels, from 6 volunteers who imagined speaking the two syllables /ba/ and /ku/ with no semantic meaning. These latter data were recorded in separate sessions, each comprising 20 trials for each of six conditions (runs), represented by different rhythms of the covertly spoken syllable. The so obtained data were preprocessed for artifact removal. For the imagined speech data, frequency filtering in the range of 4 to 25 was performed to remove electromyographic noise. A best GAR=99.76% was achieved on 6 subjects for the case of imagined speech, whereas a GAR=98.96% was obtained on 120 subjects for the VEP case. In this work the authors also observed that the classification performance does not change much when using only one rhythm or one syllable. Also Das et al. [78] used VEP data for person identification. EEG signals were collected from 20 subjects, by means of a 64 electrodes montage, during a difficult visual perceptual task in which filtered noise is added to the visual stimuli. Face and car images were sequentially presented to users as stimuli which appeared each for 40 milliseconds, after which subjects had to identify the category of the stimulus, either car or face. 1000 trials split into runs of 200 trials were presented to each subject. A subset of 20 electrodes placed in the occipital region of the head, over the visual cortex (Section 1.2.2) was selected after investigating statistical informative contribution in the spatial domain, which resulted in accordance with the experimental setup (Section 1.2.1). The same analysis showed the period $[120 - 200]ms$ after the stimulus to be the most informative with respect to discrimination between individuals, which is consistent with the latency of the visual cortex activation in visual attention tasks. Authors used the pre-stimulus and post-stimulus EEG data to discriminate between individual's neural response, obtaining classification rates ranging from 75% to 94% for the best performant post-stimulus set, which showed VEP dynamics to play a crucial role in person identification. Also Palaniappan [80] investigated VEP signals for individual identification purpose. VEP data were recorded from 20 subjects exposed

to single stimuli, which were pictures of common objects represented through black and white line drawings, easily recognizable by all the individuals. EEG measurements were taken for 1 second from 64 electrodes. Significant differences were investigated through ANOVA tests on each channel. A high classification accuracy of CRR=99.06% was obtained in this study employing all 61 channels. In another study by Palaniappan and Mandic [79] a similar protocol was employed, and 300 milliseconds VEP stimuli consisting in showing black and white drawings of common objects were used to collect EEG signals. Here a mental task consisting in recognizing and remembering shown objects was proposed. A database of 102 subjects was used and signals from 61 channels were recorded, for a total of 3560 VEP signals stored. EEG signals were filtered through a $25-56$Hz pass band filter, to retain the the γ rhythm containing the dominant frequencies within the VEP signals spectrum, which are related to perception and memory evoked when visualizing a picture. A CAR spatial filter was also applied to reduce the observed intra-class variance due to scale factors of γ band energies. A GAR of 98.12% was reached using all channels. Authors argued that the high classification result over a such large dataset could be due to the different properties of the binding process during stimulus perception and recognition for different subjects. This is in accordance with the evidence that the brain function underlying VEP generation seems to be genetically influenced [84], resulting in different levels of perception and memory between individuals.

In [81] Palaniappan also proposed a user authentication system using mental task EEG data, collected from 5 subjects and publicly available [1]. The mental tasks consisted of baseline where the subject was at rest, visual counting, geometric figure rotation, mental multiplication, and mental letter composing. These tasks were chosen since they involve hemispheric brain wave asymmetry, which was exploited for individual recognition, among other traits briefly discussed in the next section. EEG signals were recorded from the posterior part of the head on positions C3, C4, P3, P4, O1 and O2. For each mental task 10 runs lasting 10 seconds were collected for each subject within each of the different acquisition sessions performed on different days. Each mental task run was segmented into 0.5 seconds segments to increase the sample size. EEG segments were filtered using a common average referencing (CAR) filter, which consists in subtracting the mean of the entire electrode montage (i.e.the common average) from channels of interest at any one instant, and mean value was removed from each channel. Authentication was subsequently performed for each mental task separately. The obtained FRR ranged from 1.5% to 0%, while the FAR was 0% for all 5 subjects.

The results reported above have to be thoroughly evaluated and compared also considering the features extracted, the complexity of the classification algorithms employed and specially the database structures used for training and testing the classifiers. In this regards some considerations are reported below.

[1] http://www.cs.colostate.edu/eeg/main/data/1989_Keirn_and_Aunon

2.2.2 Features

The proper selection of representative and stable features from an acquired biometric signal is a key step in a recognition problem. When dealing with EEG signals, specific features of the brain activity either during resting or specific mental tasks have shown to have different degrees of distinctiveness among people.

EEG features extraction has been performed in different domains like the time domain, as well as the time-spatial or the frequency domain. Among those we can recall autoregressive (AR) coefficients, power spectrum density (PSD) function, energy of the signal, autocorrelation function, latency and area of characteristic peaks.

Coefficients from AR stochastic modeling, which characterize the power spectral density function of EEG signals, are employed as features in most of the works on EEG biometrics. Some of them rely on resting state condition. The Burg's method was employed in [74], [75] and [49] to extract the reflection coefficients from the data AR model fitting. Feature vectors were obtained concatenating the coefficients extracted from different sets of electrodes. Different analysis on the extracted features *vs* the brain rhythms were performed in [74] and [75] were 6-th and 12-th model orders were selected respectively to obtain the coefficients assorting the feature vectors. The repeatability of the obtained EEG features was furthermore addressed in [75], where a 10-th model order was adopted to fit the dataset and extract reflection coefficients. In [76] AR coefficients of order ranging in $[3 \div 21]$ were considered as features representing EO and EC resting signals, recorded with a sampling frequency of 256Hz. The best performing model order, namely $p = 21$, was empirically selected and feature vectors composed of 21 concatenated AR coefficients were obtained from single channels or their combinations.

AR features were also employed in [77] were resting EEG signals were acquired. Specifically, Lattice Equivalent Model and Levinson Recursion were employed to extract AR models from EEG traces sampled at 120Hz, and model orders ranging in $[3 \div 21]$ were tested. Only coefficients from the P4 electrode were used to assort the feature vectors. Authors observed that the discriminant power of the features improved as the model order increased up to 21. Also in [72] the EEG signals recorded during EC rest are modelled through an AR model. AR coefficients as well as other features extracted from both single channel measures and synchronicity measures between the only two forehead channels used FP1, FP2 were tested for user recognition. Signal processing consisting in EEG sampling at 256Hz, filtering in the band $[0.5, 70]$Hz, and application of a notch filter at 50Hz was performed. Both single channel and inter-channels features were tested. Specifically for the first category AR coefficients of an 100 order model and discrete Fourier transform retaining the band $[1, 40]$Hz were considered, whereas for the second category features included mutual information (MuIn), spectral coherence (COH) and cross-correlation (CC) measures obtained for the channel pair analyzed. All features were tested separately, and

later merged at the decision level, as described in Section 2.2.4. In [71] AR coefficients were extracted from the α rhythm contained in EEG signals which were recorded during EC rest, employing a bipolar measure of voltage between leads O2 and CZ. Signals sampled at 128Hz were modelled through 8 AR coefficients used as features for the authentication of four subjects. In [83] EEG data related to motion in a virtual environment were modelled through independent component analysis (ICA). The 17 acquisition channels provided signals downsampled at 125Hz clustered into 5 brain regions. ICA was performed for each scalp region separately, thus selecting the most energetic component for each region as a feature. AR modeling, with order equal to seven, was then performed on each of the selected components thus obtaining the feature vectors tested for person authentication. Different features, concatenated in a unique vector composed of 126 elements, were tested in [81] for subject authentication during thought activity. Six AR coefficients were extracted using the Burg's method from the signals acquired through the 6 employed channels, and sampled at 250Hz. Moreover, channel spectral power values in the frequency bands α, β and γ were provided thus obtaining 18 features more. Other 27 features were collected computing inter-hemispheric channel spectral power differences in the same spectral bands. The so called inter-hemispheric channel linear complexity, which accounts for the amount of spatial synchronization between channels, was also computed for each band providing 27 other features. Finally six approximate entropy values for each band, quantifying non-linear complexity, were also considered to assort the total feature vectors. Principal component analysis was then used to reduce feature size in the classification problem. Other works on EEG-based biometrics consider feature vectors composed of spectral values only, to represent inter-subject variability. Some characteristics of the EEG spectrum carry genetic information as well as personality correlates as described in Sections 2.1.7.1 and 2.1.7.2. Paulos et al. in [70] used the spectrum of the EEG signal in the α rhythm frequency band to provide feature vectors. The α rhythm, extracted from single channel EEG acquired in resting conditions, was further partitioned into three 3Hz overlapping subbands, each containing 540 spectral values, which were separately considered to solve the authentication and identification problems. Also Su et al. [73] tested PSD values as distinctive features of single channel EEG signals acquired in resting conditions, for the implementation of a biometric-based covert warning system. PSD was computes via Burg's method, and the spectral content in the range $[5, 32]$Hz was retained to generate the feature vectors, thereby removing high and low frequency noise. In [82] extracted PSD values in the frequency range $[8, 30]$Hz from 8-channels EEG signals, acquired during task performance related to motor imagery (MI) and generation of words, were considered. Electrodes and frequency band were chosen according to evidences from BCI research on the detection of the relevant information for the mental tasks considered. PSD was estimated every $62.5ms$ using windows of one second, through the Welch periodogram algorithm, obtaining a resolution of 2Hz in the range $[8, 30]$Hz. PSD values, normalized to the total energy, computed for the 8 employed channels, were concatenated so that a 96-dimensional feature vector, 8 channels $\times$ 12 frequency components, was obtained for each one second EEG sample.

Other contributions, still using features from the power spectrum of EEG signals, propose further processing to extract distinctive traits in the frequency domain. For example in [80] the estimation of γ band spectral power ratio values from each of the 61 channels employed to record VEP signals was proposed. Values from all channels were concatenated to form the feature vector for each of the 40 VEP trials for each subject. A one-way ANOVA test was employed to infer about the significance of the differences between the features extracted from all the subjects, and significant differences were observed for all the channels. Spectral features from VEP signals, filtered in the band $[25, 56]$Hz, were also extracted in [79]. Multiple Signal Classification (MUSIC) algorithm was used to estimate dominant frequency and power content, based on the eigen-decomposition of the data correlation matrix. Unique descriptors of person's brain activity and dimensionality reduction were obtained from the performed MUSIC based spectral analysis of the VEP signals in the γ band. The dominant powers within the MUSIC spectrogram extracted from each of the 61 employed channel, and normalized with respect to the total power from all channels, were concatenated into a unique feature vector. The so obtained VEP biometrics were used for subject identification. A different approach was adopted in [78], where the linear discriminant analysis' (LDA) coefficients, based on the Fisher's criterion, were extracted from EEG recordings and employed to study spatio-temporal patterns encoding discriminative information in VEP signals. More in details, after the so called "Fisher-brains" analysis, employed to select the most informative electrodes location and time interval to analyze, feature extraction was performed by projecting EEG data into the space generated by the Fisher's LDA coefficient matrix. Features from the $200ms$ pre-stimulus and $500ms$ post-stimulus EEG data were tested for person identification.

2.2.3 Database structure

As previously pointed out, for the purpose of biometric user recognition, a proper structure of the dataset under analysis is needed to evaluate the system's recognition accuracy. The dataset size, including the number of subjects and trials performed, the cross-validation framework provided and above all, the number and temporal distance of recording sessions performed are key elements that must be considered in the recognition pipeline.

Due to the difficulties of collecting EEG longitudinal recordings, EEG databases specifically acquired for biometric recognition purposes, are not publicly available. In fact the different studies discussed so far tested the implemented techniques on a variety of different datasets, some of them proprietary, showing different characteristics as reported in Table 4.1 and extensively discussed in Section 2.2.1. Most of the datasets used to investigate usability of EEG for biometric recognition are collected in different frameworks than the biometric one, mainly within the BCI context. Moreover some of these studies consider different acquisition sessions, performed on

Paper	Subjects	Trials per subject	Acquisition sessions	Training Classification	Cross Validation (CV)
Poulos et al. [70]	4 gen. 75 imp.	45 1	1	25 training 20 classification	n.a.
Das et al. [78]	20	1000	1	n.a.	10 10-fold runs
Palaniappan [80]	20	40	1	50% training 50% classification	10 10-fold runs
Palaniappan et al.[79]	102	10 to 50	1	90% training 10% classification	10 10-fold runs
He et al. [83]	7	11 per task (5 tasks)	1	10 frames for client training 1 frame for client class. 66 frames for impostor class.	leave-one-out all combinations
Paranjape [77]	40	8	1	50% training 50% classification	n.a.
Campisi et al. [74]	48	20	1	70% training 30% classification	50 runs
La Rocca et al.[75]	45	77	1	2/3 training 1/3 classification	77 runs on different partitions
Su et al. [73]	40	6 per session	2 over 2 days	50% training 50% classification	100 hold-out runs
Abdullah et al. [76]	10	11 per session per task (5)	5 over 2 weeks	90% training 10% classification	10 runs on different partitions
Palaniappan et al.[81]	5	10	5 over 5 days	50% training 50% classification	4 4-fold runs modified
Riera et al.[72]	51	12	4 over 34-76 days	training/classification on different days	8 different runs for gen./imp. tests
Marcel et al.[82]	6 gen. 3 impostors	4 per session per task (3)	3 over 3 days	training/classification on different day	n.a.
Brigham et al.[48]	6	20 per exp. (6)	4 over 3 days	training/classification on different days 25% training 75% classification	4 runs combining sessions 4 4-fold runs
La Rocca et al.[49]	9	237 per session	2 over 3 weeks	training/classification on different days	230 runs on different partitions

TABLE 2.2: Dataset characteristics

different days, while most of them present user recognition based on a single acquisition session for each user performing different runs of the same experiment, as described in the following.

In [71] and [70] a dataset of 255 EEG recordings is provided. Specifically, 4 genuine subjects and 75 impostors have been considered. For each of the 4 subjects, 45 EEG recordings, each lasting 3 minutes, have been acquired. One EEG recording has been rather acquired for each of the 75 impostors, thus obtaining a total of 255 EEG signals ($75 + 4 \times 45 = 255$). For each genuine subject 25 recordings were used for the training, while the remaining 20 for test. No cross-validation framework was provided and no information is given about recording sessions.

The dataset employed in [78] was collected from 20 subjects participating in the study. For each of them 1000 trials split into 5 runs of 200 trials were recorded on a single session. A 10-fold cross-validation scheme was implemented for the evaluation of the system's performance, and 10 independent cross-validation runs were executed to estimate classification rates. The dataset used in [80] to perform individual identification contained signals from 20 subjects, with 40 VEP trials per subject recorded on a single session. Therefore, a total of 800 trials assorted the

dataset under analysis. Half of them were used for training and the remaining half for testing, within 10 runs of a 10-fold cross validation scheme. A larger VEP dataset was used in [79], where 102 subjects were recruited for the study. A total of 3560 trials, from a minimum of 10 to a maximum of 50 blink free trials per subject, were collected during one session. Again a 10-fold cross-validation scheme was executed 10 times to statistically evaluate performance. Specifically, training was done using nine sets of feature vectors, while the remaining set was used for classification. This process was repeated 10 times, using each time nine different sets of feature vectors for training. For the authentication experiment proposed in [83] authors used data collected from 7 subjects performing 5 tasks. For each subject and each task 11 trials were recorded in one acquisition session, so that a total number of $7 \times 11 = 77$ frames per task assorted the analyzed dataset. A leave-one-out cross-validation approach is employed to evaluate performance. For a given subject ten of the eleven trials are used for training and the remaining one for testing. The trials from the other 6 subjects are used to build a set of impostors' trials. EEG data collected from 40 subjects were used in [77] to study subject identification. Each subject provided about 8 trials of 8.5 seconds during one acquisition session, hence a dataset composed of 349 frames was obtained for the analysis. 50% of frames were used to train the classifier while the remaining 50% to perform identification tests. In [74] a dataset composed of 48 subjects, each of them performing one acquisition session, has been collected. Each EEG signal had a 60 seconds duration and was segmented into frames of 3 seconds duration so that 20 feature vectors were extracted for each user and 50 independent cross-validation runs were performed to test identification accuracy, considering different frames for the training and for the test. A similar framework was proposed in [75], for a dataset composed of 45 subjects who underwent one acquisition session. Three second overlapping frames were extracted from 60 seconds recordings, in order to increase the sample size for training and test, thus obtaining 77 frames for each subject. Non-overlapping frames between the training (2/3 of the total number of frames) and the test (1/3 of the total number of frames) datasets were considered for the solution of the recognition problem within a cross-validation framework. 77 cross-validation runs were provided considering 77 different partitions of the dataset into subsets of subsequent training and test frames.

All the aforementioned papers do not allow to infer about repeatability and stability of EEG features which on the other hand represent properties of paramount importance for deploying an EEG-based biometric system in real life. Furthermore, although in some referred works, different acquisition sessions have been provided, they were considered to assort a single dataset, where randomly selected EEG segments were used for training and testing a classification algorithm for the recognition purpose. In [73] the tested dataset was composed of 40 subjects whose signals were recorded on two separate days. In each session 6 runs were performed by each user at different time points. Therefore the dataset comprised 480 EEG recordings ($40 \times 2 \times 6 = 480$) in total. Within the considered cross-validation framework half of the 12 recordings for each

subject was randomly selected and used to train the classifier, while the remaining half was employed to test the recognition accuracy. This process was repeated 100 times, and the average performance was given, losing information on the different sessions. Also in [76] EEG signals from 10 subjects were recorded in 5 separated sessions over 2 weeks. In each session 5 different runs were provided for each task, and 11 trials per task were repeatedly performed, so that a dataset composed of 275 EEG frames for each user ($11 \times 5 \times 5 = 275$) was obtained. The collected dataset was randomly divided into training and testing subsets, considering 90% and 10% of the whole data respectively, shuffling signals recorded on different sessions. 10 cross-validation runs were provided for the system's performance evaluation, considering 10 different partitions. In [81] the dataset analyzed was composed of EEG signals recorded from 5 subjects performing 10 runs for each of the proposed mental tasks, performed on 5 different single day sessions. For each subject 200 EEG segments (trials) were extracted from all the recordings related to each mental task. In the proposed recognition framework for each subject data were split into 50 randomly selected frames for training, 50 different randomly selected frames for validation and the remaining 100 frames for authentication tests. The performance was provided within a modified 4-fold cross-validation framework times to increase the reliability of the results.

Only few works test distinctiveness of EEG features for user recognition considering different acquisition sessions performed on different days for the training and the test stages separately. Riera et al. [72] tested 51 subjects, who underwent 4 different recording sessions within 34-74 days, and 36 subjects recorded just once who represented the group of intruders to be revealed. A cross-validation framework is here provided for the identification experiment, where for each of the 51 subjects 3 takes related to 3 different days are used for the training, while the remaining recording session is used for the test. For each take the first or the second minute EEG segment is considered for the training. The process was repeated for all combinations of sessions and EEG segments. In [82] the analyzed dataset contains data from 9 subjects recorded during 3 different sessions over 3 days. Each session comprises 4 runs lasting 4 minutes, which are split into 3 frames, each containing a 15 second EEG segment, related to a given mental task. Hence, the entire dataset is composed of $9 \times 3 \times 4 = 108$ frames per task used to solve the classification problem. In some of the performed experiments sessions from different days are separately considered to assort the training and the evaluation subsets. In particular in one of the experimental protocols, 3 subjects are considered as impostors and the remaining 6 as clients. Two runs from the first day were used to train the classifier on genuine users, and one different run from the same day was considered to validate the model. The last run from the first day and all runs from the second and the third days, were considered to evaluate the classification performance separately on days 1, 2 and 3. In another protocol half of the day 1 runs and half of the day 2 runs were used for client training, the remaining runs from the same days were used to validate the model, and all runs from the day 3 session were used for performance evaluation.

Finally authors tested incremental learning provided employing the first run of each session for incremental client training, and considering the remaining runs for client/impostor evaluation. This allowed to evaluate the accuracy of the system while enrolling subjects during a day, and performing recognition tests on subsequent days. In this case a degradation in performance was observed by the authors, compared to cases where training and test subsets belonged to the same day. In fact, referring to the proposed framework, they claimed that data collected only over one day is not enough for training robust models. One of the datasets analyzed in [48], related to speech imagery, contained data from 6 subjects whose signals were recorded over separated sessions, each composed of 20 trials for each of the performed experiments. A total number of 3787 trials were used in the analysis, including all 6 experiments. A 4-fold cross-validation framework was provided to evaluate performance, and 10 runs were executed keeping training and test sets distinct. In one of the performed tests data recorded on 2 different days assorted the training and test datasets, and all combinations of sessions were considered: day i to train the classifier and day j to evaluate performance, with $i \neq j$, i,j=1,...,4. Considering the obtained results, authors could observe that the tested features representing speech imagery EEG data are most likely not fully stationary with respect to time. Finally, in [49] and [85] the dataset analyzed contained signals recorded during two different acquisition sessions performed on different days, from 1 to 3 weeks apart depending on the subject. 9 subjects performing resting state were enrolled in this longitudinal study. EEG signals of duration of 60 seconds were segmented into frames of 1 second, with an overlap factor of 75%, thus obtaining a number of 237 frames for each subject and each of the two temporally separated recording sessions. Therefore, for the solution of the recognition problem frames for the training and for the recognition datasets have been obtained from two different acquisition sessions in order to infer about the repeatability of the EEG features over the considered interval, for the acquired dataset. Performance evaluation is provided within a cross-validation framework, obtained selecting for each user 75% of feature vectors related to cyclically subsequent training frames, while 75% from subsequent test frames. Moreover, within the cross-validation framework, classification results were reported separately considering the two combinations obtained training on day i and performing recognition tests on day j, with $i \neq j$, $i, j = 1, 2$.

2.2.4 Classification algorithms

The efficiency of the classification algorithms employed for user biometric recognition based on EEG depends on the specific distribution of the observed vectors in the feature space. In fact, for a proper solution of the classification problem it is important to use a suitable classifier fitting the scattering distributions generated by the different classes to distinguish among. Different machine learning algorithms present specific capabilities in approximating different boundary surfaces between the actual decision regions in the feature space, representing the classification

problem. The most commonly employed algorithms used in literature for EEG biometrics are based on Neural Networks (NNs), suitable in the classification of data not linearly separable in the feature space. Several architectures of NN based classifier have been proposed in the published studies, with different numbers of nodes for each of the considered layers, and different training functions, such as the scaled-conjugate training function [76], the back propagation algorithm [80], [79], the Kohonen's Liner Vector Quantizer [71], [70].

Some other works rely on the use of the k-Nearest Neighbor (KNN) classifier, based on different distance measure techniques [79], [73], [78]. Also Discriminant Analysis based on different linear and non-linear discriminant functions have been exploited for the solution of the recognition problem based on EEG [73], [77] [72]. In [48] a support vector machine classifier with a linear kernel to identify subjects based on EEG features was used. Other employed classification algorithms can be found in [82], [81], and [83]. In [82] Maximum a Posteriori training was employed to adapt a generic model to a client-dependent model. In [81] the Manhattan distances between feature vectors from training and from validation datasets were computed, in order to implement a two-stage biometric authentication method. It was based on the computation of threshold values used to improve accuracy in the classification of the test dataset, in terms of reduction of FAR and FRR respectively. Polynomial regression has been employed in [74] and [75] where different expansion degree values were tested, while the MMSE criterion was used in [49] to perform a linear classification. A naive Bayes approach was adopted in [83] to probabilistically model the observed feature vectors, assuming gaussian distribution and statistical independence of elements from the generic feature vector.

2.3 Research directions

As outlined in the previous Sections, EEG biometrics poses several new challenges to be tackled by researchers. Many issues are shared also by other biometrics, but many others are peculiar of EEG based systems. For example permanence and uniqueness are two basic requirements that need to be well analyzed for each candidate biometrics to be employed in actual systems. However, when dealing with EEG biometrics, the target brain responses need to be elicited using some specific protocols, ranging from resting state to imagined movements to speech imagery and so forth. This variety of elicitation methods has not equals within the biometric field and, with the exception of the resting state condition which has been deeply analyzed mainly in the neurophysiology area, they have not been received the necessary attention from the biometric scientific community. Therefore, permanence and uniqueness need to be analyzed with respect to the protocol employed and also with respect to the extracted features which of course posses different levels of permanence and uniqueness. It is worth pointing out that, the elicitation methodology is just one aspect of the protocol definition. For example, electrodes positioning

and number need to be optimized and of course this is dependent on the employed elicitation mechanism. Despite the several advantages of EEG biometrics, already listed in the previous Sections, against conventional biometrics, the major obstacle towards the deployment of EEG based biometric systems is mainly related to the inconvenient acquisition setup for users, consisting of a number of electrodes placed on the scalp, usually employed with conductive gel to reduce skin impedance. Therefore, the minimization of the number of employed electrodes is a crucial issue that needs to be tackled in order to improve user's quality of experience. However, some EEG based products, mainly for entertainment purposes, which employ only few electrodes, have already been commercialized. Although, they are not implementing any biometric system, they can be seen as a proof of concept that the electrodes number can be reduced. Moreover, recently, dry electrodes, not requiring any conductive gel have been introduced in the market. Their use would alleviate the user inconvenience with no degradation of performance but at an increasing cost price. Therefore, improvements in EEG signal acquisition and technological advances in sensor design, which could dramatically improve the system usability, need to be addressed by researchers in order to outline some guidelines for practical system implementation which could trigger attention from industry, and which can be a reference to lead future research towards feasible EEG biometric systems. Some developments in this regard have been presented in [86] where some prototypal contactless electrodes, that is not requiring any electric contact with the scalp, made of flexible polymeric material have been proposed. Also the reduction of the acquisition session length as well as the relaxation of the acquisition conditions are important research lines that need to be addressed by researchers. Specifically, EEG signals are usually acquired in dim lit rooms where no external visual or audio stimuli are present. Of course this is not a realistic condition for systems that need to operate in un unprotected environment. However, some attempts to use EEG based systems, in real life conditions have been already taken into account as in [87] where single trial EEG signal collection in outdoor walking for brain computer interface purpose has been addressed, or as in [88] where a mobile based scenario, employing low cost acquisition devices, is considered for EEG based recognition systems. Public databases, collecting data using different acquisition protocols, are strongly needed. Only few, collected for other purposes rather than biometric recognition, are available. The spoofing issue is an open research topic. At the present stage of research, no attempts to spoof EEG based recognition systems have been documented in literature. A thoughtful analysis on possible spoofing methodologies could help in either corroborating or criticize the statement that EEG based systems are more secure than systems based on other biometrics at least at the sensor level.

The review study reported in this chapter has lead to a survey contribution published in an international journal [89].

Chapter 3

EEG Feature Engineering

Most of the approaches adopted in neuroimaging signal processing focus on feature engineering, that is the extraction of significant and distinctive features from the signals, for a compact and efficient representation of the measured brain activity related to the task or mental state under analysis.

The employed methods can involve parametric or non-parametric representation of data, whose convenience depends on *a priori* knowledge of the properties of signals, and on the needs of compactness.

In this chapter the main feature engineering approaches investigated within the present work for biometric recognition purpose will be reported, making distinction between parametric and non-parametric analyses. For each method the related results obtained and published as scientific research contributions will be shown and discussed.

A preliminary section on the general description of the employed datasets and the pre-pocessing steps performed before the analysis is also reported. Since different analyses have been conducted on different datasets, reference is made to the particular publications for further details on signal acquisition and data structure, beyond the aim of this work.

Eventually, an insight is also given on a performed study employing spectral non-parametric feature extraction in the context of brain activity correlates of efficient language comprehension and processing.

3.1 Dataset and Preprocessing

The different approaches developed and adopted within the herein presented doctoral thesis work have been tested on different datasets mainly acquired within Brain Computer Interface

contexts. Some of them are publicly available [90], while some others have been collected by expert technicians in equipped laboratories [75] and shared with our research group within a cross-disciplinary collaboration. The acquisition of our own dataset designed for the specific requirements of EEG biometric recognition purposes is detailed in Chapter 4, and the related analyses are reported in Chapter 5.

As discussed in Section 2.2.1 EEG signals can be recorded during the performance of different sensory, motion, concentration and cognitive tasks, or during specific mental states. Among these acquisition protocols a particular interest has been shown for the study of the brain ongoing activity (i.e. spontaneous brain activity at rest) for biometric recognition purpose.

This interest is mainly due to the early evidence of the influence of personality and genetic factors on specific features of brain activity at rest as measured by resting state EEG (see Sections 2.1.7.2 and 2.1.7.1 for references). Moreover brain ongoing activity is likely to reflect mechanisms like self-perception and other inner processes that are supposed to show individual-specific aspects.

Guided by the mentioned reasons, the investigation that we carried out in the context of EEG-based biometric recognition have focused on the analysis of datasets recorded in resting state (RS) condition with both eyes closed (EC) and open (EO). In general, the enrolled subjects have been asked to sit on a chair in a dim lit room and to rest for few minutes (T in the range of $[1, 4]min$) remaining awake, avoiding focusing and concentration. During the eyes open RS condition the subjects are asked to fix a green cross on a black screen in order to reduce artifacts due to eyes movement.

While subjects were at rest EEG signals have been recorded through medical systems, employing sensor headset spanning the whole scalp at different spatial resolution. In all acquisition sessions conductive gel have been also used to keep the skin-contact impedance low to $10k\Omega$.

For further details on the analyzed datasets (e.g. number of subjects N, duration of each recording I (Number of time samples), number of acquisition sensors N_{ch}, etc.) reference is made to the specific contributions reported in the next sections.

Before extracting features to represent EEG signals, a preprocessing is generally carried out on the data to improve the SNR. As a first step, a common average referencing (CAR) filter is applied to signals according to the formula:

$$v_{i,t}^{(k)} = V_{i,t}^{(k)} - \frac{1}{N_{ch}} \sum_{j=1}^{N_{ch}} V_{i,t}^{(j)}, \tag{3.1}$$

where $V_{i,t}^{(j)}$ is the potential between the j-th electrode and the reference electrode, $j = 1, \ldots, N_{ch}$ (number of channels), $t = 1, \ldots, I$ (number of time samples), $i = 1, \ldots, N$ (number of subjects). Such spatial filter is employed to reduce artifacts related to inappropriate reference choices in monopolar recordings or not expected reference variations [91], providing nearly reference-free EEG recordings. This procedure functions as an high-pass spatial filter, and results in an increased SNR [92] reducing components that are present in most of the montage, especially when the reference is not external to the neurophysiological system, like in this case (see Section 4.1.2).

Data are subsequently downsampled after applying a proper anti-aliasing low-pass filter. A pass-band filter is also applied to retain spectral components contained in the main EEG rhythms of interest for the resting state (see specific contribution referred within the description of the results for further details).

A z-score normalization is typically applied to the signals to reduce variations between recordings due to scale factors:

$$x_{i,t} = \frac{v_{i,t} - E\left[v_i\right]}{\sigma_{v_i}}$$

where $E\left[v_i\right]$ is the espected value for v_i, and σ_{v_i} its standard deviation, replaced by sample estimates.

The so obtained signals are typically windowed generating T consecutive (eventually overlapping) frames of few seconds (up to $3s$). For resting state recordings these epochs are considered as different observations of the same mental state. In order to extract features the EEG signals are further processed accordingly to the model employed.

3.2 Parametric Features

3.2.1 Auto Regressive Stochastic Modeling

One of the parametric approaches adopted in the herein presented work of doctoral thesis for the representation of the data is the Auto-Regressive (AR) stochastic modeling, widely employed in EEG signal processing to provide parametric estimations of signal power spectra. According to this method, each frame τ, whit $\tau = 1, \ldots, T$, is modeled as an AR stochastic process, that is as the output of an all-poles filter receiving at its input a white noise process. A realization x_t of an AR process obeys to the following recursion:

$$x_t = -\sum_{q=1}^{Q} a_{Q,q} \cdot x_{t-q} + w_t$$

where w_t is a realization of a white noise process with variance σ_Q^2, and $a_{Q,q}$ are the regression coefficients of the model of order Q. They form the denominator of the all-poles filter of the model (see Figure 3.1), whose transfer function is:

$$H(z) = 1/\left(1 + \sum_{q=1}^{Q} a_{Q,q} z^{-q}\right)$$

The regression coefficients can be obtained solving the system of Yule-Walker equations that for causal processes can be expressed as:

$$R_{x,m} = -\sum_{q=1} Q\dot{a}_{Q,q} R_{x,m-q} + \sigma_Q^2 \delta_m, m = 0, \ldots, Q$$

The so-called Levinson recursion is a recursive approach to solve the Yule-Walker equations, obtaining the AR coefficients of increasing order

$$a_{Q,q} = a_{Q-1,q} - K_Q \cdot a_{Q-1,Q-q}, Q = 1, \ldots, Q-1$$

$$\sigma_Q^2 = \sigma_{Q-1}^2 \cdot 1 - K_Q^2$$

The factor K_Q is the so-called *reflection coefficient* of order Q, expressed as a function of the auto-correlation sequence $R_{x,m}$ of x_t.

$$K_Q = -\left(R_{x,Q} + \sum_{q=1}^{Q-1} R_{x,q} \cdot a_{Q-1,Q-q}\right) / \sigma_{Q-1}^2$$

There are several methods to estimate the sequence of reflection coefficients [93] when $R_{x,m}$ is not known. The Burg method [94] estimates Kq, for $q = 1, \ldots, Q$, operating directly on the observed data x_n rather than estimating the auto-correlation samples $R_{x,m}$. Given the forward and backward linear prediction estimates

$$\hat{x}_t = -\sum_{q=1}^{Q} a_{Q,q} \cdot x_{t-q}$$

$$\hat{x}_{t-Q} = -\sum_{q=1}^{Q} a_{Q,q}^* \cdot x_{t-Q+q}$$

the problem is solved minimizing the arithmetic mean of the forward and beckward linear prediction error variances, $\hat{\rho}_f(q)$ and $\hat{\rho}_b(q)$, respectively

$$\hat{K}_q = \min_{k_q} \frac{1}{2}[\hat{\rho}_f(q) + \hat{\rho}_b(q)]$$

$$\hat{e}^{(f)}_{q,t} = x_t + \sum_{i=1}^{q} a_{q,i} \cdot x_{t-i}$$

$$\hat{e}^{(b)}_{q,t} = x_{t-q} + \sum_{i=1}^{q} a^*_{q,i} \cdot x_{t-q+i}$$

$$\hat{e}^{(f)}_{q,t} = \hat{e}^{(f)}_{q-1,t} + \hat{K}_q \hat{e}^{(b)}_{q-1,t-1}$$

$$\hat{e}^{(b)}_{q,t} = \hat{e}^{(b)}_{q-1,t-1} + \hat{K}^*_q \hat{e}^{(f)}_{q-1,t}$$

$$\hat{K}_q = \frac{-2\sum_{t=q+1}^{I} \hat{e}^{(f)}_{q-1,t} \hat{e}^{(b)*}_{q-1,t-1}}{\sum_{t=q+1}^{I} [|\hat{e}^{(f)}_{q-1,t}|^2 + |\hat{e}^{(b)}_{q-1,t-1}|^2]}$$

where $\hat{e}^{(f)}_q$ and $\hat{e}^{(b)}_q$ are the farward and backward errors estimetes and

$$\hat{e}^{(f)}_{0,t} = \hat{e}^{(b)}_{0,t} = x_t$$

.

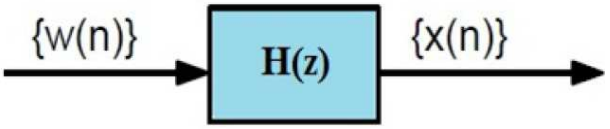

FIGURE 3.1: AR filter.

The set of reflection coefficients represents the second order statistics of a stationary time series x, given the one-to-one relationship between the sequences $[R_{x,0}R_{x,1}R_{x,2}\ldots]$ and $[R_{x,0}K_1K_2\ldots]$, as discussed in [95]. In that work Burg shows that the description of the second order statistics based on reflection coefficients presents practical advantages over auto-correlation function- and power spectrum-based representations when dealing with many short data samples, avoiding the end-effect problem and obtaining a new definition of a power spectrum.

The AR *reflection coefficients* K_q of increasing order $q = 1, \ldots, Q$, obtained according to the Burg method are considered to assort the feature vectors $\chi^{(I)}$ representing each frame of the EEG signals. The value for the parameter Q of the AR model has been selected according to the Akaike Information Criterion (AIC) which minimizes the information loss in fitting the AR model [96] according to the formula:

$$\text{AIC}(Q) = I \ln \sigma^2_Q + 2Q \tag{3.2}$$

being I the sequence length, and σ^2_Q the prediction error power (variance). An example of the AIC function estimated for sample dataset is shown in Figure 3.2.

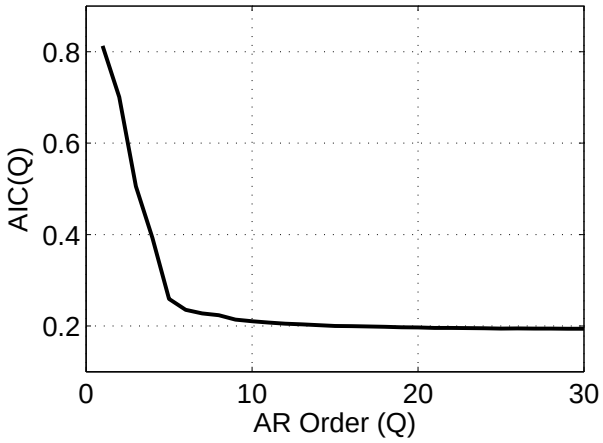

FIGURE 3.2: Akaike Information Criterion for the estimation of the AR model order Q.

Therefore a sample dataset $\chi^{(I)}_{i,\tau}$, where $\chi^{(I)}_{i,\tau} \in \mathbb{R}^d (d = Q$, number of AR features), $i = 1, \ldots, N$ (number of subjects), and $\tau = 1, \ldots, T$ (number of time frames), is obtained for each channel. A graphical representation of the AR features for 10 sample subjects is shown in Figure 3.3.

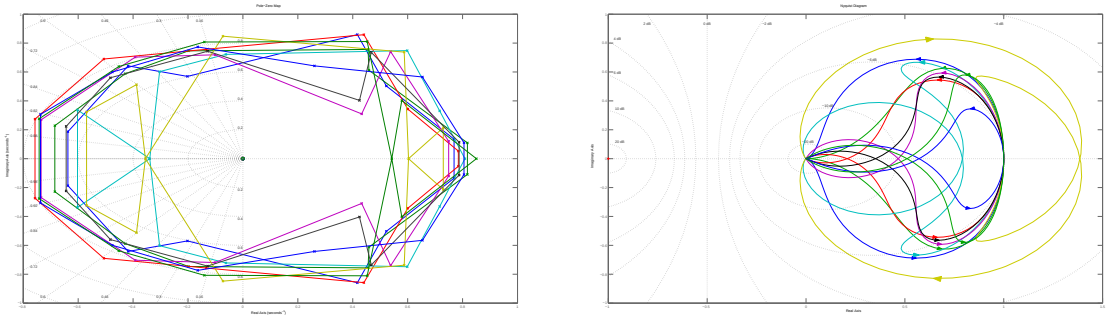

(a) (b)

FIGURE 3.3: Pole-zero map (a) and Nyquist diagram (b) of the transfer functions of the models represented by the feature vectors $\chi^{(I)}_{i,\tau} \in \mathbb{R}^{12}$ for 10 sample subjects. The feature vectors reported are extracted from EEG frames τ. The colormap codes the subjects $i = 1, \ldots, 10$.

3.2.1.1 Results in EEG biometrics

A first evidence of the potentials of EEG biometrics is given by the analysis of RS data modeled as AR processes employing the methods reported in Section 3.2.1. A systematic analysis of all the involved parameters is performed on the EEG signals acquired through a 64 channels acquisition system from 45 healthy subjects at rest with eyes closed, in order to obtain the best fit of the current dataset for recognition purpose. $N_{ch} = 56$ channels are retained after a preliminary screening on the whole dataset to reduce artifact occurrence.

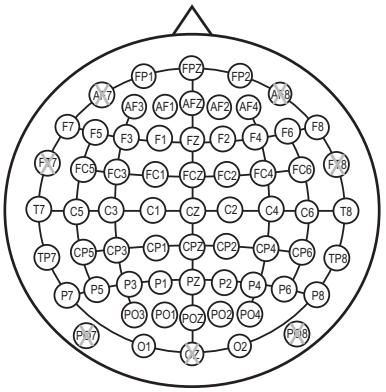

FIGURE 3.4: Scalp electrodes positioning according to an extension of the standard 10-20 montage. Electrodes positioning in the employed protocol is shown by the uncrossed circles.

Given the 56 employed channels shown in Figure 3.4, different subsets of them are considered in order to find the best performing spatial arrangements of electrodes while minimizing their number. To achieve this goal we consider sets of two, three, and five electrodes, listed in Tables 3.1 and 3.2. Symmetrical configurations are selected, spanning the entire scalp for sets of two and three channels (Tables 3.1 and 3.2).

AR modeling is employed to extract the feature vectors from EEG recordings, which have been first pre-processed as described in Section 3.1. Specifically, in that stage signals have been decimated to a sampling rate $S_r = 60$Hz, in order to maintain the frequency components in the range of interest $[0 - 30\text{Hz}]$, and band pass filtered to further extract and analyze the brain rhythmic activity in the frequency bands δ, θ, α and β, which are predominant in resting state with eyes closed, and in some of their combinations. A spatial filter has been then employed to improve the SNR, controlling artifacts that may occur on the single reference electrode. Furthermore, the so obtained signals have been normalized, segmented into overlapping frames of I/S_r with an overlapping factor O_L between consecutive frames, and the linear trend has been removed. Values of $I/S_r = 3s$, and $O_L = 75\%$ have been selected in order to capture locally stationary and repeatable features, while providing a proper number of frames to train the classification algorithm. In fact we have experimentally verified that increasing the dataset size through the overlapping factors of 25% 50% and 75%, leads to improved performance due to a better estimation of the matrices involved in the classification algorithm.

A number of $T = 77$ frames has been obtained in the pre-processing stage, and AR reflection coefficients are estimated from each of them to generate features vectors. The order $Q = 12$ of the AR model has been properly estimated using the AIC function [94], but different orders $Q \in \{6, 8, 10, 12\}$ are tested providing an experimental validation of the adopted model in terms of performance. In Figure 3.5 it can be observed that increasing the model order up to $Q = 12$ leads to improved performance for all the considered sets of channels. For each frame a template is obtained by concatenating the reflection coefficients referring to the signals from

electrodes	$\delta \cup \theta \cup \alpha \cup \beta$	$\delta \cup \theta \cup \alpha$	δ	θ	α	β
Fp1 Fp2	77.66	73.54	54.34	40.75	56.05	22.80
AF3 AF4	83.67	78.44	57.00	43.38	57.86	24.10
F7 F8	81.18	79.48	56.28	35.99	59.02	23.84
FC5 FC6	90.33	79.88	61.79	44.33	63.64	26.84
FC3 FC4	90.91	82.94	56.16	44.99	61.21	32.03
FC1 FC2	90.39	78.35	59.71	40.89	61.15	28.51
T7 T8	91.52	84.04	68.28	54.17	65.37	35.56
C5 C6	89.73	76.25	58.90	44.33	62.40	32.53
C3 C4	90.71	83.64	59.37	48.31	60.52	36.19
C1 C2	93.16	76.45	57.17	44.33	62.28	37.60
TP7 TP8	89.18	82.16	64.59	55.12	67.99	29.99
CP5 CP6	86.41	79.28	60.06	47.36	56.97	28.17
CP3 CP4	90.48	74.14	63.92	49.06	58.21	33.04
CP1 CP2	86.12	70.76	56.05	41.33	54.89	29.81
P7 P8	91.98	84.44	70.79	58.07	69.61	39.08
P5 P6	94.26	80.58	68.34	53.02	66.64	28.48
P3 P4	92.09	82.71	62.74	51.40	67.76	27.13
P1 P2	90.65	81.15	59.71	46.52	66.12	30.68
PO3 PO4	96.57	87.65	77.58	62.83	72.70	38.61
O1 O2	95.41	87.59	72.73	56.57	74.60	41.10
F5 F6	84.10	83.15	55.18	42.22	60.52	26.55
F3 F4	86.58	80.23	61.15	43.81	59.68	32.67
F1 F2	87.50	73.22	52.01	45.11	57.03	30.04
Fpz AFz	86.15	73.28	58.99	44.18	59.51	29.47
AFz Fz	88.83	79.08	61.15	42.94	56.59	26.23
Fpz Cz	93.19	85.08	69.21	53.25	67.13	33.25
Fpz FCz	91.86	88.23	70.74	55.21	66.61	33.07
Fpz Fz	89.55	82.57	62.74	54.92	62.37	31.08
Fpz CPz	88.92	83.55	65.66	51.72	64.50	33.02
Fpz Pz	88.98	83.41	64.88	51.98	68.57	30.68
Fpz POz	89.73	84.82	72.90	57.84	68.92	34.92
AFz FCz	93.51	85.22	67.91	48.95	65.48	32.18
AFz Cz	94.52	82.37	66.87	52.18	69.47	34.83
AFz CPz	89.90	81.04	64.56	50.71	68.11	35.61
AFz Pz	91.28	84.13	64.39	44.99	70.07	34.57
AFz POz	91.89	84.56	72.73	51.86	71.20	42.97
Fz FCz	91.60	80.72	59.16	45.83	56.39	26.00
Fz Cz	95.32	85.89	66.03	53.30	62.91	36.22
Fz CPz	92.78	85.22	62.68	56.02	66.06	38.27
Fz Pz	93.77	86.81	64.73	48.66	68.63	35.21
Fz POz	95.24	89.03	74.34	55.84	69.75	43.64
FCz Cz	96.59	88.23	65.02	51.23	57.63	37.60
FCz CPz	94.49	90.25	71.72	58.99	66.23	36.71
FCz Pz	95.12	88.77	73.28	55.30	75.47	37.20
FCz POz	97.09	90.07	76.68	59.51	75.18	41.10
Cz CPz	91.11	80.32	64.99	47.07	62.16	37.17
Cz Pz	93.65	86.32	68.66	55.79	71.40	39.62
Cz POz	94.89	85.89	77.66	56.05	73.02	35.93
CPz Pz	91.66	81.99	62.25	53.82	63.12	35.44
CPz POz	92.87	88.95	73.56	58.44	71.14	40.32
Pz POz	90.22	83.75	69.87	47.79	66.61	32.53

TABLE 3.1: Classification results in $\%$ obtained for the subbands δ, θ, α, β, and the fusions $\delta \cup \theta \cup \alpha \cup \beta$ and $\delta \cup \theta \cup \alpha$ for sets of two electrodes. Values for overlap and AR model order are $O_L = 75\%, Q = 12$, respectively.

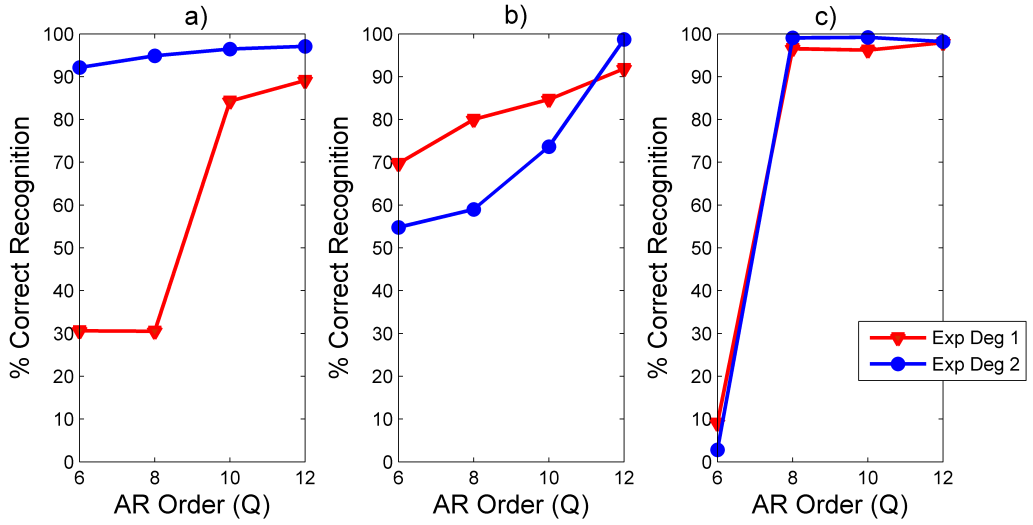

FIGURE 3.5: Recognition performance *vs* AR model order, with overlap factor of 75% for: a) best couple; b) best triplet; c) best set of five 5 electrodes.

electrodes	$\delta \cup \theta \cup \alpha \cup \beta$	$\delta \cup \theta \cup \alpha$	δ	θ	α	β
Fp1 Fpz Fp2	79.65	78.47	58.96	45.69	58.61	26.26
AF3 AFz AF4	88.25	80.55	63.35	45.25	63.64	26.64
F7 Fz F8	92.76	89.61	70.97	55.44	71.28	31.75
FC5 FCz FC6	95.56	89.93	74.57	62.86	78.93	39.97
T7 Cz T8	97.75	92.70	81.62	72.67	83.61	47.42
C5 Cz C6	96.57	89.81	80.58	62.05	77.14	41.24
C3 Cz C4	97.52	92.70	75.90	67.01	73.42	47.01
C1 Cz C2	95.50	82.57	65.66	52.09	66.67	45.54
TP7 CPz TP8	95.70	90.22	79.54	68.72	78.15	46.18
P7 Pz P8	96.51	90.10	79.45	67.33	81.76	49.96
PO1 POz PO2	95.04	88.54	78.33	57.32	76.57	45.95
PO3 POz PO4	98.10	93.04	84.68	71.14	84.91	51.66
O1 POz O2	98.73	90.59	77.37	61.41	84.79	53.88

TABLE 3.2: Classification results in % obtained for the subbands δ, θ, α, β, and the fusions $\delta \cup \theta \cup \alpha \cup \beta$ and $\delta \cup \theta \cup \alpha$ for sets of three electrodes. Values for overlap and AR model order are $O_L = 75\%, Q = 12$, respectively.

the electrodes set under analysis, thus generating feature vectors of length $24, 48, 60$ for the sets of two, three, and five electrodes respectively.

A polynomial classifier [97] is then employed using an expansion factor $D = 2$. It is worth pointing out that the expansion factor has been kept low, since, given the dimension of the feature vector considered in this study, a higher expansion factor would lead to a dimensionality curse resulting in heavy computational load and matrices estimation problems. In Figure 3.5 it is shown the comparison between recognition performances obtained employing a simple linear classifier based on the Minimum Mean Square Error (MMSE) and a 2-degree polynomial classifier. Results show that best performance of 97.09% and 98.73% are obtained setting $Q = 12$ and $D = 2$ for sets of two and three channels respectively, while remaining below 90% for $D = 1$. Referring to sets of five channels it should be noticed that the space expansion doesn't provide

significant improvements in the recognition performance. In this case a correct recognition rate of about 99% is obtained for $Q = 10, 12$ and $D = 2$, which differs not significantly from the best performance achieved by using three channels, while requiring an inconvenient greater number of electrodes. Finally, a cross-validation framework is provided for all the considered sets of channels and frequency bands, obtaining results shown in Tables 3.1 and 3.2. The set of frames used for training and test have been kept disjoint. It should be noticed that the channel spatial configurations giving the best performance appear to be located mainly in the parieto-occipital area PO of the scalp (O1-POz-O2, PO3-POz-PO4, Cz-TP7-CPz-TP8-Pz, Cz-P7-CPz-TP8-Pz), while the worst performing sets of electrodes are placed in the fronto-polar region FP (FP1-FP2, FP1-FPz-FP2). This is in agreement with the experimental finding that α and β rhythms carry individual-specific traits, claimed to be genetically induced [56], and with the observation that the oscillatory α activity is the most dominant rhythm which emerges from the PO region in a condition of relaxation with closed eyes [15], corresponding with the herein employed experimental protocol. According to this evidence, the most considerable contribution to the correct recognition performance, for the given dataset, comes from the α band followed by the β band, as it can be observed comparing the column 3 of each table to the columns 4, 5 and 6. Moreover, as it can be observed in Figure 3.6, the worst performing FP region doesn't show α activity, while it is strongly detected in the PO area. Besides, eyes movement artifacts mostly affect the FP region, due to the proximity of the involved muscles.

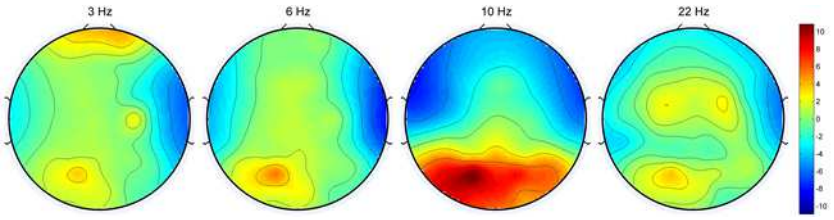

FIGURE 3.6: Spectral maps for the EC resting state protocol. The spatial distribution on the scalp of spectral EEG amplitudes at given frequencies, specified above each map, is shown. Each circle represents the top view of a head, where the highest point is the nasion while the lowest is the inion.

In conclusion, the contribution of this analysis concerns the investigation of the most characteristic combination of subbands to analyze, the proper segmentation and spatial configuration of electrodes to employ, while using an efficient polynomial regression classifier. It proves that a preliminary data screening is needed for the optimal setting of the involved parameters. This analysis shows that, within the employed classification framework, the α rhythm can be successfully employed for recognition purposes, since the used acquisition protocol and the proper choice of the electrodes number and their positioning allowed reaching recognition rates equal almost to 99% through a second order polynomial regression. The obtained results achieves more accuracy compared with previous works carried out on one-session recordings investigating the EC condition cited in Chapter 2, especially considering the size of the employed datasets and the separation of the training and the test datasets. A better result is obtained also with

respect to other acquisition protocols, such as open eyes condition in [76]. The results reported in this section have been published in [75], to which the reader is referred to for further details on the performed analysis and the polynomial classification approach employed.

3.2.2 Bump Modeling

The second parametric approach adopted in the present work to extract features from EEG data involves the analysis of time-frequency maps of the acquired signals, in order to identify specific map parameters for each individual.

In order to achieve this goal, we use bump modeling [98], which is a technique for modeling a time-frequency map, with the aim of representing the map with a limited number of elementary functions. The purpose is to reduce the huge quantity of parameters that describe a time-frequency map, tens to hundreds of thousands, to a sum of parametric functions, a few functions with some tens of parameters.

The main idea of this method is to approximate a time-frequency map with a set of predefined elementary parameterized functions called bumps; therefore, the map is represented by the set of parameters of the bumps, which is a very sparse encoding of the map, resulting in information compression rates that range from one hundred to one thousand (rationales for this procedure, proofs and technical details are explained in [98]).

The algorithm performs the following steps on the time-frequency maps (after appropriate normalization):

i. window the map in order to define the zones to be modelled (those windows form a set of overlapping sub-areas of the map);

ii. find the window that contains the maximum amount of energy;

iii. adapt a bump β to the selected zone, and withdraw it from the original map. The parameters of the bumps are computed using the BFGS algorithm [99] in order to minimize the cost function C defined by:

$$C = \frac{1}{2} \sum\nolimits_{t,f \in W} (z_{f,t} - \beta(f,t))^2 \tag{3.3}$$

where the summation runs on all pixels within the window W, $z_{f,t}$ are time-frequency coefficients at time t and frequency f, and $\beta(f,t)$ is the value of the bump function at time t and frequency f;

iv. if the amount of information modelled by the bumps reaches a threshold, stop; else return to (iii).

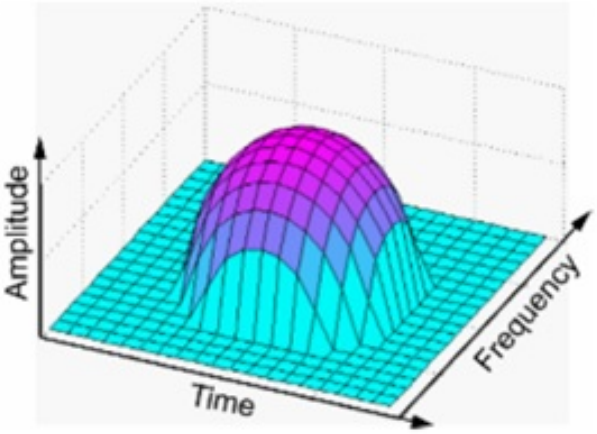

FIGURE 3.7: Half ellipsoid bump function.

EEG signals are transformed to time-frequency maps using Complex Morlet wavelets, as they are appropriate for time-frequency analysis of electroencephalographic signals because of its symmetrical and smooth Gaussian shape both in time and frequency domains [100].

$$w(t) = \exp(-t^2/2{\sigma_t}^2)\exp(2i\pi rt) \tag{3.4}$$

Bump functions used are half ellipsoids. Half ellipsoids (see Figure 3.7) are defined by:

$$\begin{aligned} \beta(f,t) &= a\sqrt{1-v} \quad for \quad 0 \leq v \leq 1 \\ \beta(f,t) &= 0 \quad for \quad v > 1 \end{aligned} \tag{3.5}$$

where $v = ({e_f}^2 + {e_f}^2)$ with $e_f = \frac{f-\mu_f}{l_f}$ and $e_t = \frac{t-\mu_t}{l_t}$. μ_f and μ_t are the coordinates of the center of the ellipsoid, l_f and l_t are the half-lengths of the principal axes, α is the amplitude of the function, t is the time and f the frequency.

Figure 3.8 shows a typical example of bump modeling of the time-frequency map of an EEG recording. Each bump is described by 5 parameters: its coordinates on the map (2 parameters), its amplitude (one parameter) and the lengths of its axes (2 parameters). All the experiments performed in the present work is done using the BUTIF Toolbox [101][1]

In particular, to assort the feature vectors for each subject i and each channel ch, the wavelet decomposition of EEG signals is computed employing the Complex Morlet waveform, so that each frame τ is represented by the extracted wavelet coefficients in the time-frequency space. Bump modelling is then employed to obtain a parametric description of most energy contained in the wavelet maps, so that the 5 parameters are extracted for each bump fitting the energy spots in the time-frequency representation of the EEG signals.

[1] publicly available at: http://www.bsp.brain.riken.jp/~fvialatte/bumptoolbox/toolbox_home.html

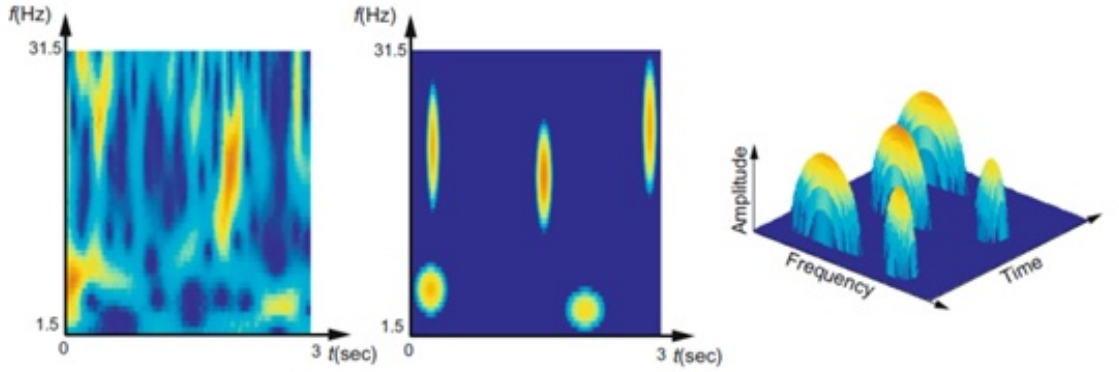

FIGURE 3.8: Left: normalized time-frequency map of an EEG recording; middle and right: 2D and 3D bump modeling of the map.

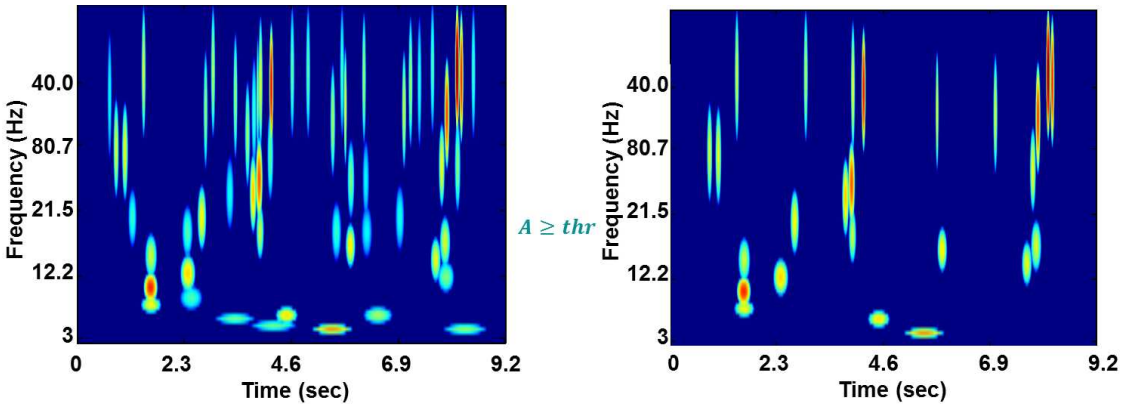

FIGURE 3.9: Parametric time-frequency map of an EEG epoch for a sample subject (left) and the result of its amplitude filtering (right).

Subsequently, discriminant features of the so obtained parametric maps are computed considering the median values for the amplitude (A), the central frequency (f_c), the volume (v), the surface of the meridian ellipse (a), the height (extension in frequency h) and the width (extension in time w) of each bumps modelling the time-frequency maps. To obtain feature vectors we also consider the total number of bumps for each map, the sum and max values of A, f_c, v, a, h and w, the number of bumps within different ranges of the investigated time-frequency domain, the amplitudes and central frequencies of bumps showing max values of parameters a, v, w and h. Moreover for each bump map we compute the spectral centroid $c(t)$, that is the "center of mas" of the bumps in the frequency domain defined for each time step t, computed as the weighted mean of the frequencies present in the map for each instant, with the corresponding map amplitudes as the weights. The average value over time of $c(t)$ is considered as a further feature. Furthermore, each of the listed parameters are also computed for filtered maps where a threshold value $thr = 0.4$ is applied to the bump amplitude A. An example of the obtained parametric maps and their amplitude filtering is shown in Figure 3.9 for a sample subject.

Therefore feature vectors of 39 components $\chi_{i,\tau}^{(II)} \in \mathbb{R}^d (d = 39$, number of parametric map features),

with $i = 1, \ldots, N$ and $\tau = 1, \ldots, T$ (number of time frames), are obtained for each channel, where parameters referred to the unfiltered and the filtered maps are concatenated.

3.2.2.1 Results in EEG biometrics

This section report the results obtained employing parametric bump maps for the purpose of user identification. EEG signals acquired through a $64-$channels system from $N = 36$ subjects in resting conditions are modeled in the time-frequency domain to extract distinctive features. A pre-processing stage has been first performed on the acquired EEG signals(see Section 3.1), including decimation with sampling rate of $S_r = 100$Hz, band-pass filtering to remove very low and high frequency noise, normalization and segmentation into overlapping frames of $I = 15s$.

Then, as described in Section 3.2.2, the obtained frames are modeled through wavelet decomposition and parametric functions are used to obtain compact representations of the extracted wavelet coefficients in the time-frequency domain, employing the BUTIF toolbox. Bump modeling is employed to reduce the dimensionality of the time-frequency representation of each EEG segment τ, while retaining most of the energy content. 39 features are extracted from the bump maps, and the analysis of variance is employed to evaluate the inter-subject variability of each of them, so that $d = 13$ features are selected (refer to [102] for further details on the statistical analysis).

Different tests are carried out in order to infer about the best electrodes configuration and to analyze the distinctive contribution of each brain rhythm. More in detail, given the "resting state with eyes closed" acquisition protocol here investigated and the $N_{ch} = 56$ artifact-free channels shown in Figure 3.4, different subsets of acquisition sensors are considered in order to find the best performing spatial arrangements of the electrodes while minimizing their number. To achieve this goal we select sets of three symmetrical inter-hemispheric and sets of mid-line electrodes. The subbands related to the different brain rhythms $\theta, \alpha, \beta, \gamma([30 - 40]$Hz), which are the ones interested by the "resting state with eyes closed" protocol, and their combination $[3-40]$Hz are individually modeled and analyzed. For each identity the template is subsequently obtained by concatenating the selected features related to the different electrodes in the set under analysis, thus generating feature vectors of length 13×3 for the sets of three electrodes listed in Table 3.4, first column.

In Table 3.3 the results obtained from the analysis of different subbands, using a classifier based on the Mahalanobis distance, are given for some of the tested electrodes configurations. The correct recognition percentages reported in the table refers to overlapped training and test datasets, and are obtained within a cross-validation framework (for further details on the classifier and on the cross-validation framework reference is made to [102]). In Table 3.4 the same analysis for a larger set of scalp electrodes configurations is provided considering disjoint datasets, which are

obtained by removing overlapping frames. It is worth pointing out that the classification performance varies considerably for the different scalp regions and rhythms under analysis. Moreover the performance significantly decreases for the disjoint datasets than for the overlapped frames. On the other hand, a match score fusion obtained performing the sum of scores (Mahalanobis distances) related to specific rhythms and different sets of channels, leads to a dramatic increase in recognition accuracy, especially for the otherwise poorly performing case of disjoint training and test datasets, as observed in Figure 3.10. In this case a selection of the best performing channels configurations and frequency bands to combine provides the good result of 99.69% of correct recognition percentage, which differs not significantly from 99.75% obtained for the case of overlapped datasets. For the selection of the frequency bands to combine, the best performing set of three channels $PO_3 - PO_z - PO_4$ (see Table 3.4) is considered, and subsequent score fusions are performed. To this aim the brain rhythms are previously sorted in descending order of performance achieved individually, and sequentially combined within a forward-backward step-wise approach, retaining in the information fusion only those bands which improved the correct classification. Results reported in Figure 3.10 show that a significant improvement is obtained combining β, α and θ rhythms. The same approach is considered to select the combination of electrodes configurations, while considering the best performing band fusion $\beta \cup \alpha \cup \theta$. For the case of disjoint training and test datasets the best correct recognition percentage of 99.69% can be achieved when the sets of three inter-hemispheric and mid-line channels $PO_3 - PO_z - PO_4, O_1 - PO_z - O_2, CP_5 - CP_z - CP_6, TP_7 - CP_z - TP_8, PO_1 - PO_z - PO_2, PO_z - P_z - CP_z, T_7 - C_z - T_8, P_5 - P_z - P_6, CP_z - C_z - FC_z$, and the three rhythms θ, α, β containing most information are combined into the match score fusion. It should be noticed that the selected channels result located in the posterior region of the head, where the considered rhythms are mainly detected. Figure 3.10 reports the improvements obtained in the subsequent steps of the information fusion. Moreover the resulting misclassification matrix shows that a 100% of correct identification is obtained for all users but one, who presents correct recognition rate of about 89%. The result obtained doesn't differ significantly from the perfect recognition performance (100%) obtained for the case of overlapped datasets, within the same information fusion approach and cross-validation framework.

The results reported in this section have been published in [102], to which the reader is referred to for further details on the performed analysis and the classification approach employed.

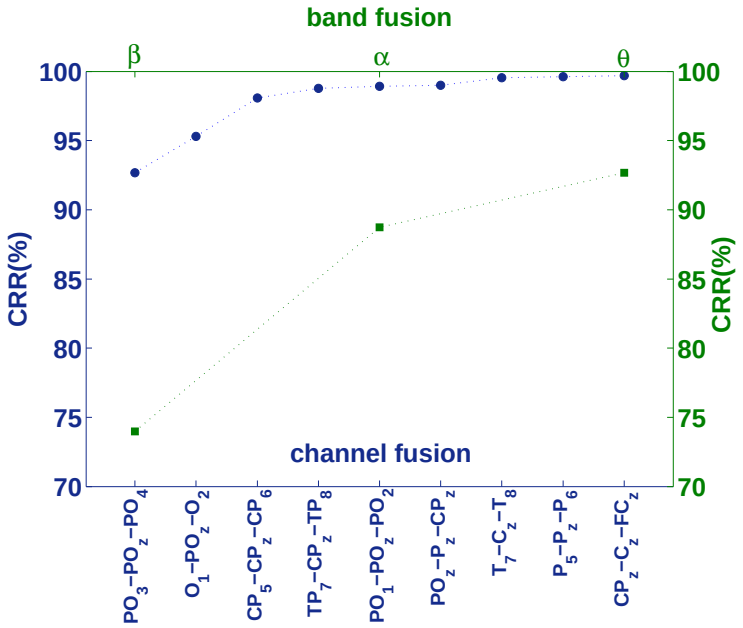

FIGURE 3.10: Improvement of the correct recognition rate obtained performing subsequent score fusions. Curves refer to the combination of different brain rhythms (top x-axis) and different electrodes sets (bottom x-axis). Labels in the x-axes refers to the score added at the related step.

Channels	$3-40$Hz	θ	α	β	γ
C1 Cz C2	62.22	76.60	83.02	83.21	73.27
C3 Cz C4	73.27	84.26	87.10	87.90	76.67
C5 Cz C6	75.56	86.54	89.94	91.67	83.64
T7 Cz T8	78.83	85.43	93.09	92.96	85.19
PO1 POz PO2	79.69	86.23	90.43	93.77	79.01
TP7 CPz TP8	80.68	87.90	92.65	93.70	83.09
P7 Pz P8	81.60	89.44	94.57	92.90	83.33
O1 POz O2	82.59	86.30	94.14	94.38	83.70
PO3 POz PO4	84.69	**89.69**	**95.74**	**95.19**	83.21

TABLE 3.3: Classification performance in terms of correct recognition rate. Results refer to overlapped training and test datasets. The analysis of individual subbands is reposted in subsequent columns, and the set of 3 channels considered is listed in the first column.

3.3 Non-Parametric Features

3.3.1 Power Spectral Density

Although parametric linear or non-linear EEG signal processing has been successfully employed for biometric purposes [75], [103], a non-parametric Fourier Transform-based spectral analysis is also considered in the present work of doctoral thesis due to its obvious physical interpretation in terms of EEG rhythms. The classical Spectral Analysis based on the estimation of the Welch's periodogram is here employed to obtain the Power Spectrum Density (PSD) of the EEG epoch. The PSD function extracted from each channel and each epoch allows to account for the

Channels	$3-40$Hz	θ	α	β	γ
C1 Cz C2	24.81	38.61	43.70	45.65	35.56
CP1 CPz CP2	28.98	42.69	44.35	48.61	33.89
FCz Fz AFz	29.54	42.13	47.96	46.57	34.44
F3 Fz F4	29.63	41.02	54.35	51.39	38.98
Cz FCz Fz	30.19	39.17	49.07	46.85	39.44
CPz Cz FCz	30.46	44.81	49.72	53.70	41.02
C3 Cz C4	31.76	43.80	48.43	52.22	40.00
Pz CPz Cz	32.59	42.96	57.78	55.83	39.72
Fz AFz Fpz	34.17	38.43	44.63	51.20	31.30
CP5 CPz CP6	37.04	50.28	53.61	53.43	36.20
CP3 CPz CP4	37.59	45.09	49.35	55.28	36.76
FC3 FCz FC4	37.87	43.06	52.69	56.67	47.31
C5 Cz C6	40.00	46.11	57.78	58.70	48.98
P5 Pz P6	41.57	49.63	69.17	63.06	40.65
T7 Cz T8	42.41	42.41	62.41	62.69	50.09
POz Pz CPz	42.87	49.17	59.54	61.02	37.41
PO1 POz PO2	46.57	52.78	62.13	66.39	45.56
P7 Pz P8	46.94	53.98	71.11	62.31	47.50
TP7 CPz TP8	49.07	48.61	64.44	69.26	48.52
P3 Pz P4	49.91	45.28	64.91	62.04	43.98
O1 POz O2	52.59	51.57	64.91	69.91	52.04
PO3 POz PO4	52.78	**55.56**	**67.31**	**73.98**	49.81

TABLE 3.4: Classification performance in terms of correct recognition rate. Results refer to disjoint training and test datasets. The analysis of individual subbands is reposted in subsequent columns, and the set of 3 channels considered is listed in the first column.

contribution of each EEG rhythm to the significant differences under analysis, e.g. between subjects.

Specifically, the PSD of the EEG signals are extracted from each EEG epoch (see Section 3.1) by computing the Welch's averaged modified periodogram. A sliding Hanning window of $0.5s$, with an overlap of $0.25s$, is applied to improve the estimation quality. The number of FFT points is set in order to have a PSD estimate with a frequency resolution of 1Hz. The resulting function $PSD(f)$ for the electrode j, with $j = 1, \cdots, N_{ch}$, is a vector of N_{FT} elements characterizing the power of the EEG oscillations.

A logarithmic transformation is applied to the obtained PSD values to provide a Gaussian distribution of values, needed for further analysis.

Therefore a sample dataset representing the spectra of the EEG recordings $\chi_{i,\tau}^{(III)}$, where $\chi_{i,\tau}^{(III)} \in \mathbb{R}^d (d = N_{FT}$, number of spectral features), $i = 1, \ldots, N$, and $\tau = 1, \ldots, T$ (number of time frames), is obtained for each acquisition channel.

3.3.2 Pairwise Spectral Coherence

Over the past decades, different methods have enabled the study of whole-brain functional connectivity patterns, and advances in neuroimaging have provided new insight into plasticity changes associated with language comprehension. In the present work of thesis, in order to further represent features of the brain activation patterns measured by EEG, the linear relationships between simultaneously recorded signals (channels) is measured employing coherence (COH) analysis. Being a bivariate method frequently used due to its practical and intuitive interpretation, spectral coherence gives insight into the way functional networks cooperate with each other during the different mental states. In fact different brain functions rely on distributed patterns of information transfer between the different brain regions involved in specific processes. In this context, COH quantifies the level of synchrony between two signals at a specific frequency f. Given two signals obtained from channels $j1$ and $j2$, the spectral coherence $COH_{j1,j2}(f)$ for a particular frequency f is computed as follows:

$$COH_{j1,j2}(f) = \frac{|S_{j1,j2}(f)|^2}{S_{j1,j1}(f) \cdot S_{j2,j2}(f)} \tag{3.6}$$

where $S_{j1,j2}(f)$ is the cross-spectrum of the signals acquired from channels $j1$ and $j2$, while $S_{j1,j1}(f)$ and $S_{j2,j2}(f)$ are the respective autospectra. By definition $COH_{j1,j2}(f)$ ranges between 0, which corresponds to no synchrony at the frequency f and 1, which corresponds to maximum synchrony at the frequency f. Here, $S_{j1,j2}(f)$, $S_{j1,j1}(f)$ and $S_{j2,j2}(f)$ are computed by means of the Welch's averaged modified periodogram, with same parameters used for the computation of the PSD (see Section 3.3.1). In particular the use of $1s$ Hanning windows should improve the stationarity of the segmented EEG signals [104]. For each electrode pair $(j1, j2)$, we obtain a vector $\chi_{i,\tau}^{(IV)} \in \mathbb{R}^d (d = N_{FT}$, number of frequency points) cof COH values.

A Fisher's Z transformation is applied to COH data to obtain a Gaussian distribution, similarly to what performed for PSD data.

3.3.3 Results in EEG biometrics

In this section the results of the analysis performed for subject recognition based on EEG signals employing non-parametric spectral features are reported and discussed. Scalp EEG signals were gathered from the freely online database PhysioNet BCI [105]. The database consists of $N = 108$ healthy subjects recorded in two different baseline conditions, i.e. 1-minute EC resting state and 1-minute eyes closed EO resting state. The EEG data recorded with a 64-channel system but 5 electrodes are excluded so that only $N_{ch} = 56$ electrodes (see Figure 3.13) are retained for the subsequent analysis. For each subject and condition (EO, EC) the obtained EEG signals are segmented into $T = 6$ non-overlapping frames of $I = 10s$.

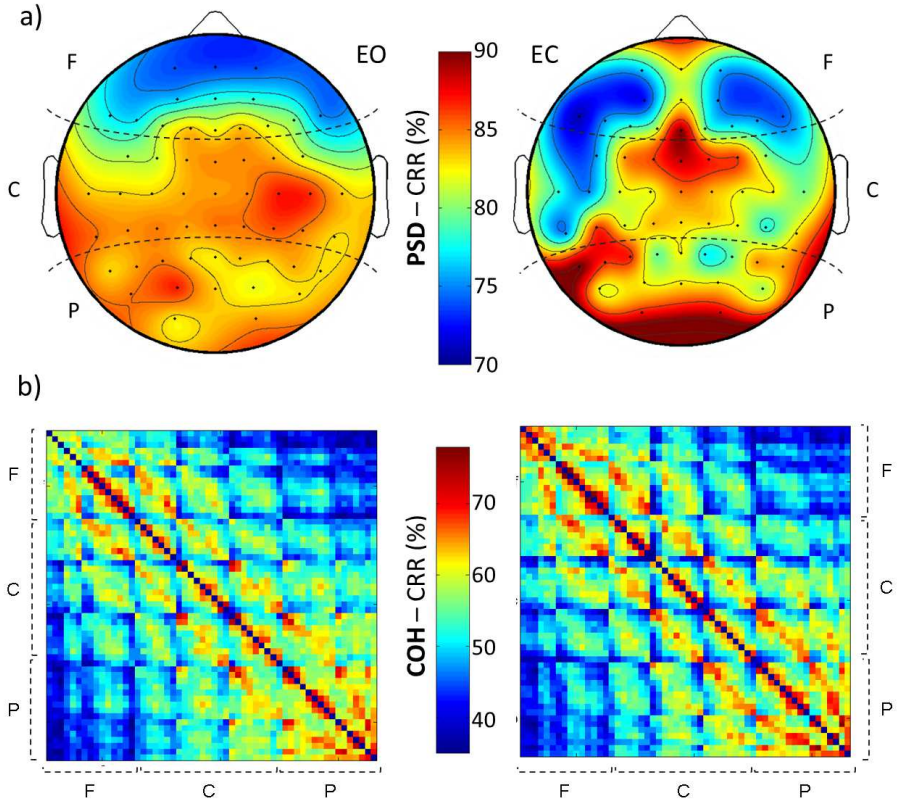

FIGURE 3.11: Spatial distribution of CRR values obtained considering a) PSD features $\chi^{(III)}$ from single EEG channel and b) COH features $\chi^{(IV)}$ from single channel pairs. In b) the elements of the adjacency matrices code all the possible EEG channel pairs. They are organized in order to highlight the connectivity within and between three zones: frontal (F), central (C), and parieto-occipital (P). The two analyzed conditions EO (on the left) and EC (on the right) are reported for each of the two investigated spectral features.

Resting state conditions EO and EC are investigated separately and the related outcome is here compared for all the performed tests. Two different characterizations of the brain signals are considered as distinctive features to test within the provided biometric framework. In particular, PSD and COH estimates are obtained as reported in Sections 3.3.1 and 3.3.2, to generate the representations $\chi^{(III)}$ and $\chi^{(IV)}$ respectively. As previously pointed out, PSD measures the activity of single brain regions while COH rather measures their functional connectivity. In this study we consider a restricted range of frequency, namely $1 - 40$Hz. This choice covers the standard spectrum of physiologic EEG oscillations from low (Delta (δ) and Theta (θ)) to intermediate (Alpha (α)) and high frequency bands (Beta (β) and Gamma (γ) up to 40Hz). In order to obtain a frequency resolution of 1Hz, given a downsampling to $S_r = 100$Hz, we set the number of FFT points to $NFT = 100$. Then, two different sets of feature vectors $\chi^{(III)}(f)_{i,\tau}, \chi_{(IV)}(f)_{i,\tau} \in \mathbb{R}^{NFT}$, are extracted for each channel (channel pair for COH) according to the previously described methods. A classification based on Mahalanobis distance, is then carried out to evaluate the distinctiveness of the two considered feature vectors in all tested conditions, in terms of correct recognition rate (CRR).

3.3.3.1 Single-element classification

A preliminary test on distinctiveness related to each feature is reported in Fig. 3.11. The CRR values obtained within a cross-validation framework, (reference is made to [90] for further details on the tests of recognition performance provided), are shown in false colors. In particular the scalp maps shown in Fig. 3.11 (a) represent the spatial distribution of the CRR values obtained through single channel PSD features $\chi^{(III)}$, in the EO and EC conditions. The adjacency matrices shown in Fig. 3.11 (b) report the CRR values of the COH features $\chi^{(IV)}$ for each channel pair. Given the $N_{ch} \times N_{ch}$ adjacency matrix $\mathbf{Adj}$, each element $Adj_{j1,j2}$ represents the CRR obtained considering the COH between channels $j1, j2$ as feature vector. According to this representation, the position of the EEG channels over the head is coded by the x and y axes of the adjacency matrix.

The CRR scalp maps for the PSD features $\chi^{(III)}$ show that the most distinctive regions appear in the central part of the head (C) during EO (max CRR $= 86.91\%$),while the parieto-occipital zone (P) is more predominant during the EC condition (max CRR $= 90.49\%$). The better distinctiveness of the posterior areas during EC condition was already reported in previous EEG studies [106], [74], [75] and it is probably related to well-known physiological increase of the parieto-occipital Alpha power in such condition [11]. A possible explication for this evidence is that eyes-closed resting states interrupt the visual processing while enhancing endogenous and autonomic related brain activity [15], which reflects the influence of genetic factors [107]. For the CRR adjacency matrices in the EC condition the best discriminant channel pairs are mainly located in the parieto-occipital zone P (max CRR $= 78.5\%$). In the EO condition, the CRR values are generally lower compared to EC (max CRR $= 75.86\%$). In both conditions, short-range functional connectivity carries more distinctive information as can be observed by the tendency of the highest CRR values to stay close to the main diagonal of the $\mathbf{Adj}$ matrices.

Taken together these findings show that COH features $\chi^{(IV)}$ are less distinctive than PSD features $\chi^{(III)}$ in a single-element approach. This outcome is in line with the tested hypothesis that a functional brain network consisting of more elements "linked" together can better characterize different people, describing some aspects of brain organization assumed to be specific of each subject.

3.3.3.2 Match-score fusion

To improve performance, a fusion of the elements at the match score level is obtained for each cerebral zone (F, C and P), within the same cross-validation framework. In particular the sum of

scores related to different elements is considered:

$$S_{m,n} = \sum_{e \in E} \frac{1}{d^e_{m,n}} \tag{3.7}$$

where E is a selection of elements e from the set of 56 channels for PSD, or from 1540 channel pairs when considering COH. The elements to consider in the match score fusion are selected according to a forward-backward approach. Specifically only elements which improve accuracy are retained in the fusion. First, all the elements are sorted in a descending order of accuracy according to the single-element classification results. Starting from the first one, each single element is then added stepwise in the subset E to compute equation (3.7). If the inclusion of the i-th element improves the resulting accuracy then it is retained for the final fusion, otherwise it is removed (see Figure 3.13). More details about the pseudo-code implementation of the match score fusion can be found in Appendix A. The related CRR improvements with respect to the single element approach are shown in Figure 3.12. Here the two conditions EO and EC, and the two considered features $\chi^{(III)}$ and $\chi^{(IV)}$, are compared. In general, the match-score fusion approach improves the performance with respect to the single element approach for each zone, condition and feature. Notably, a perfect recognition rate (CRR $= 100\%$) is obtained when fusing the scores of the COH features $\chi^{(IV)}$, for the EC condition (in all the zones) and for the EO condition (in the frontal zone). The different behavior in performance improvement between $\chi^{(III)}$ and $\chi^{(IV)}$ features can be in part explained by the lower variability of the PSD features vector $\chi^{(III)}$ across different brain regions (Appendix D). In this regard, most of distinctive information is supposed to be contained in the single elements. Instead, COH features vector $\chi^{(IV)}$ tends to be more variable across brain regions and the inclusion of more COH elements can eventually improve the correct recognition rate, while single elements represent very partial information.

Figure 3.13 shows the optimal combination of channel pairs in every zone for COH features $\chi^{(IV)}$. Results are shown for the two conditions EO (a) and EC (b). The plots shown on the bottom part of the figure represent the steps of the match score fusion. Here, each highlighted symbol represents a subsequent improvement of the overall CRR, which leads to include the related channel pair in the final distinctive connectivity pattern represented in the upper part of the figure. It can be noticed that the maximum value of CRR is achieved more rapidly for the EC condition, as shown by the vertical lines in the plots on the bottom part of the figure. The resulting distinctive connectivity patterns consist mainly of short-range COH elements, a result which is in line with the previous outcome reported in the single-element classification analysis. The topology of the more discriminant COH elements reveals a hemispheric symmetry with respect to the longitudinal line. In particular, the predominance of the frontal electrode pairs (line $F7 - F8$) can be observed in both the EO and EC conditions. Neurophysiological evidence shows that specific genetic factors can influence EEG frontal activity [58]. Thus the

highly discriminant spectral coherence observed in this zone could in part reflect a subjective distinctiveness of brain functioning. We also report the involvement of temporo-parietal and dorsal centro-parietal electrodes of the central zone C. Brain regions near the temporo-parietal junction play a specific role in self-other distinction processes and in representing thoughts, beliefs, desires, and emotions [108], influenced by a combination of biological and environmental factors. A comprehensive analysis reporting the fusion steps for the spectral coherence features in all the conditions and zones is detailed in Table 3.5, along with a description of the obtained identification accuracy and topology. A predominance of short-range connectivity characterizes the distinctive patterns for all the considered brain zones.

Notably, the inclusion of the long-range (i.e. inter-zone) connectivity in the fusion algorithm does not improve the recognition performance (Appendix B). The superiority of short-range over long-range connectivity could be partially imputed to volume condition effects, which are known to affect spectral coherence measurements [109]. Although removing those effects is important in general to estimate true interactions between the cortical generators, this would not represent an issue in our study. In fact, volume conduction effects depend on the morphology and electrical conductibility of the subject's head structures. In this regard, any possible volume conduction contributions on the EEG signals could instead represent a relevant personal trait to be exploited for the biometric recognition. As a partial confirmation of this claim it can be shown that the recognition performance of the imaginary coherence (robust to volume conduction effects [109]) is significantly lower than standard spectral coherence (Appendix A).

To sum up, the results of the herein proposed analysis show that a perfect identification of 108 subjects (CRR $= 100\%$) can be obtained considering spectral coherence features within specific regions of the head, and fusing the respective information at the match score level. This result outperforms the state-of-the-art recognition performance obtained with single-session EEG during resting states, notably a CRR $= 98.73\%$ for a dataset of 45 subjects [75] and a CRR $= 97.5\%$ for a dataset of 40 subjects [73].

3.3.4 Results in Language Processing

The same feature engineering approach based on non-parametric spectral representation of EEG signals ($\chi^{(III)}$and$\chi^{(IV)}$) is employed in the present work of doctoral thesis to quantitatively evaluate oscillatory brain activity during language processing and comprehension, which is the subject of a current study. Although sentence processing has been at the center of much psycholinguistic speculation, its neural underpinnings delineate a relatively recent strand of research.

Following [110] and more recent contention [111], we outline the Given (G)/New (N) opposition as bearing upon activation states of information in discourse and in the receivers conscious

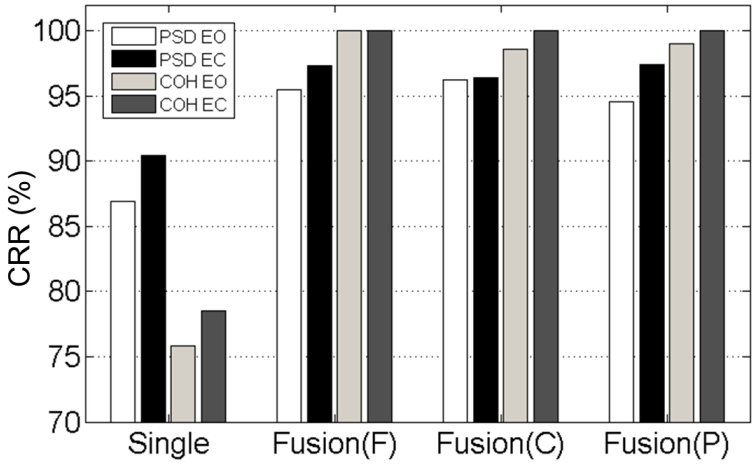

FIGURE 3.12: Performances in terms of CRR (y-axis) obtained considering single-element classification versus match-score fusion in each cerebral zone (x-axis). The color of the bars codes the spectral feature and the condition according to the legend.

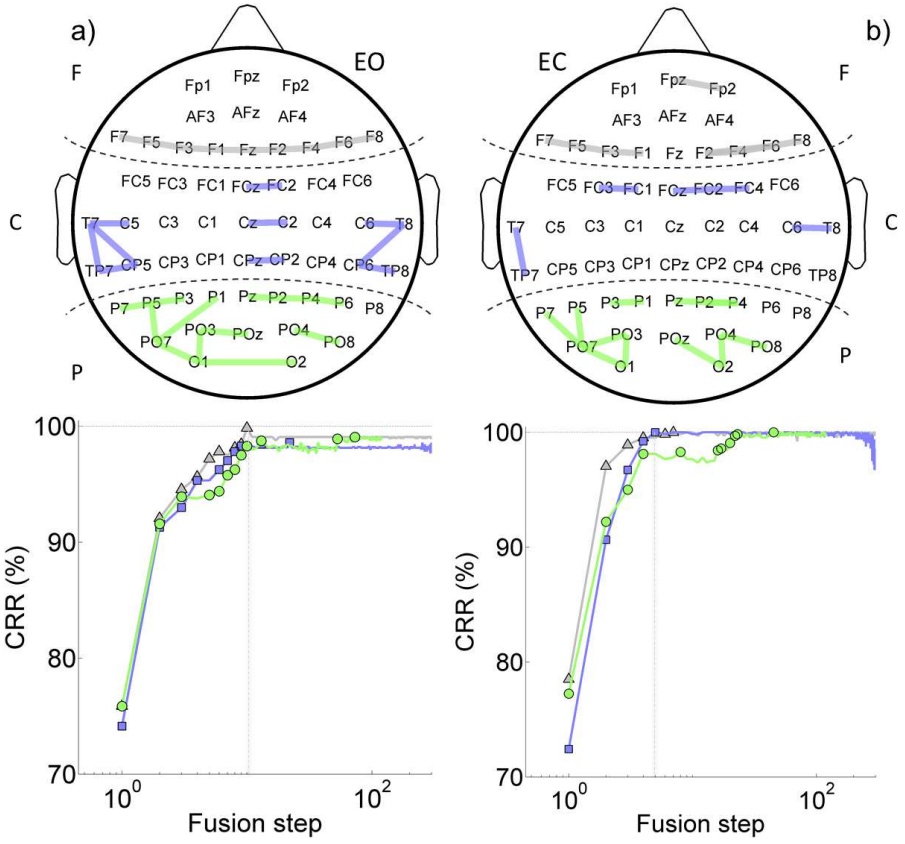

FIGURE 3.13: Distinctive functional connectivity patterns in each cerebral zone (on the top) and related steps for the match score fusion selection (on the bottom). Results for the EO and EC to conditions are reported in a) and b) respectively. The color of each line in the bottom panels codes the CRR values obtained for different cerebral zones, according to the top panels. Symbol markers highlight the fusion steps that increased the overall CRR accuracy. Different symbols are used for different cerebral zones (F-triangles, C-circles, P-squares). X-axes are put into logarithmic scales for the sake of representation.

Eyes-Open												
F	72,74 F2-F4	91,43 F1-F3	94,55 F4-F6	97,2 F3-F5	97,82 F6-F8	99,06 F1-Fz	99,84 F5-F7	100 F2-Fz				
C	74.14 TP7-T7	91.28 CP5-TP7	92.99 C5-T7	95.33 T8-C6	96.26 FC2-FCz	97.04 C2-Cz	97.82 CP2-CPz	98.29 CP5-T7	98.44 TP8-CP6	98.6 CP6-T8		
P	75.86 P7-P5	91.59 PO4-PO8	93.92 O1-PO3	94.08 O1-PO7	94.39 P2-P4	95.79 PO7-P5	96.26 O1-O2	97.51 P2-Pz	98.29 P3-P5	98.75 P4-P6	98.91 POz-PO3	99.07 PO7-P1
Eyes-Closed												
F	77.26 F2-F4	97.04 F3-F5	97.82 F1-F3	98.6 F5-F7	98.75 F6-F8	99.06 F4-F6	99.69 Fp2-Fpz	100 F2-F6				
C	72.43 TP7-T7	90.65 FC2-FCz	96.73 FC2-FC4	99.22 C6-T8	100 FC1-FC3							
P	78.5 PO3-O1	92.21 PO4-PO8	95.01 PO7-O1	98.13 PO3-PO7	98.29 P2-P4	98.44 PO7-P7	98.6 PO7-P5	99.06 P1-P3	99.69 O2-PO4	99.84 O2-POz	100 P4-Pz	

TABLE 3.5: CRRs for COH features $\chi^{(IV)}$, obtained through the fusion of the channel pairs reported in each row. Each column represents a step of the fusion, and the related accuracy achieved is reported together with the channel pair considered in that step (see Appendix A). Results for EO, EC, and the three investigated brain zones are shown.

attention. Given, in this sense, is equated with information recently introduced in discourse and active in the addressee's Short-Term Memory. New designates information with no recent introduction in prior discourse or situation, and therefore inactive in the addressee's Short-Term Memory.

We refer the Topic (T)-Focus (F) (or Topic-Comment) dichotomy to the illocutionary level of utterances, i.e. a level in which cues to the detection and interpretation of communicative purposes are provided [112], [113], [111]. On this account, Focus represents the unit conveying information proposed by the speaker as his main contribution to the ongoing interaction; whereas Topic provides the semantic domain that makes the Focus understandable, and links focal information to the foregoing discourse. Correspondingly, the Focus conveys the illocutionary force of the utterance [114], while the Topic only proposes information that is useful to understand the Focus.

In much literature, the Given/New and Topic/Focus pairs have been treated as coterminous (with Topic referring to given, and Focus to new information). However, the inter-independence between the two levels is shown by occurrences which are by no means rare in ordinary communication [2]. As is known, the alignments T/G and F/N is the most typical, since it is more probable for new information to bear the illocutionary force of the utterance (i.e. the speaker's communicative goal), while given information is more often presented as Topic. This pattern appears altogether reversed in the misalignment T/N and F/G, in which new content is encoded in the sentence Topic and given content in the Focus, respectively. A number of psycholinguistic studies highlight that anticipation is one of the key strategies to ease automation in processing and reduces cognitive overloading of the executive working memory channels, which are temporary and capacity-limited. Building on these findings the investigation detailed in this section aims to

[2] [115]"The distinction between topic and comment is autonomous, in the sense that it cannot be derived from the distinction between "given" (i.e. the known from the preceding context or situation, contained among the presuppositions) and "new" (not given)".

assess the effects of encoding given/new contents in aligned or misaligned configurations with respect to topical vs. focal packaging.

The results of the performed analysis are reported together with a discussion on the significance of the observed brain activity changes related to different activation states and packagings of information items.

The experimental analysis is carried out on EEG signals acquired in the Biometrics and Multimedia Forensics Laboratory using a 19-channels system (GALILEO Be Light amplifier), with an original sampling rate of $S_r = 256$Hz. The database consists of EEG recordings collected from $N = 54$ healthy subjects. EEG signals are recorded during the listening of a text suitably provided to emphasize different activation states and packaging conditions of information. EEG recordings have been time-locked to the listened utterances by means of a synchronization signal which marks each occurrence of a relevant sentence on the raw traces. Ongoing EEG activity lasting four minutes has also been recorded for each subject before the performance of the linguistic task. For further details on the acquisition protocol reference is made to [116]. After a preprocessing following the steps described in Section 3.1, PSD and COH estimates are obtained as reported in Sections 3.3.1 and 3.3.2, respectively, for each EEG epoch time locked to the occurrence of the utterances under analysis. In order to find markers of significant differences between conditions, we separately analyze single channels (and single channel pairs for COH) and predefined Regions Of Interest (ROIs) to find overall differences in brain oscillatory activity. The four contrasts of interest (F/N vs T/N, F/G vs T/G, F/N vs T/G and T/N vs T/G) are addressed performing the *paired-sample t-test* to assess the significance of the observed differences. The effect of packaging and informational status (alignment or misalignment) is tested across all PSD (COH) levels separately for each channel (channel pair) and each ROI using the False Discovery Rate (FDR) method which provides corrected *p-values* for multiple comparisons. We adopt the FDR procedure, which provides a less stringent control over false discovery compared to Family-wise Error Rate (FWER) procedures (such as the Bonferroni correction), since it results more suitable for our study where the great number of variables (frequency bands, channels, channel pairs) would lead to zero the significance level (impossible to reject the *null hypothesis*). Normalized values of PSD and COH with respect to ongoing activity are considered for each contrast. The significant effects are depicted in the following for PSD and COH levels separately.

3.3.4.1 Power Spectrum Analysis

PSD functions are estimated for all subjects and all channels, and mean values are obtained for each brain rhythm computing the average over the related frequency band (δ, θ, α, β and γ up

to40Hz). The significance of the obtained features as markers of language processing efficiency are tested within both a single-channel and a ROI-based analyses.

Single-Channel Analysis

In a first analysis PSD levels are tested independently for each channel in order to find significant differences in the contrasts of interest. In Figures 3.14 and 3.15 the map of the significant changes between conditions (eg. condition F/N and condition T/N for the contrast F/N vs T/N) for each brain rhythm (δ, θ, α, β and γ up to40Hz) are reported in subplots c). The lower and upper values of the 95%-confidence interval on the difference of population means for each contrast are also reported in subplots a) and b), respectively. As shown in Figure 3.14 c) significant differences (FDR corrected p-values≤ 0.05) are observed between the conditions F/N and T/N for the β rhythm in the right centro-parietal region of the head. As can be inferred from the related confidence intervals reported beside, β oscillations present a larger amplitude for the F/N condition compared to the T/N condition. Equally significant differences for the same contrast are observed for the α brain rhythm in the central, parietal and temporal regions. Also in this case we can observe a larger power amplitude for the F/N condition. The results in these two frequency bands suggest a larger Event-Related Desincronization (ERD) for the T/N condition, which could indicate a less efficient processing due to the misalignments between packaging and informational status. This is supposed to determine growing difficulty in integrating information needed for understanding, due to the search for a missing antecedent in prior discourse. In general power of α and β rhythms has been shown to be inversely related to task complexity, attentional and processing demand [117]. Accordingly, in language processing power reduction in the frequency band $[13, 30]$Hz due to phrase structure violation has been linked to an increased involvement of neural resources for sentence processing after mismatch [118]. Furthermore, β ERD over posterior regions has been observed for semantic and prosodic mismatches during language processing [119] and increased difficulty in language integration and comprehension due to semantic incongruence [120], [121].

A less extensive but equally significant difference of PSD features is observed for the contrast F/G vs T/G reported in Figures 3.15, where F/G condition shows a greater left temporal θ power. This suggests a major ERS that could be due to a not met expectation on the organization of information in the sentence. The misalignment is supposed to perturb an efficient information processing involving short-term memory. In general θ synchronization has been linked to increased working memory load [122].

The results reported above suggest specific effects of packaging on the PSD correlates of efficient processing for different informational statuses (New and Given). The specificity of this effect observed in the θ, α and β frequency bands suggests that the two linguistic processing

mechanisms (information encoding and retrieval in working memory) involve different underlying neural subsystems which are differently sensitive to linguistic packaging.

A further contrast is between brain responses to alignment and misalignment, and significant and extensive lower levels of the PSD are observed for the misalignment condition in the β frequency band, as shown in Figure 3.16. A narrow but equally significant difference observed in the α band involves the right temporal region, where the misalignment condition shows lower EEG power. This analysis suggests possible common patterns of power changes in the α and β bands between alignment and misalignment conditions, whatever the informational status.

ROI analysis

A further approach is also carried out to find significant differences between conditions considering brain oscillatory activity in predefined Regions Of Interest (ROIs). For each frequency band 27 features are obtained as reported in Table 3.6, representing EEG power averaged across each region of the head (frontal (F), centro-temporal (C) and parieto-occipital (P) bilateral and hemispheric regions, i.e. considering right(r) and left(l) hemispheres separately), and EEG power gradients between different regions (antero-posterion, controlateral, cross-hemispheric). The same statistical analysis employed within the single-channel approach is performed to test the significance of the so obtained spectral features as markers of language processing efficiency related to information packaging and informational status. The obtained results, reported in Figures 3.17 and 3.18, support some findings discussed for the previous analysis. As shown in Figure 3.17 for the F/N vs T/N contrast significant effects of the packaging of new information are observed on the right central and right parieto-occipital power levels in the β frequency band, higher in the F/N condition. A significant effect is also observed on the right centro-temporal power level in the α frequency band, again higher in the F/N condition.

Accordingly to the single-channel analysis of the contrast F/G vs T/G, a significant difference is detected for the right centro-frontal power gradient within the θ rhythm, higher in the F/G condition. The ROI-based analysis of this contrast also reveals a significant difference for the centro-frontal power gradient within the β band, lower in the F/G condition. It is worth to point out that θ and β rhythms are known to be involved in language processing (including encoding new information [14] and [122]), and to show inverted behavior with respect to processing load [123].

Finally, a result consistent with the previous analysis is observed for the contrast between alignment and misalignment within the ROI-based approach, as shown in Figure 3.19, where lower mean power of the β rhythm in the right hemispheric parieto-occipital region is reported for the misalignment condition. Within the same frequency band also lower right and cross-hemispheric centro-frontal and parieto-frontal power gradients are detected for the misalignment condition.

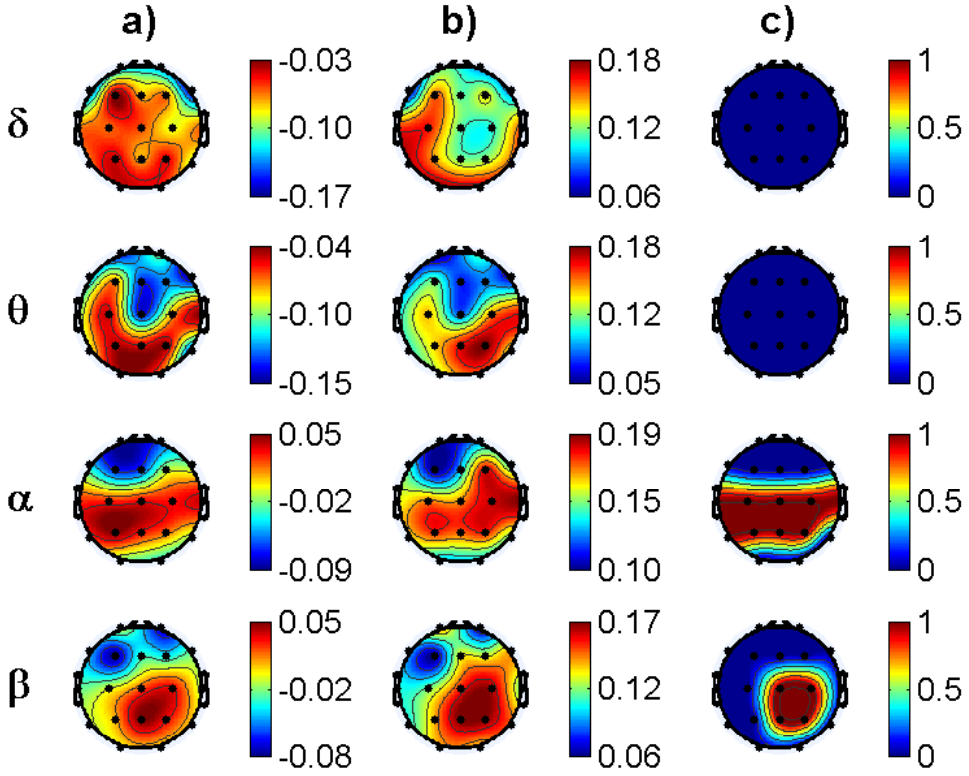

FIGURE 3.14: FNvsTN PSD. The different rhythms $\delta, \theta, \alpha, \beta$ and γ in the subsequent rows. Lower and upper limits of the confidence interval (a) and b)) and map of the significant differences (c) in the subsequent columns.

These results suggest a more rich framework of changes in rhythmic activation patterns, to be further explored in order to infer about the underlying mechanisms.

3.3.4.2 Cross-Spectrum Analysis

Similarly to the analysis performed for the power spectrum features, we estimate COH functions for all subjects and all channels pairs, obtaining normalized mean values for each brain rhythm. Also for these features, which describe the linear dependencies within pairs of channels, we perform a single-element and a ROI-based analysis to test significant changes between the conditions of interest, that would represent different language processing modalities.

Channel-Pair Analysis

The same contrasts of interest discussed above are addressed within the single-element analysis of the COH function. Spectral coherence levels are independently tested for each channel pair and frequency band. The results of this analysis are shown in Figures 3.20 and3.21, for the

Feature	Description
P_F	mean power in the frontal region
P_C	mean power in the cento-temporal region
P_O	mean power in the parieto-occipital region
$P_{F,r}$	mean power in the right hemispheric frontal region
$P_{F,l}$	mean power in the left hemispheric frontal region
$P_{C,r}$	mean power in the right hemispheric centro-temporal region
$P_{C,l}$	mean power in the left hemispheric centro-temporall region
$P_{O,r}$	mean power in the right hemispheric parieto-occipital region
$P_{O,l}$	mean power in the left hemispheric parieto-occipital region
$P_F - P_c$	fronto-central power gradient
$P_F - P_o$	fronto-occipital power gradient
$P_C - P_o$	centro-occipital power gradient
$P_{F,r} - P_{F,l}$	frontal hemispheric power asymmetry
$P_{C,r} - P_{C,l}$	centro-temporal hemispheric power asymmetry
$P_{O,r} - P_{O,l}$	parieto-occipital hemispheric power asymmetry
$P_{F,r} - P_{C,r}$	right fronto-central power gradient
$P_{F,l} - P_{C,l}$	left fronto-central power gradient
$P_{C,r} - P_{O,r}$	right centro-occipital power gradient
$P_{C,l} - P_{O,l}$	left centro-occipital power gradient
$P_{F,r} - P_{O,r}$	right fronto-occipital power gradient
$P_{F,l} - P_{O,l}$	left fronto-occipital power gradient
$P_{F,r} - P_{C,l}$	cross-hemispheric fronto-central power gradient
$P_{F,l} - P_{C,r}$	cross-hemispheric fronto-central power gradient
$P_{C,r} - P_{O,l}$	cross-hemispheric centro-occipital power gradient
$P_{C,l} - P_{O,r}$	cross-hemispheric centro-occipital power gradient
$P_{F,r} - P_{O,l}$	cross-hemispheric fronto-occipital power gradient
$P_{F,l} - P_{O,r}$	cross-hemispheric fronto-occipital power gradient

TABLE 3.6: Regions Of Interest (ROI) PSD.

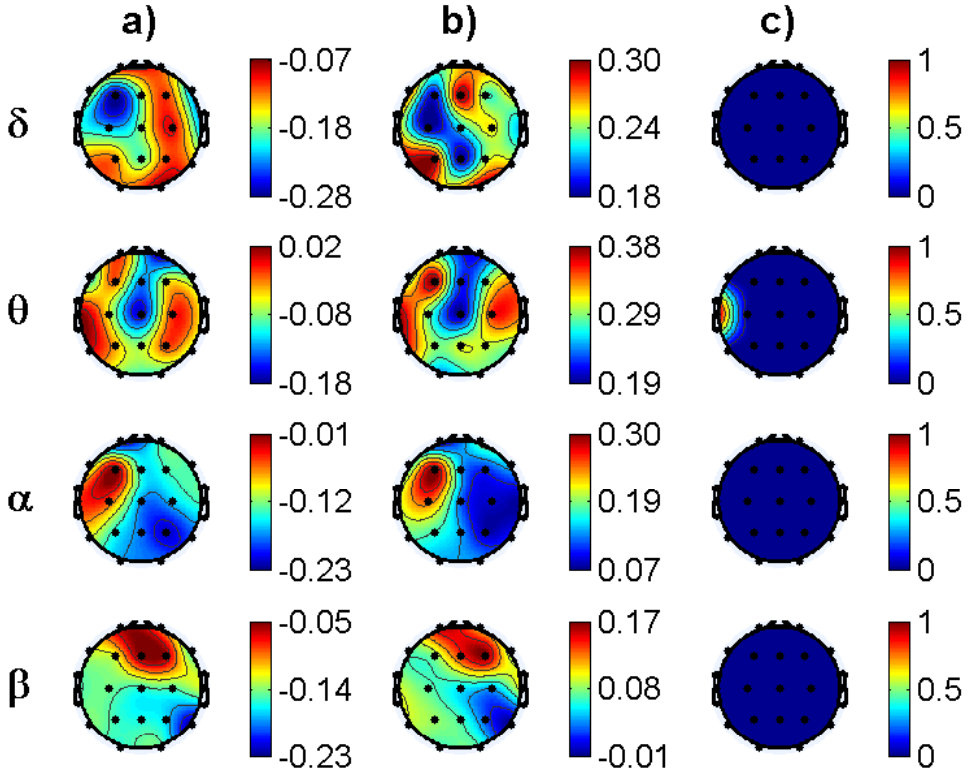

FIGURE 3.15: FGvsTG PSD. The different rhythms $\delta, \theta, \alpha, \beta$ and γ in the subsequent rows. Lower and upper limits of the confidence interval (a) and b)) and map of the significant differences (c) in the subsequent columns.

contrasts F/N vs T/N and F/G vs T/G, respectively. In each figure the significant differences observed in the frequency bands under analysis are reported separately. Subplots c) show the map (distribution across the adjacent matrix $[N_{ch} \times N_{ch}]$ representing all channel pairs) of significant changes between conditions (FDR corrected p-values≤ 0.05), while for each channel pair subplots a) and b) report the lower and upper values of the 95%-confidence interval on the difference of population means, respectively. In Figure 3.20 referring to the contrast F/N vs T/N a significant effect of language packaging can be observed for specific channel pairs in all frequency bands. In particular, the analysis of the connectivity maps reveals that the T/N condition shows significant differences with respect to the F/N condition, such as a greater frontal controlateral $Fp_2 - F_7$ coherence level and lower left posterior (involving temporal region T_3) and centro-occipital ($C_z - O_1$ and $C_z - O_2$) coherence levels in the δ band; greater long-range cross-hemispheric coherence involving the frontal region Fp_2, and lower right posterior and fronto-occipital ($C_z - P_z$) levels in the α band; lower ipsilateral long-range (antero-posterior) connectivity and cross-hemispheric fronto-temporal ($F_8 - T_3$) level in the β band.

As regards the significant differences within the contrast F/G vs T/G (Figure 3.21), we can notice that the T/G condition shows lower left ipsilateral short-range coherence involving region C_3,

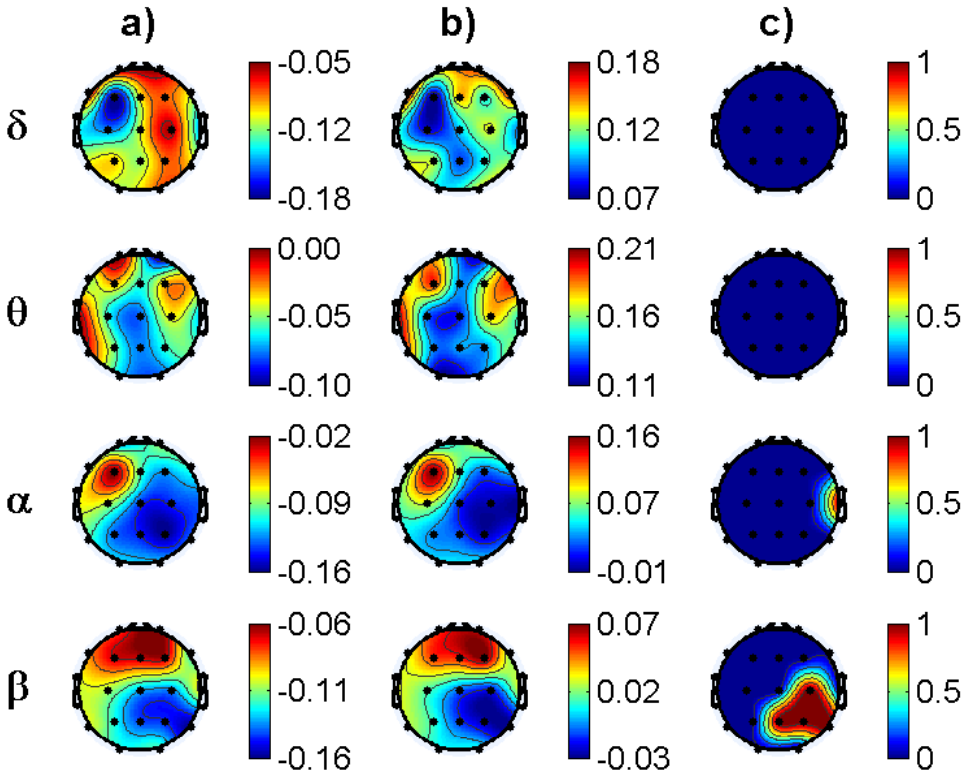

FIGURE 3.16: Misalignment vs Alignment PSD. The different rhythms $\delta, \theta, \alpha, \beta$ and γ in the subsequent rows. Lower and upper limits of the confidence interval (a) and b)) and map of the significant differences (c) in the subsequent columns.

and right short-range fronto-temporal ($F_8 - T_4$) coherence in the θ band. In the α and β bands the T/G condition shows a significant greater posterior connectivity involving the right temporal region T_4. In the β band we also observe a greater central and centro-posterior coherence for the T/G, and a greater cross-hemispheric fronto-parietal ($Fp_2 - P_3$) coherence for the F/G condition.

It should be noticed that previous literature has shown that the processing of different kind of sentences elicit different coherence patterns in different frequency bands, possibly reflecting various aspects of sentence understanding like memory, semantic and syntactic integration, parsing and so on [124]. In particular COH increase in the "slow" frequency range (especially involving θ band) has been shown to correlate to increased demand on working memory during sentence processing [125]. On the other hand, coherence increase in the higher frequency range (especially involving the β rhythm) seems to be related to efficient semantic integration and parsing processes (higher for congruous than non-congruous sentences) [121]. Moreover complex language stimuli have shown to increase right hemispheric involvement [126].

Given those findings our results suggest a main involvement of semantic and syntactic integration processes in the differences observed for the contrast F/N vs T/N. In this regard, given the results in the α and β bands, the F/N condition seems to lead a more efficient information

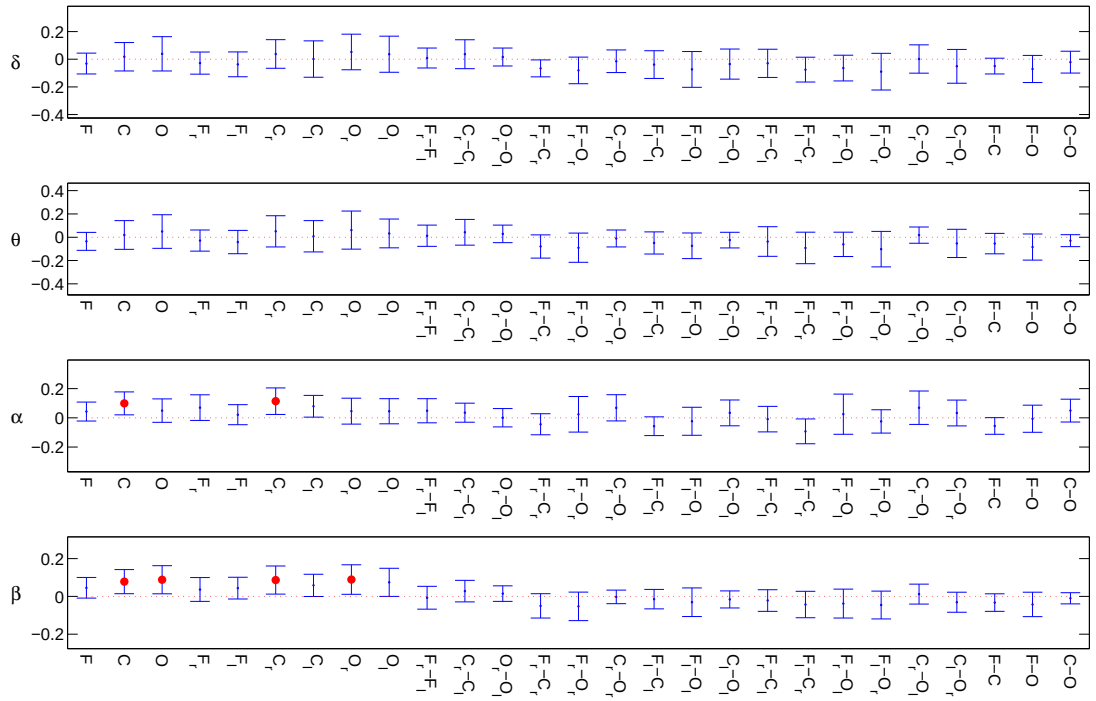

FIGURE 3.17: FNvsTN PSD ROI. The different rhythms $\delta, \theta, \alpha, \beta$ and γ in the subsequent rows. Lower and upper limits of the confidence interval in the vertical bars. Different tested features (PSD values within and between ROIs) on the x-axis. Red spots highlighting significant differences.

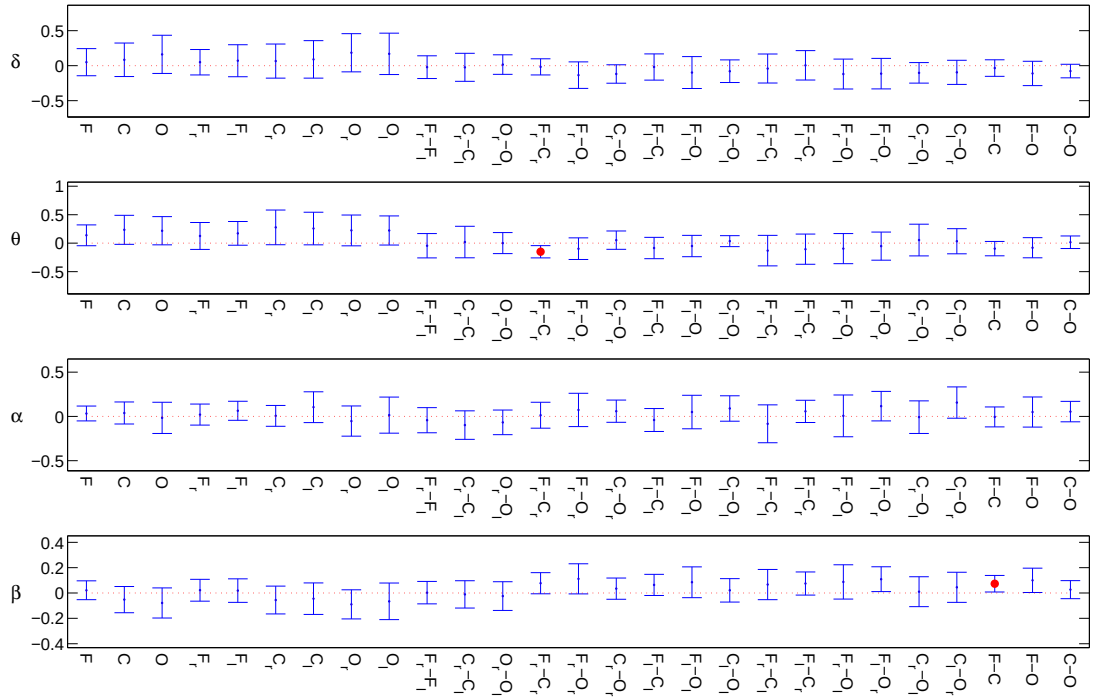

FIGURE 3.18: FGvsTG PSD ROI. The different rhythms $\delta, \theta, \alpha, \beta$ and γ in the subsequent rows. Lower and upper limits of the confidence interval in the vertical bars. Different tested features (PSD values within and between ROIs) on the x-axis. Red spots highlighting significant differences.

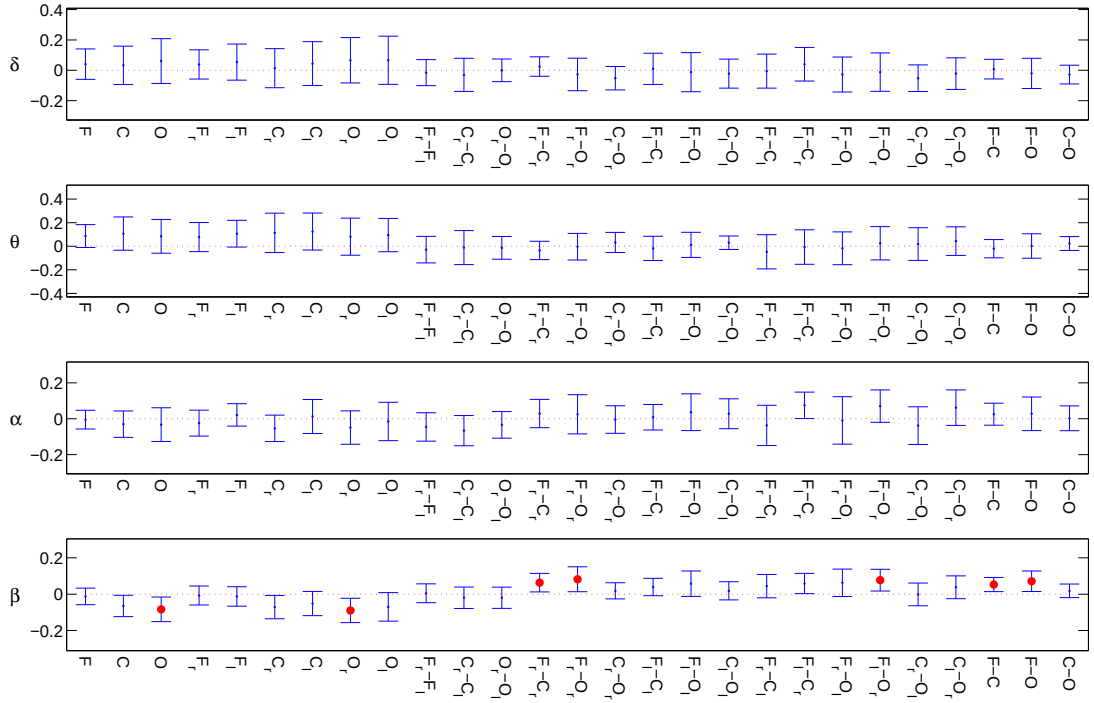

FIGURE 3.19: Misalignment vs Alignment PSD ROI. The different rhythms $\delta, \theta, \alpha, \beta$ and γ in the subsequent rows. Lower and upper limits of the confidence interval in the vertical bars. Different tested features (PSD values within and between ROIs) on the x-axis. Red spots highlighting significant differences.

processing. A further involvement of specific working memory processes in the T/G vs F/G differences is suggested by the related results in the θ band. This is in accordance with the evidence that given information require retrieval processes involving working memory.

As for the PSD analysis, the same contrast is performed between brain responses to alignment and misalignment, and significant lower levels of the COH are observed in the posterior region for the misalignment condition in the β frequency band, mainly involving right centro-temporal and occipital regions C_4, T_4, T_6 and O_1, as shown in Figure 3.16. A similar but less broad result is observed in the α band for the posterior connectivity levels involving the same regions. Fewer COH patterns showing more strength for the alignment condition are observed in the α and β bands involving antero-posterior long-range cross-hemispheric connectivity. Slow waves (δ and θ frequency bands) show more strength of few short range intra-hemispheric COH patterns ($T_4 - P_4$ for δ rhythm; frontal COH, $C_3 - O_1$ and $P_3 - O_1$ for θ rhythm) for the misalignment condition. These findings support the discussion reported on the analysis of single contrasts, and highlight common pattern of significant changes between alignment and misalignment conditions, beyond the differences observed in specific contrasts.

ROI analysis

The same approach carried out for the analysis of PSD data is adopted to investigate the effect of information structure on coherence levels within and between predetermined ROIs. Following the analogous definitions reported in Table 3.6 for PSD, we extract 46 COH features (9 within-region coherence levels, 3 between-region coherence levels, 15 antero-posterior coherence gradients, 3 controlateral coherence asimmetries, 12 cross-hemispheric and ipsilateral antero-posterior long- and mid-range coherence levels, and 4 controlateral coherence levels) to be tested. The results shown in Figures 3.23 and 3.24 support the observations provided within the channel-pairs analysis.

Specifically, as shown in Figure 3.23, in the δ band a greater coherence in the C_l region and a lower value in the F region, together with a greater left centro-occipital (CO_l) COH, are found for F/N compared to T/N. Within the same contrast F/N shows a geater right centro-occipital (CO_r) COH in the β band.

For the contrast F/G vs T/G reported in Figure 3.24, in the θ band we observe a greater coherence in C_l, O_l and CO_l, and a lower value in O_r for F/G (accordingly, lower gradients $C_r - C_l$ and $O_r - C_l$). Also in the α band we find a lower $C_r - C_l$ gradient for F/G. The β rhythm shows lower F, inter-hemispheric C_rC_l, right and cross-hemispheric CO mean coherence for the F/G condition.

A further analysis on the contrast between alignment and misalignment conditions, similar to those performed for the previously discussed features, is carried out to identify patterns of COH between ROIs typical of the misalignment/alignment contrast. The result reported in Figure 3.25 shows that the significant differences involve mainly the β rhythm in the centro-posterior region of the head, accordingly to previously discussed channel-pairs and ROI-based analyses. In particular lower values of β COH are observed for the misalignment conditions in the right centro-occipital (CO_r), controlateral central (C_rC_l), cross-hemispheric centro-occipital (C_rO_l) and fronto-central (FC) patterns. It should be noticed that the right central, temporal and parietal regions appear more involved in the significant differences observed between alignment and misalignment within the β rhythm, compared to the respective controlateral regions. Accordingly to the channel-pairs analysis, a less broad but significant difference in the CO_r COH (weaker for misalignment) is observed also within the α band. On the other hand θ left centro-occipital (CO_l) COH appears stronger for the misalignment condition, supporting the same reverse trend observed in the previous analysis of the this study.

The results of the ROI-based analysis suggest some notable aspects of the complex framework representing the differences of COH patterns between conditions, in accordance with related findings in previous literature.

Feature	Description
P_f	mean coherence in the frontal region
P_c	mean coherence in the cento-temporal region
P_o	mean coherence in the parieto-occipital region
$P_{f,r}$	mean coherence in the right hemispheric frontal region
$P_{f,l}$	mean coherence in the left hemispheric frontal region
$P_{c,r}$	mean coherence in the right hemispheric centro-temporal region
$P_{c,l}$	mean coherence in the left hemispheric centro-temporall region
$P_{o,r}$	mean coherence in the right hemispheric parieto-occipital region
$P_{o,l}$	mean coherence in the left hemispheric parieto-occipital region
$P_f - P_c$	fronto-central coherence gradient
$P_f - P_o$	fronto-occipital coherence gradient
$P_c - P_o$	centro-occipital coherence gradient
$P_{f,r} - P_{f,l}$	frontal hemispheric coherence asymmetry
$P_{c,r} - P_{c,l}$	centro-temporal hemispheric coherence asymmetry
$P_{o,r} - P_{o,l}$	parieto-occipital hemispheric coherence asymmetry
$P_{f,r} - P_{c,r}$	right fronto-central coherence gradient
$P_{f,l} - P_{c,l}$	left fronto-central coherence gradient
$P_{c,r} - P_{o,r}$	right centro-occipital coherence gradient
$P_{c,l} - P_{o,l}$	left centro-occipital coherence gradient
$P_{f,r} - P_{o,r}$	right fronto-occipital coherence gradient
$P_{f,l} - P_{o,l}$	left fronto-occipital coherence gradient
$P_{f,r} - P_{c,l}$	cross-hemispheric fronto-central coherence gradient
$P_{f,l} - P_{c,r}$	cross-hemispheric fronto-central coherence gradient
$P_{c,r} - P_{o,l}$	cross-hemispheric centro-occipital coherence gradient
$P_{c,l} - P_{o,r}$	cross-hemispheric centro-occipital coherence gradient
$P_{f,r} - P_{o,l}$	cross-hemispheric fronto-occipital coherence gradient
$P_{f,l} - P_{o,r}$	cross-hemispheric fronto-occipital coherence gradient

TABLE 3.7: Regions Of Interest (ROI) COH

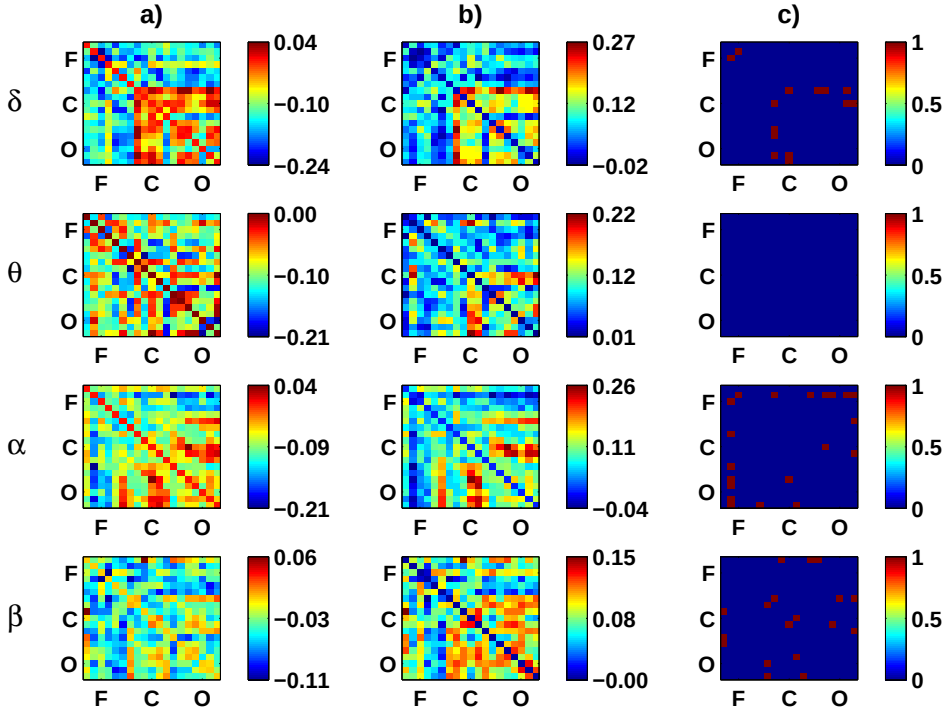

FIGURE 3.20: FNvsTN COH. The different rhythms $\delta, \theta, \alpha, \beta$ and γ in the subsequent rows. Lower and upper limits of the confidence interval (a) and b)) and map of the significant differences (c) in the subsequent columns.

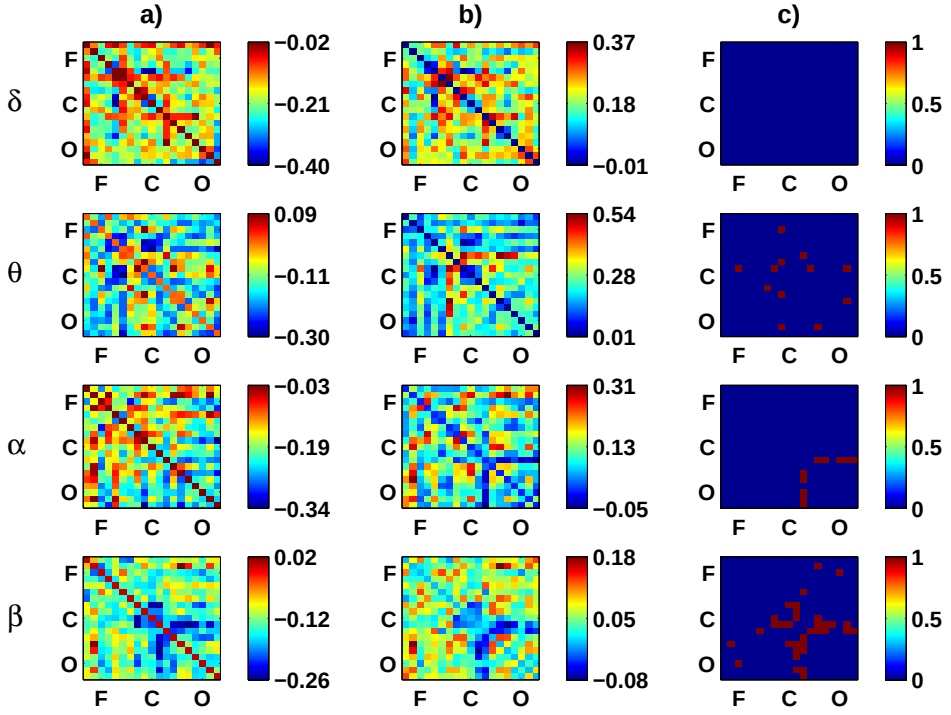

FIGURE 3.21: FGvsTG COH. The different rhythms $\delta, \theta, \alpha, \beta$ and γ in the subsequent rows. Lower and upper limits of the confidence interval (a) and b)) and map of the significant differences (c) in the subsequent columns.

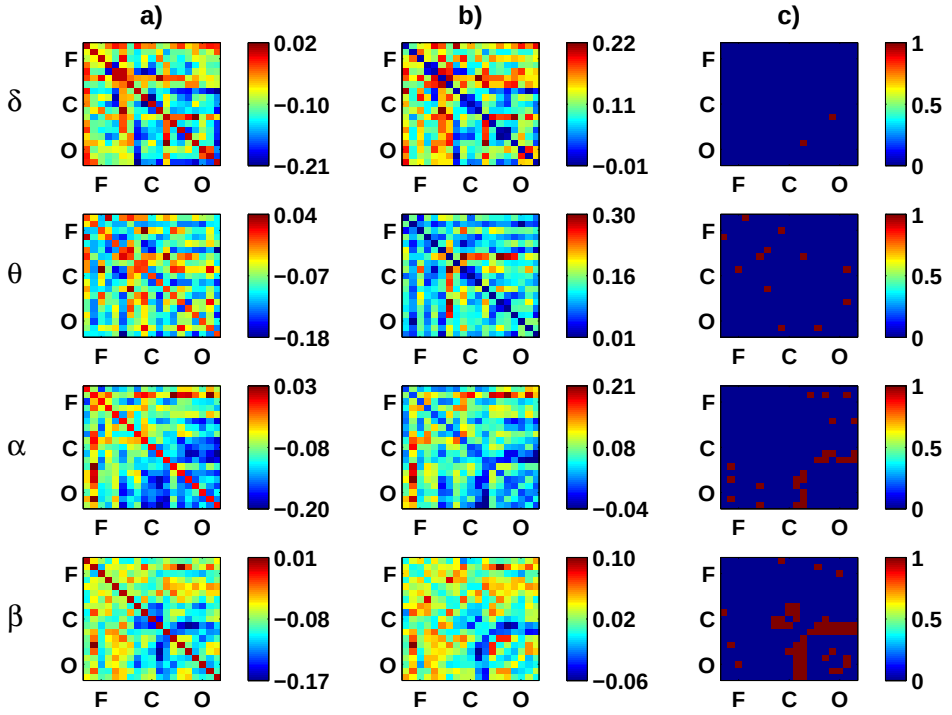

FIGURE 3.22: Misalignment vs Alignment COH. The different rhythms $\delta, \theta, \alpha, \beta$ and γ in the subsequent rows. Lower and upper limits of the confidence interval (a) and b)) and map of the significant differences (c) in the subsequent columns.

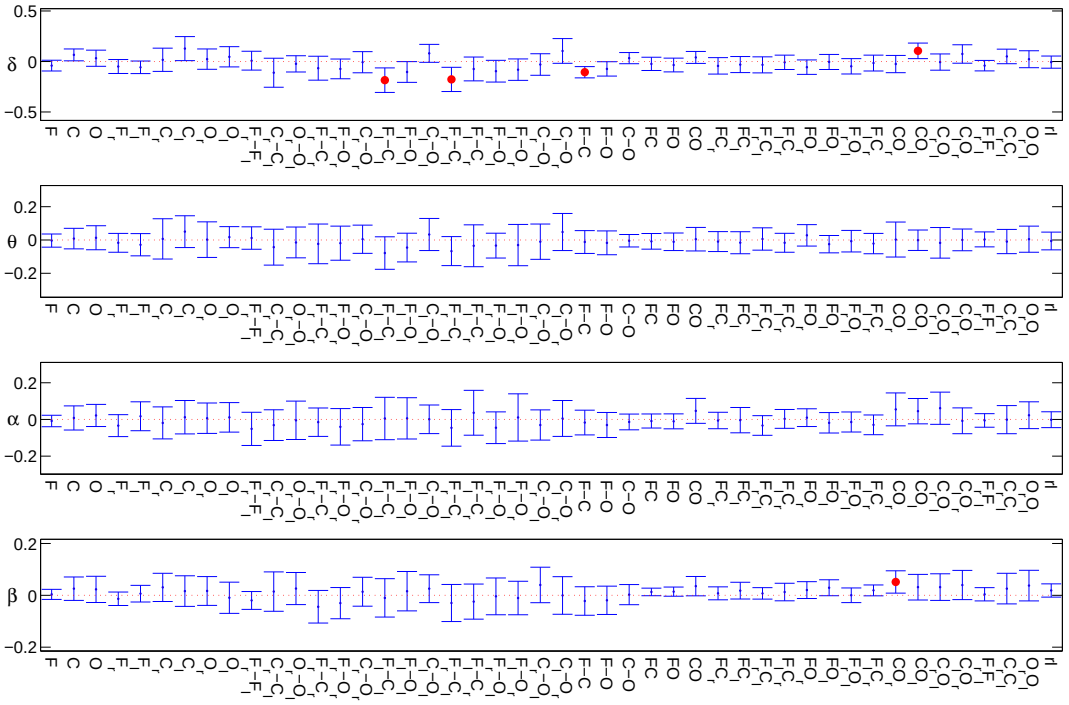

FIGURE 3.23: FNvsTN COH ROI. The different rhythms $\delta, \theta, \alpha, \beta$ and γ in the subsequent rows. Lower and upper limits of the confidence interval in the vertical bars. Different tested features (COH values within and between ROIs) on the x-axis. Red spots highlighting significant differences.

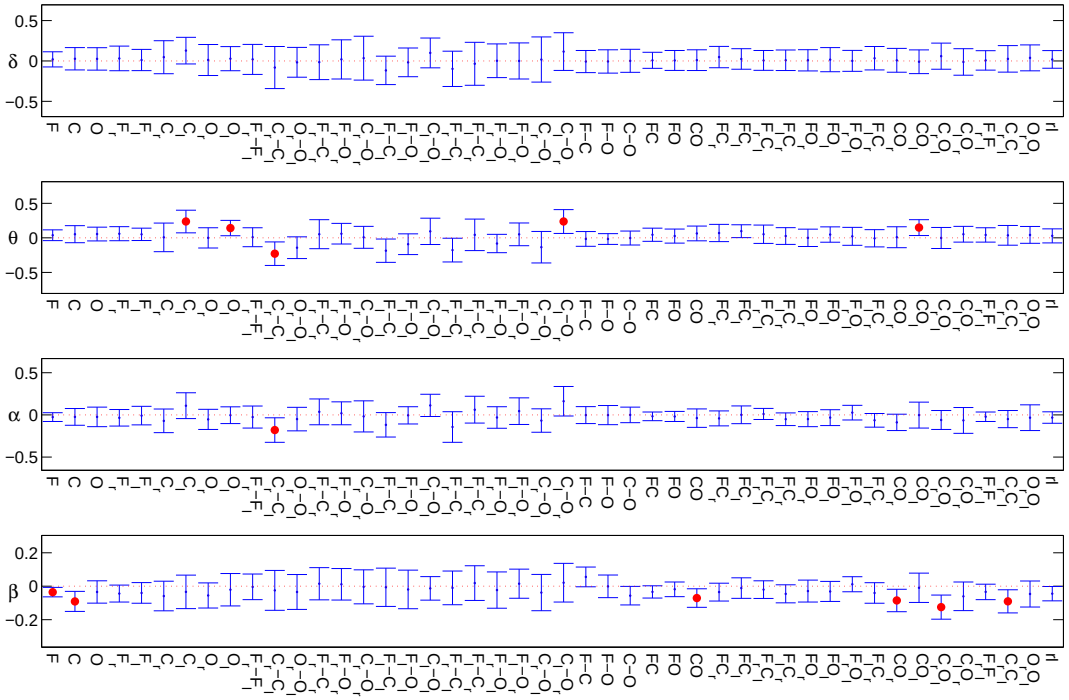

FIGURE 3.24: FGvsTG COH ROI. The different rhythms $\delta, \theta, \alpha, \beta$ and γ in the subsequent rows. Lower and upper limits of the confidence interval in the vertical bars. Different tested features (COH values within and between ROIs) on the x-axis. Red spots highlighting significant differences.

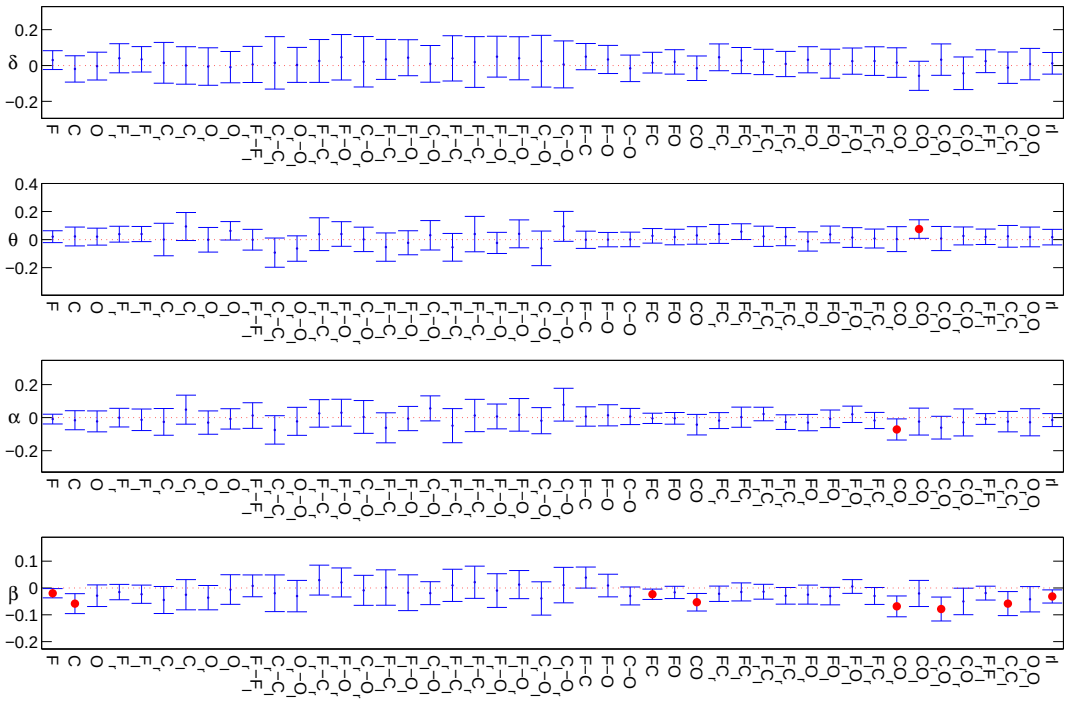

FIGURE 3.25: Misalignment vs Alignment COH ROI. The different rhythms $\delta, \theta, \alpha, \beta$ and γ in the subsequent rows. Lower and upper limits of the confidence interval in the vertical bars. Different tested features (COH values within and between ROIs) on the x-axis. Red spots highlighting significant differences.

Chapter 4

Longitudinal Dataset

4.1 Main issue in EEG biometric context

Among the studies proposed so far on the research of distinctive patterns in EEG signals, very few works employ a longitudinal dataset, i.e. a dataset containing several EEG recordings for each subject acquired on different days. Nevertheless this is an aspect of primary importance in order to evaluate individual-specific features in EEG signals for biometric recognition purpose.

Most of the works in literature analyze signals recorded within Brain Computer Interface (BCI) contexts. Typically these datasets provide a single acquisition session for each subject. In general, different partitions are obtained from the same recording to generate the enrolling and the test samples. It is worth to point out that this procedure prevents to determine whether the system's accuracy evaluates features specific of each individual or typical of each acquisition/recording session.

In fact, as mentioned in Section 1, EEG signals are affected by physiological and exogenous noise. The latter can be responsible for erroneous interpretations of the performance of a byometric systems based on single EEG-aqcuisition sessions.

Some of the issues preventing to test the permanence of EEG features for biometric applications are the lack of publicly available longitudinal datasets, and the difficulties to assort a database of statistically significant dimension.

Nonetheless, the research of repeatabile and individual-specific EEG patterns is supported by the results of neurophysiology studies on genetic influence in brain signals [58] and on test-retest reliability in EEG analysis [45].

Recently an attempt to consider the repeatability of EEG features for biometric applications has been shown in some works, performing several acquisitions on different days for each subjects.

In [76] a biometric system was evaluated on 10 subjects, who underwent 5 acquisition sessions. In that work EEG segments of n seconds were randomly selected among the 5 recordings to assort the enrollment and the test subsets, so that the information about the acquisition session was not considered. Authors obtained a Correct Recognition Rate (CRR) of 97% considering the Auto Regressive (AR) coefficients as features.

Also the dataset employed in [73] was considered to randomly assort the enrollment and the test subsets in an EEG-based identification system. In that work 2 resting state recordings were acquired on 2 separate days for each of the 40 subjects, and a CRR of 95% was obtained considering spectral features. It should be noticed that, due to the shuffling procedure, also in this case the enrollment and test samples didn't belong to different recording sessions/days.

The same approach can be observed in [81], where an EEG-based authentication system was tested on 5 subjects who underwent 5 recording sessions on 5 different days. Again the database was randomly split into enrollment and test subset to evaluate the recognition accuracy. The authors extracted AR coefficients as feature vectors and obtained a False Rejection Rate (FRR) in the range of $[1.5 - 0]\%$ depending on the subject, and a null False Acceptance Rate (FAR) for all subjects.

In [82] Marcel and Millan first considered enrollment and test performed on different acquisition sessions. They tested 9 subjects, each of them recorded on 3 different days during an imagination task. The obtained Half Total Error Rate (HTER) for spectral features ranged in $[19.3, 36, 2]\%$ when considering training/validation and evaluation on different days. Authors observed that robust models needed incremental learning on subsequent days.

Later Riera et al. [72] tested 51 subjects recorded in resting conditions on 4 separate days. They obtained the best result of Equal Error Rate (EER) of $3, 4\%$ in an EEG-based identity verification system, using a combination of features and classifiers, where the decision was taken on 1-minute EEG segments. In the same work the best accuracy obtained within an identification approach was a CRR of $94, 5\%$.

Also Brigham and Vijayakumar in [48] proposed a biomeetric EEG-recognition system based on an imagination task performed by 6 subjects, each of them recorded on different days. AR features were employed, and all combinations of enrolling and test sessions were considered to test the system. Given the deterioration of accuracy compared to other tests where all sessions randomly assorted the enrollment and test subsets, the authors observed that the employed features were most likely not fully stationary with respect to time.

More recently in [49] 9 subjects, each recorded on 2 different days, were tested in an identification framework where enrollment and test trials of 1-second length belonged to different sessions. A perfect recognition rate was there obtained employing AR features.

Paper	Protocol	Database	Channels	Features	Classifier	Performance	sessions
Riera et al. [72]	EC	51	2 (FP1, FP2)	AR (100th) & DFT MI&Coh.&CC	DA	EER=3.4%	4
Su et al. [73]	EC	40	1 (FP1)	PDS	k-NN	CRR=97.5%	2
La Rocca et al. [49]	EC/EO	9	3, 5	AR	LDA	CRR=100%	2
Abdullah et al. [76]	EC/EO	10	4	AR	NN	CRR=97%	5
Palaniappan [81]	Mental tasks	5	6 P-O	AR, PSD, synchr., entropy	Manh. dist.	FRR==1.5-0% FAR=0%	5
Marcel and Millán [82]	MI	9	8 C-P	GMM	MAP	HTER=8.1%-12.3%	3
	Word gen.	9	8 C-P	GMM	MAP	HTER=12.1%	1
Brigham and Vijaya Kumar [48]	SI	6	128	AR (2nd)	SVM	GAR=99.76%	4
	VEP	120	64	AR (4th)	SVM	GAR=98.96%	4

TABLE 4.1: State-of-the-art contributions using EEG signals as a biometrics, and investigating multi-session datasets.

The reported works, summarized in 4.1, demonstrate the potentials of EEG signals to be used in real-life biometric scenarios where enrollment and recognition are different processes. The few works in literature also suggest the need for an effort to systematically study the repeatability of subject-specific EEG features.

4.1.1 The EEG longitudinal database

In order to address the repeatability of distinctive EEG features, required to assess the feasibility of an EEG-based biometric recognition system, scalp EEG signals have been acquired within the present work of doctoral thesis in the Biometrics and Multimedia Forensics Laboratory using a 19−channels system (GALILEO Be Light amplifier), shown in Figure 4.1.

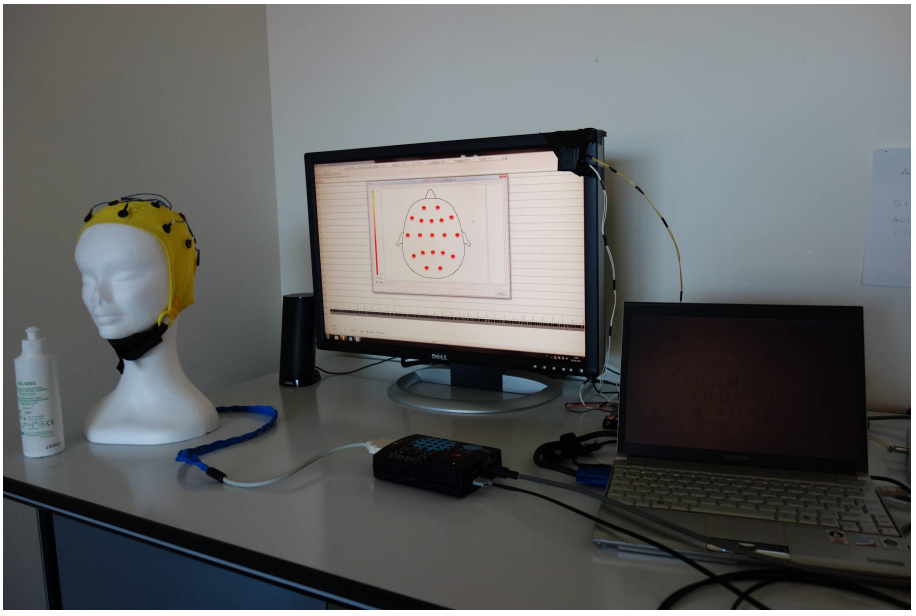

û

FIGURE 4.1: EB Neuro Galileo BE Light acquisition system.

The database consists of EEG recordings collected with an original sampling rate of 256Hz from $N = 60$ healthy subjects, whose ages range from 20 to 35 years old. The considered population contains 40 male and 8 female subjects. During each EEG acquisition, subjects are comfortably seated on a chair in a dimly lit room and asked to perform specific tasks.

For the signal detection, the 19 electrodes are placed on the scalp according to the standard $10-20$ montage (see Figure 1.1), and the electrical impedance of each electrode is kept under 10 kΩ using conductive gel at the beginning of each acquisition. The EEG measures are referenced to the AFz position. The headset and the material used are shown in Figure 4.2.

The EEG signals of the considered subjects are collected during five distinct acquisition sessions, indicated in the following as S1, S2, S3, S4 and S5. Specifically, having performed the first recording of EEG signals at t_1 during S1, for each subject the second session S2 is performed at $t_2 = t_1 + 1$ week; the third set of acquisitions for S3 is carried at $t_3 = t_1 + 1$ month; the forth acquisition for S4 is performed at $t_4 = t_1 + 6$ months and the last fifth acquisition for S5 at $t_5 = t_1 + 1$ year. This time scheme was adopted in order to infer about short-, mid- and long-range repeatability, relative to the considered time interval.

It has to be remarked that the enrolled subjects didn't had to attend any restriction regarding the activities they could have carried out or the diet they should have followed, neither between an EEG acquisition and the following one, nor during the days of the recordings. Such freedom has been allowed in order to process data acquired in conditions as close as possible to those associated with an actual use of EEG signals for practical biometric recognition applications.

4.1.2 tasks

During the recording session each subject was asked to subsequently perform different tasks. Each acquisition protocol was designed to emphasize specific mental states, cognitive and sensory processes that are supposed to show distinctive features for each individual. The performed tasks and conditions include RS, MI, SI, P300 elicitation and mental calculation.

The stimulation protocols, the cues for the performance timing and all instruction for the subjects have been implemented using the software BCI2000 [127]. The specific protocols are detailed in the following.

- **Rest**. Two resting conditions are performed by the subjects, namely with eyes open and closed. Each recording lasts 4 minutes. For the eyes-open condition a green cross shown in Figure 4.3 is continuously presented on the display and the enrolled subject has to fix it in order to reduce eyes movements.

FIGURE 4.2: Headset composed of 19 electrodes used for acquisitions.

- **MI**. According to this protocol subjects have to perform the imagination of hands and feet movements. In particular when a cue is presented to the subject he/she has to imagine the sensation of moving the specified limb for 3 seconds (one trial). The inter-trial interval is set to $1s$. Two upper arrows are used to indicate right and left hands movements, while lower arrows point feet movements, as shown in Figure 4.4. 10 runs are provided, each containing 5 sequences of the 4 imaginary movements (trials) to be performed. The interval between the runs is set to 6 seconds, to allow rest. This protocol lasts around 20

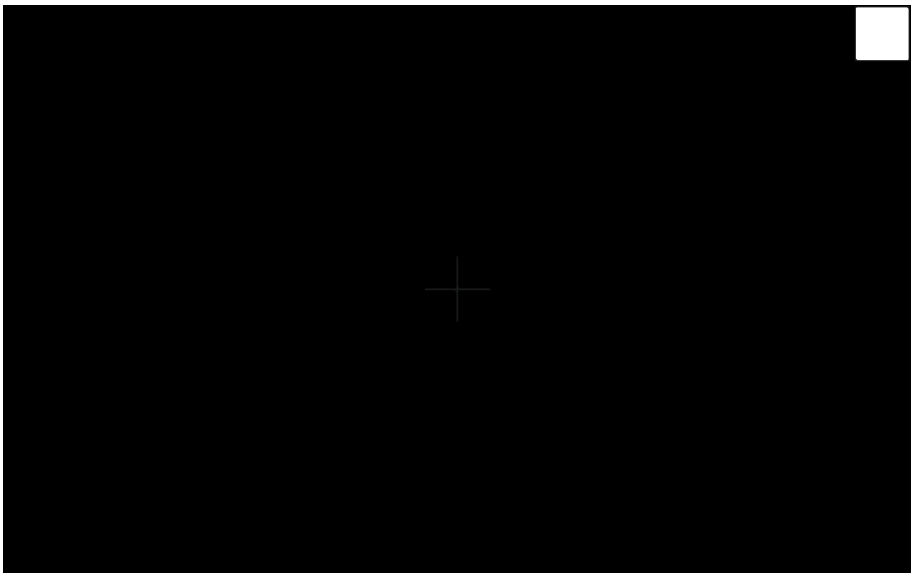

FIGURE 4.3: Green cross to be fixed during rest with eyes open, to avoid eyes' movement.

minutes.

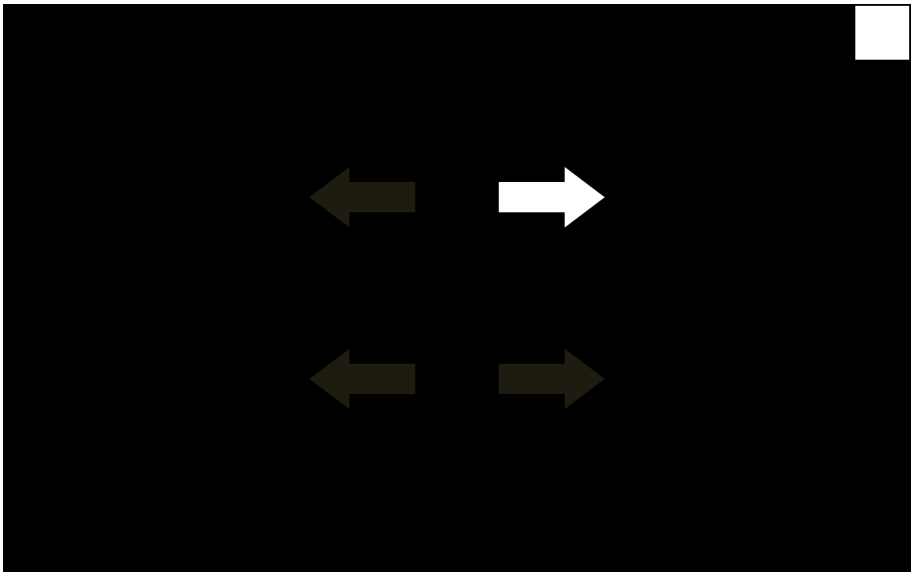

FIGURE 4.4: Frame of the MI task.

- **SI**. Similarly to what performed for the MI protocol, this one consists in imagining the pronunciation of vowels. When a vowel is presented at the center of the display to the subject, as shown in Figure 4.5, he/she has to imagine the sensation of pronouncing the specified phoneme for 3 seconds (one trial). The timing of this protocol is the same as the previous one, but each sequence contains 5 trials to perform (one trial for each vowel) and each run is composed of 2 sequences.This protocol lasts around 15 minutes.

- **ERP Elicitation**. During this protocol an oddball paradigm is adopted to elicit the P300 event-related brain response (see Section 1.2.1). In particular 8 different geometric shapes

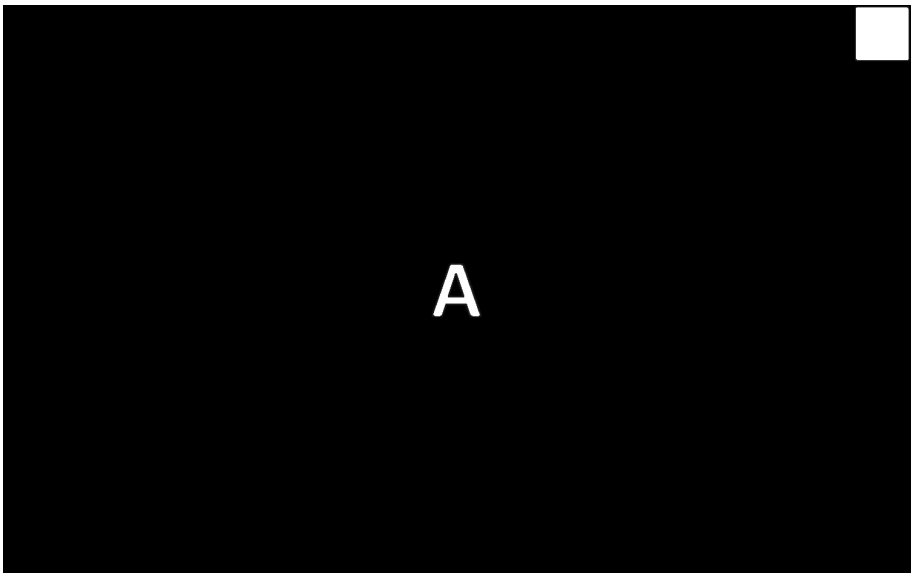

FIGURE 4.5: Frame of the SI task.

are presented at the center of the display, as shown in Figure 4.6, and the subjects are instructed to focus on the detection of the circle among them. According to this sequence the circle represents the target infrequent stimulus in the oddball paradigm, and it elicits the P300 potential. Each trial is composed of one stimulus lasting $350ms$ and the inter-trial interval is set to $350ms$. 20 trials for each stimulus are randomly presented to assort a sequence. This protocol lasts around 10 minutes. A similar protocol is also performed using letters as frequent stimuli and numbers as infrequent target stimuli.

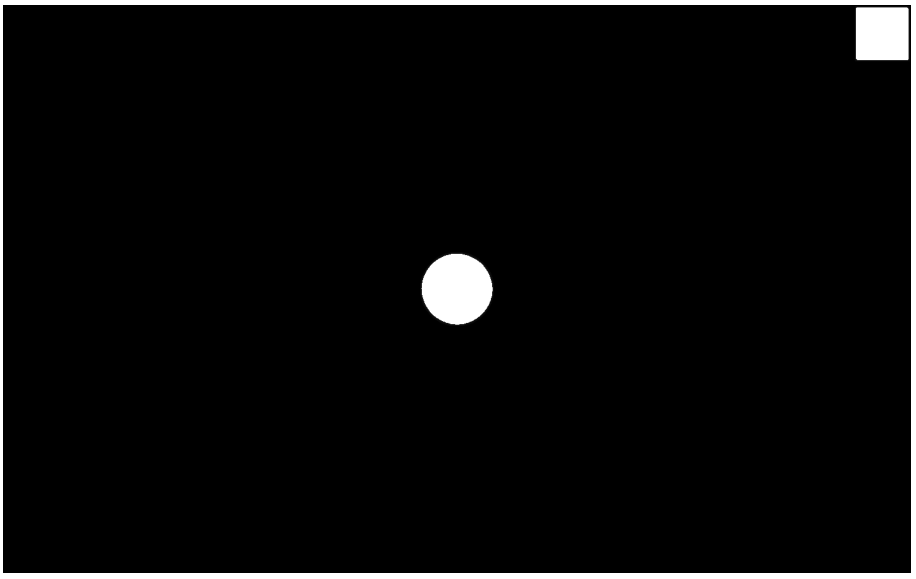

FIGURE 4.6: Frame of the oddball (P300) task.

- **Mental Calculation**. This protocol consists in performing mental algebraic summation between couples of integer (20 trials) or decimal (28 trials) numbers. Summands are shown at the center of the display, and they are horizontally (for integers) or vertically (for

decimals) aligned as shown in Figures 4.8and4.7, respectively. Each trial lasts $6s$ during which the enrolled subject has to mentally perform the result. The inter-trial interval is set to $3s$ to allow resting and just one sequence is provided. This protocol lasts around 7 minutes.

FIGURE 4.7: Frame of the mental calculation task for algebraic sum of integer numbers.

FIGURE 4.8: Frame of the mental calculation task for algebraic sum of decimal numbers.

The synchronization between the recorded EEG traces and the specific protocol timing has been provided through a trigger generator device based on a photodiode, implemented in our laboratory and placed as shown in Figure 4.9 on the upper-right corner of the display used to present stimulus sequences and instructions. The pixels in the area under the photodiode are switched on when a stimulus or cue is presented, producing an output current. A resistor is then calibrated to collect a proper voltage signal. This device detects the timing of each acquisition protocol

and send the obtained trigger voltage signal to the amplifier. This signal is conveyed on a digital acquisition channel (the 20th in the GALILEO system) and stored jointly to the EEG signals, identifying segments on the raw traces time-locked with cues or stimuli.

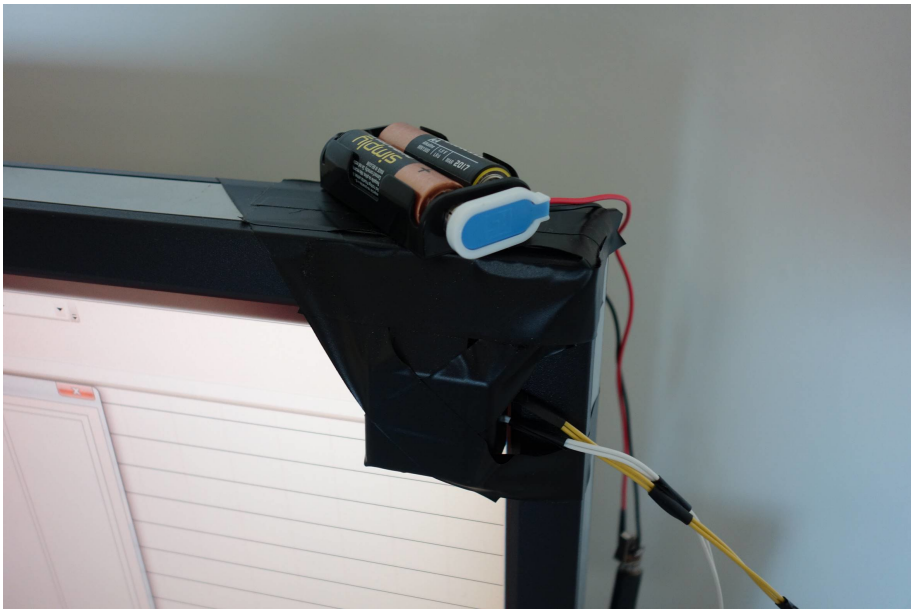

FIGURE 4.9: Photodiode used to implement the trigger system.

The RS collected database is analyzed within the system described in the following chapter. The other protocols performed are the subject of current investigations.

Chapter 5

Pattern Recognition/Classification

In this chapter different classification approaches are reported, as used in the present work to predict the class, namely the subject identity, to which the observed feature vector belongs. We separately consider approaches based on metrics and on machine learning algorithms. Metric-based approaches have the advantage to be less time consuming straightforward methods providing an immediate interpretation of the resulting scores (precisely distances). On the other hand the exploitation of the advances of machine learning allows to automatically reveal information about particular aspects of the structure of the data by means of intelligent classifiers.

5.1 Metric-based Approach

The model we use for the discriminant analysis based on metrics assumes that the feature vectors χ form a Gaussian mixture distribution. For this reason, before the classification, we apply a proper transformation to the data depending on the computed features vectors, as pointed out in Sections 3.3.1 and 3.3.2 for PSD and COH, respectively.

One of the methods implemented to to perform pattern recognition using a simple metric approach is the Mahalanobis distance-based classifier. This method is a second order metric-based classifier as it requires the computation of the covariance matrix of the feature vectors of each class. Nevertheless, when few observations are given for each subject the covariance matrices cannot be robustly computed. In these cases a common procedure consisting in the simplification to equal covariance matrices [97] is typically adopted. Specifically, a pooled covariance matrix is obtained by merging the class-specific distributions of the feature vectors after removing their mean value. Notably, a previous normalizing transformation applied to the feature vector distribution supports such approximation. Within this work of doctoral thesis, to perform biometric recognition employing the Mahalanobis based classifier a partition k ($0 \leq k \leq T$) of

the $T \times N$ normalized feature vectors extracted from the dataset under analysis is used to enroll the subjects and generate templates representing the class distributions.

A cross-validation framework is then considered to assess the recognition performance. In each cross-validation run, for each subject i, kNT epochs are used to generate the class distributions (i.e. enrollment phase), while the remaining epochs are employed to perform the recognition (i.e. test phase). A number r of runs are provided, considering all possible partitions (leave-one-out framework). The Mahalanobis distances are computed between each observation $m, m = 1, \ldots, (1-k)NT$ in the test dataset, and the class distributions i obtained in the enrolling, according to the formula:

$$d_{m,i} = (\chi_m - \mu_i)\Sigma_N^{-1}(\chi_m - \mu_i)^T \tag{5.1}$$

with $i = 1, \cdots, N$, N being the number of classes (subjects), χ_m the observed feature vector from subject m, μ_n the mean vector for the class distribution n, and Σ the covariance matrix.

A misclassification (or confusion) matrix $\mathbf{M}$ can be used to evaluate the recognition performance for the identification scenario, where the aim is to assess the identity of the user comparing the matching scores of the template of all the subjects enrolled in the systems. Each column of this $N \times N$ matrix represents the instances in a predicted subject identity (i.e. class), while each row represents the instances in an actual class. For a given test observation m, the predicted subject identity $\hat{i}$ is obtained according to:

$$\hat{i} = \arg\min_i d_{m,i}. \tag{5.2}$$

Eventually, for each run the correct recognition rate (CRR) is defined as the average over the diagonal of the resulting misclassification matrix $\mathbf{M}$:

$$\text{CRR} = \left(\frac{1}{N} \sum_{i=1}^{N} M[i,i] \right) \times 100. \tag{5.3}$$

The results obtained adopting the Mahalanobis distance-based classifier are shown in the next section, compared to those achieved using a machine learning method implemented to improve recognition performance. This metric-based classification approach has also been employed to obtain the results discussed in Chapter 3 focused on feature engineering techniques.

5.2 Machine Learning Approach

An approach based on machine learning is implemented within the present work in order to improve the performance of the classification algorithm. Given N sample sequences $\chi_{i,\tau}$ (feature vectors) for the enrollment, where $\chi_{i,\tau} \in \mathbb{R}^d$, the goal is to learn F_i, $i = \dots N$ such that

$$F_i(\chi_{i,\tau}) \text{ sufficiently often different from } F_i(\chi_{j,\tau'}), \forall j \neq i$$

This might be expressed as an optimization problem where the goal is to find F_i, a_i, b_i, with $[a_i, b_i]$ an interval in $\mathbb{R}$ such that, out of $p < T$ consecutive time steps, the number of times $\chi_{i,\tau}$ belongs to $[a_i, b_i]$ is significantly higher than for any $j \neq i$.

It should be noticed that this F_i can also be used as a tool to assess the variability of the signal from one session to another; in fact it can be evaluated the range of $F_i(\chi_{i,\tau})$ when $\chi_{i,\tau}$ is not part of the training sample.

As a first step we define the search space for F_i as a linear transformation on $\mathbb{R}^d$ [1]

$$F_i(\chi) = \langle w, \chi \rangle.$$

5.3 Experiments

The sample datasets $\chi_{i,\tau}^{(I)} \in \mathbb{R}^d$, $i = 1 \dots N$ and $\tau = 1 \dots T$, obtained through the methods discussed in Chapter 3) for different acquisition sessions within the longitudinal experiments (see Chapter 4 for a detailed description of the longitudinal dataset), are analyzed to evaluate variability between subjects. The EEG ongoing activity measured during the rest protocol is considered for this analysis. Two recording sessions S_1 and S_2 (training sessions) are used in order to find w, a, b which optimizes F. For each subject $i, i = 1, \cdots, N$, the optimization of F_i is obtained employing the Covariance Matrix Adaptation Evolution Strategy (CMA-ES). This is a black-box second order optimization approach, mainly used to solve complex problems, which estimates a covariance matrix within an iterative procedure [2]. Given p consecutive frames, where $p < T$, we have

$$\nu_{True} = \#\{\theta_i | F_i(\chi_{i,\theta_i}) \in [a_i, b_i], \theta_i \in [\tau, \tau + p]\}$$

[1] A different search space can also tested for F_i modeled as a L_1 distance on $\mathbb{R}^d$:

$$F_i(\chi) = \sum_{\ell} w_\ell |\chi_\ell - c_\ell|$$

where c is a central point $c \in \mathbb{R}^d$. In this case the evaluation of the objective function for the train data gave worse results compared to the first search space tested (see Section 5.3), and also the obtained recognition accuracy for the test data was lower (see Section 5.3.1).

[2] matlab tool provided at https://www.lri.fr/~hansen/cmaes_inmatlab.html

$$\nu_{False} = \#\{\theta_j | F_i(\chi_{j,\theta_j}) \in [a_i, b_i], j \neq i, \theta_j \in [\tau, \tau + p]$$

The objective function we want to minimize for each tested identity is

$$J(w, a, b) = \nu_{False} - \nu_{True}$$

Given the subject i, for the optimization of F_i, a_i and b_i we use $2T$ frames obtained from the two acquisition sessions S_1 and S_2(each recording contains T frames). For the estimation of ν_{False}, 50% of the $K - 1$ false identities $j, j \neq i$ are randomly selected to assort the $2T$ frames to be used for learning. Results of the training in the search space $F_i(\chi) = \langle w, \chi \rangle$ employing the EEG waveform $x_{i,t}$ as features for 9 sample subjects are shown in Figure 5.1 , while in Figures 5.2 and 5.4 the training scores on the AR features $\chi^{(I)}_{i,\tau}$ and COH features $\chi^{(IV)}_{i,\tau}$, respectively, are reported for the same subjects. In Figures 5.3 and 5.5 similar training scores are shown for an L_1 distance as search space using AR and spectral coherence features, respectively. It should be noticed that better train scores are obtained for the search space $F_i(\chi) = \langle w, \chi \rangle$ using both AR and spectral coherence features. In particular raw signals seem to provide not significantly different scores $F_i(\chi_{i,\tau})$ and $F_i(\chi_{j,\tau})$.

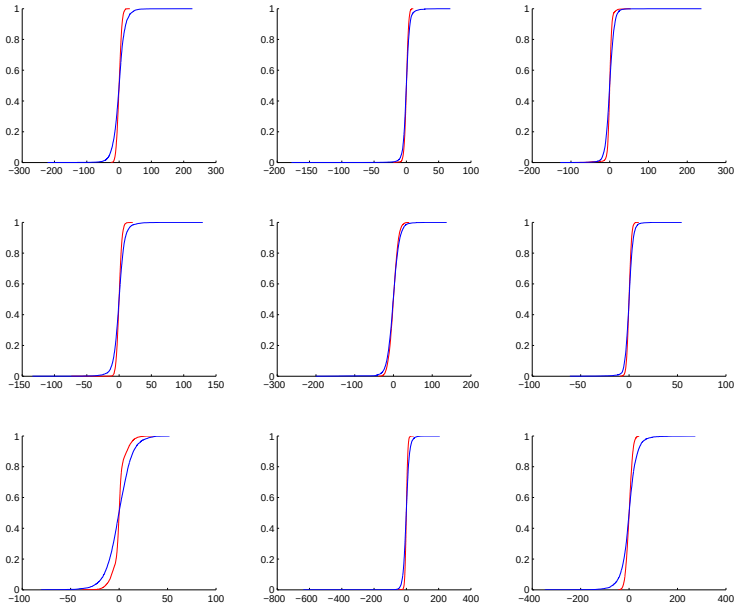

FIGURE 5.1: Cumulative distibutions of $F_i(x) = \langle w, x \rangle$. The curves refer to the training raw data from sessions S_1 and S_2. The red curve represents the scores of the genuine vector x_i, while the blue one represents the impostor x_j. The cumulative distributions of 9 sample subjects are shown in different subplots, for channel C_z and for a single run of the employed algorithm.

The third acquisition session S_3 (test session) is considered to evaluate the performance within a cross-validation (CV) framework. In particular 20 independent learning and test runs have

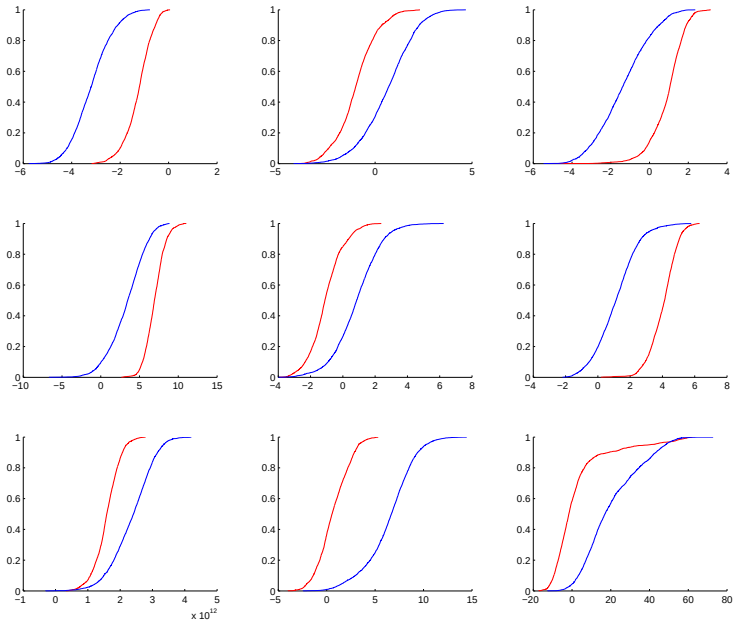

FIGURE 5.2: Cumulative distibutions of $F_i(\chi) = \langle w, \chi \rangle$. The curves refer to the training AR data from sessions S_1 and S_2. The red curve represents the scores of the genuine vector χ_i, while the blue one represents the impostor χ_j. The cumulative distributions of 9 sample subjects are shown in different subplots, for channel C_z and for a single run of the employed algorithm.

been performed on different partitions of the dataset, considering $p = 3T/4$ frames of sessions S_1 and S_2 for learning. Moreover, for each of the 20 CV runs the CMA-ES stochastic algorithm is executed 20 times gving 20 different learned vectors $[w_i, a_i, b_i], i = 1, \ldots, K$ (see Figure 5.6).

5.3.1 Results

5.3.1.1 Identity Verification

For the identity verification approach the goal is to verify the identity claimed by the subject i. The tests are performed as follows.

5.3.1.1.1 Genuine Acceptance Rate

Given the genuine subject i (subject i who claims identity i), and the vector of weights $w_i \in \mathbb{R}^d$ obtained from the learning, the values of ν_{True} are obtained for the test session S_3 considering l consecutive frames. The claimed identity i for the subject i is accepted if $\nu_{True,i}(F_i(\chi_{i,\tau}), l) \geq$

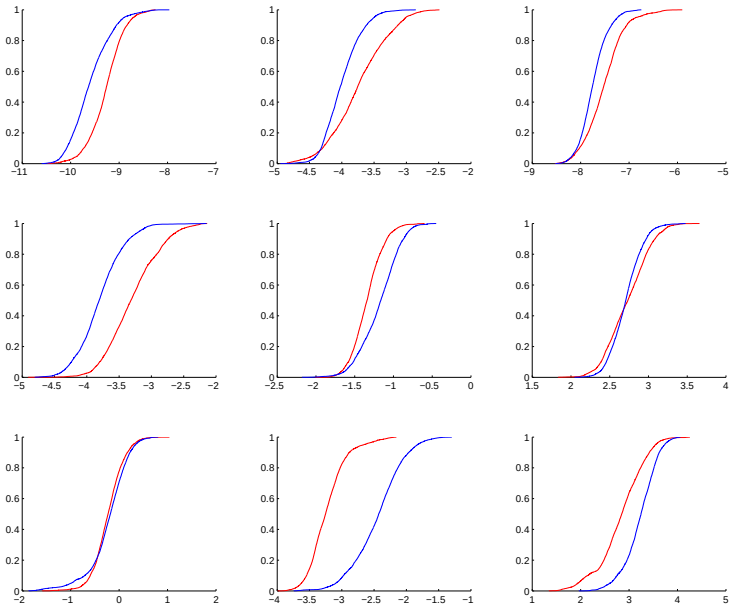

FIGURE 5.3: Cumulative distibutions of $F_i(\chi) = \sum_\ell w_\ell |\chi_\ell - c_\ell|$. The curves refer to the training AR data from sessions S_1 and S_2. The red curve represents the scores of the genuine vector χ_i, while the blue one represents the impostor χ_j. The cumulative distributions of 9 sample subjects are shown in different subplots, for channel C_z and for a single run of the employed algorithm.

t_h, where t_h is a threshold value. Then, the Genuine Acceptance Rate (GAR)is obtained as the ratio between all genuine identities accepted and all genuine identities tested.

As mentioned above, a CV framework is obtained by randomly selecting a sequence of l consecutive frames out of T from the test session. Different tests are performed for values of l in a range which spans the interval $[1, 40]s$. It is worth noting that the aim is to minimize the number of consecutive frames, employed to achieve a good accuracy, that is the duration of the recognition test. In fact, for a longitudinal experiment, this would be an important improvement with respect to the state-of-the-art, as reported in Chapter 4, where the best accuracy is an Equal Error Rate (EER) of $3,4\%$ obtained for 51 subjects employing 1-minute test EEG segments [72].

5.3.1.1.2 False Acceptance Rate

Similarly to what discussed for the GAR, given the randomly selected impostor user $j \neq i$ (subject j who claims identity i), ν_{False} is obtained for the test session S_3 considering l consecutive frames. Therefore,the claimed identity i for the impostor subject j is accepted if $\nu_{False,j}(F_i(\chi_{i,\tau}), l) \geq t_h$, where t_h is the same threshold value introduced above. The False Acceptance Rate (FAR) is obtained as the ratio between all false identities accepted, and all

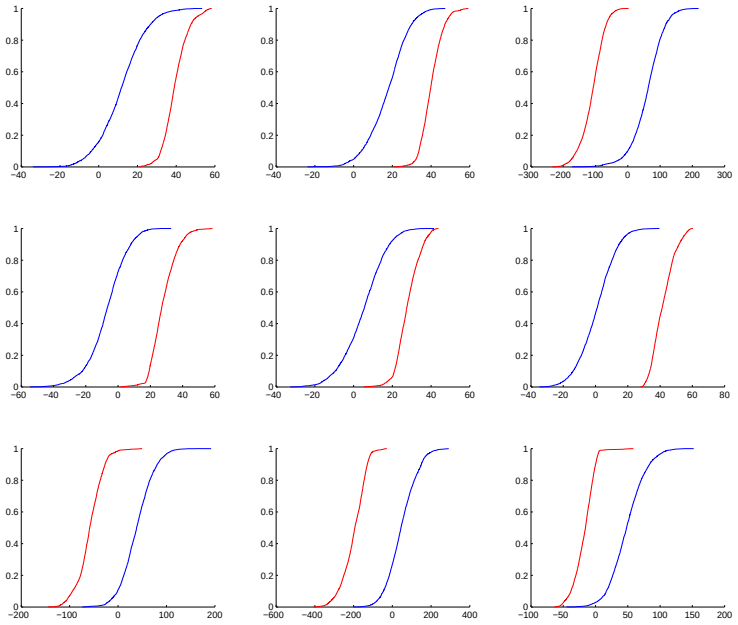

FIGURE 5.4: Cumulative distibutions of $F_i(\chi) = \langle w, \chi \rangle$. The curves refer to the training spectral coherence data from sessions S_1 and S_2. The red curve represents the scores of the genuine vector χ_i, while the blue one represents the impostor χ_j. The cumulative distributions of 9 sample subjects are shown in different subplots, for channel C_z and for a single run of the employed algorithm.

false identities tested. It is worth noting that for a given identity i the FAR is evaluated considering false test identities j other than the false identities used during the training to learn F_i, a_i and b_i. As for the GAR, the same CV framework is considered to average the FAR, and the same values of l were tested.

5.3.1.1.3 Ensemble Testing and channel selection

In order to improve the system accuracy an averaging procedure at the decision level is considered during the test stage. Specifically, different representations of the same information employing AR reflection coefficients are obtained for different values of parameter Q (see Section AR) and different channels. Each representation is considered to evaluate $\nu_{True,i}$ and $\nu_{False,j}$, and the average over the different representations is performed to improve the decision process. Moreover, the different instances of $[w, a, b]$ for each identity obtained from the 20 executions of the CMA-ES stochastic algorithm on the same data (see Section 5.3) are also considered to evaluate $\nu_{True,i}$ and $\nu_{False,j}$, and the same average is performed before taking the decision. The different representations of the data given by channels are ranked according to the minimum value obtained for the objective function in the training stage. A selection of channels for the ensemble averaging is performed according to that ranking, retaining N_{ch} elements. In Figures

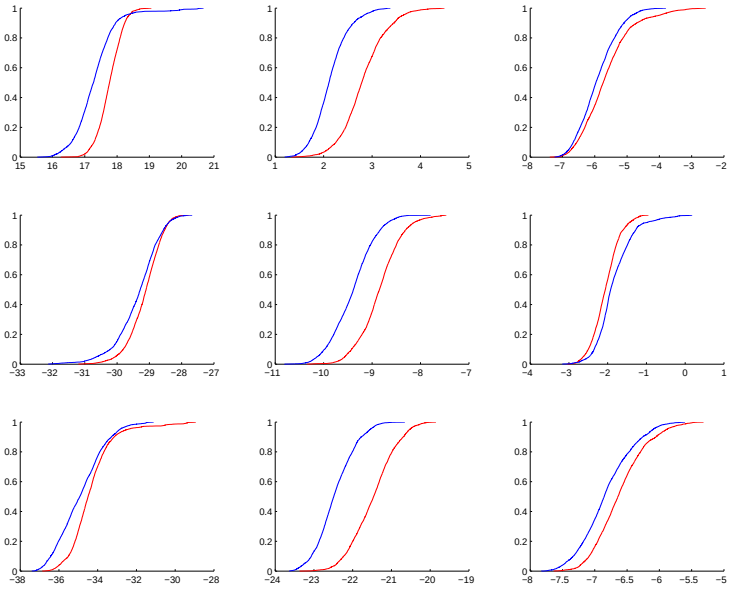

FIGURE 5.5: Cumulative distibutions of $F_i(\chi) = \sum_\ell w_\ell |\chi_\ell - c_\ell|$. The curves refer to the training spectral coherence data from sessions S_1 and S_2. The red curve represents the scores of the genuine vector χ_i, while the blue one represents the impostor χ_j. The cumulative distributions of 9 sample subjects are shown in different subplots, for channel C_z and for a single run of the employed algorithm.

5.7 the channel selection is shown, reporting the ranking order in false colors. As can be observed, most of the channels providing best training scores are placed along the midline and in the left hemisphere of the head

5.3.2 Discussion

As a first experiment we tested the system accuracy employing the representation of the data $\chi^{(I)}_{i,\tau}$ based on AR coefficients, for a single channel, a single value of Q, and a single execution of the CMA-ES algorithm for each CV run. The result is shown in Figure 5.8, where a comparison between the employed learning approach and a second order metric-based classifier (Mahalanobis distance) is provided (black and green lines). The Figure reports the achieved accuracy in terms of Equal Error Rate (EER) on the y-axis, versus the duration of the EEG segment tested during the recognition session on the x-axis. It can be noticed that an acceptable accuracy is obtained for 45-seconds EEG segments. The same information is provided in Figure 5.9 for spectral coherence features considering a single representation, that is a single channel pair.

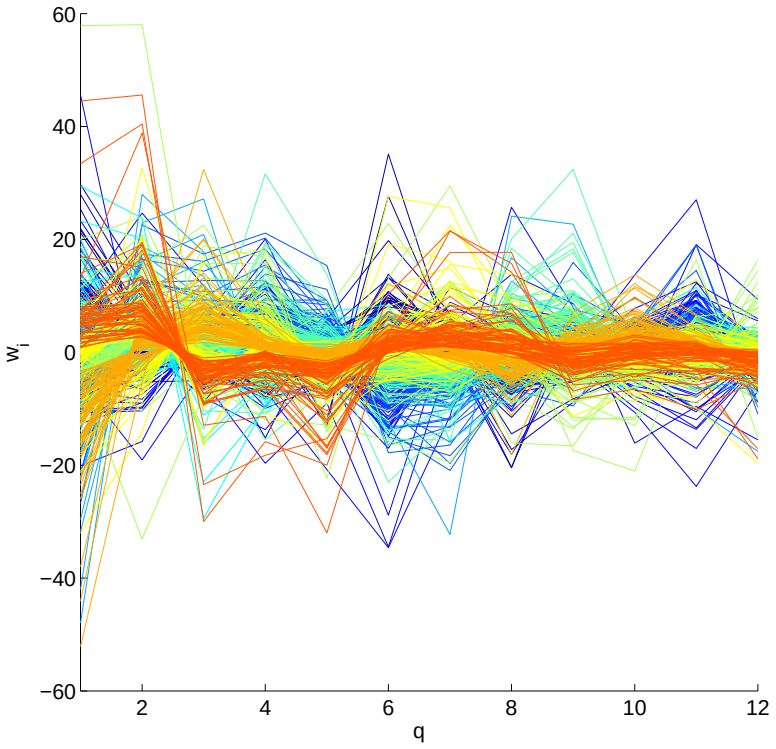

FIGURE 5.6: Vectors $w_i \in \mathbb{R}^{12}$ for 10 sample subjects, obtained from 20 executions of the stochastic optimization algorithm (CMA-ES) on the sessions S_1 and S_2. The colormap codes the subjects $i = 1, \ldots, 10$.

In Figure 5.10 the system accuracy is reported considering AR features $\chi^{(I)}_{i,\tau}$ for the case of performing the average along different representations of the scores given by the different channels. Here the achieved accuracy in terms of Equal Error Rate (EER) is reported on the y-axis, versus the number of channels considered for the ensemble average on the x-axis. This result refers to tested EEG segments of 5 seconds. We can observe that an acceptable EER is obtained performing the ensemble testing, reducing the duration of the recognition test to only $5s$.

Results for the averaging of scores related to the different channels and the different values of Q used to represent data are shown in Figure 5.11, where the values of Q considered in the average are reported on the x-axis. Here the result refers again to EEG segments of 5 seconds. It should be noticed that a good EER is obtained averaging along all the considered representations of the data ($EER = 0.02\%$) reducing the duration of the recognition test to only $5s$.

The same information is reported in Figure 5.12 for spectral coherence features $\chi^{(IV)}_{i,\tau}$, with the number of channel pairs considered in the ensemble averaging shown on the x-axis. Also in this case an improvement is observed for $5s$ EEG frames, despite a better accuracy is obtained using AR features $\chi^{(I)}_{i,\tau}$.

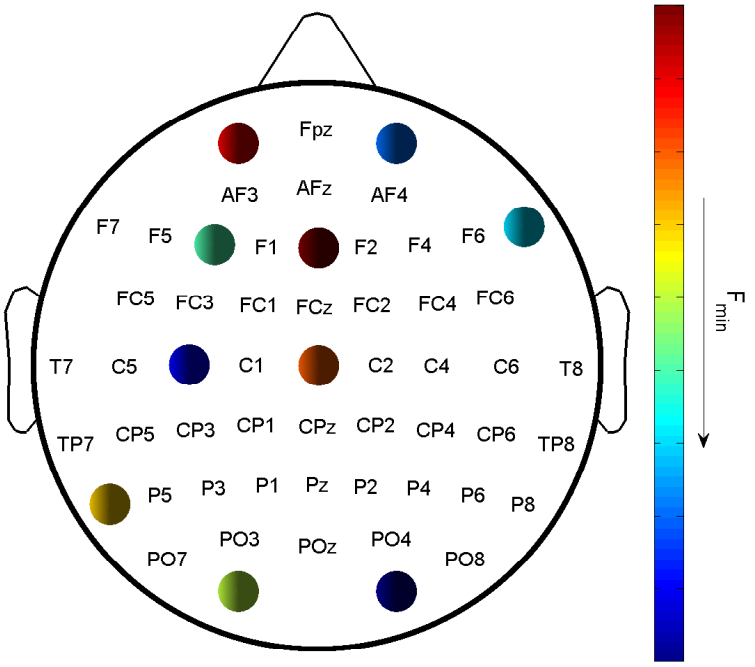

FIGURE 5.7: Channel selection based on the minimum value of the objective function achieved in the training.

In Figure 5.13 we can observe the accuracy obtained using AR features $\chi_{i,\tau}^{(I)}$ for different lengths of the tested EEG segments, considering the averaging of the scores along all the considered representations of the data. As can be noticed an enhanced accuracy of $EER = 0.015$ is obtained employing 10-seconds EEG segments, while an $EER = 0.008$ is achieved for 45-seconds EEG segments.

Figure 5.14 shows the EER obtained for each subject, considering train and test frames separately. Also the results for channel selection, obtained as discussed in Section 5.3.1.1.3, are reported in the same figure. In general an improvement of the system accuracy can be observed employing the CMA-ES optimization approach and the channel selection for all subjects except one ($i = 30$), for which the recognition rate is still high ($EERi = 30 = 90\%$).

The system accuracy for the ensemble of subjects versus time is shown in Figure 5.15 for AR features $\chi_{i,\tau}^{(I)}$. A good result of EER in the range of $[0.003, 0.023]$ is obtained selecting the best channels from training data. In general a significant improvement is observed employing the CMA-ES algorithm compared to metric-based approaches. Also the ensemble averaging of the test scores and the channel selection seem to provide enhanced recognition accuracy.

The same plot as for AR modeling are shown in Figures 5.16 and 5.17 for coherence features $\chi_{i,\tau}^{(IV)}$. In general similar consideration can be raised in this case. Nevertheless the achieved

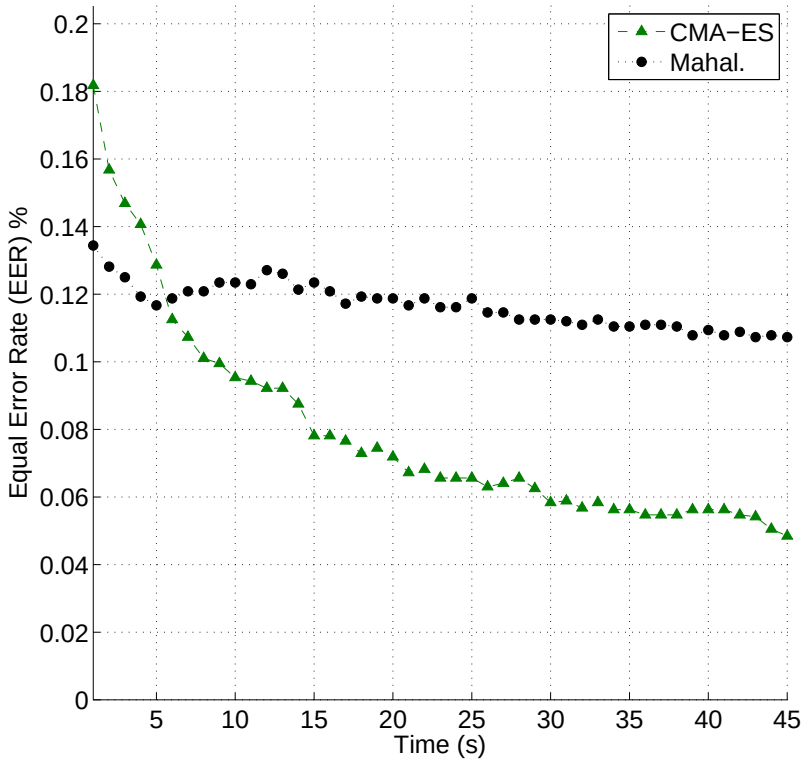

FIGURE 5.8: EER versus time obtained for a single representation of the data through the AR coefficients. The shown result refers to channel C_z and $Q = 12$, that are the channel and the AR model order which give better accuracy. Green markers refer to the CMA-ES optimization algorithm, while black markers refer to Mahalanobis-based classifier.

accuracy worsens compared to the AR features, and the curves shown appear discontinuous, especially foe EER versus time plots, so that more caution is needed to support a general trend according to the involved parameters. In fact, despite the good training scores obtained for spectral coherence features, shown in Section 5.3, the optimized coefficients of the linear transformation applied to the data does not seem to enhance repeatability of such connectivity patterns.

Finally for AR features $\chi^{(I)}_{i,\tau}$ the ROC curves for the different averaging steps and 5-seconds EEG segments are shown in Figure 5.18, while in Figure 5.19 the same curves are reported for the different lengths of the tested EEG segments.

The result obtained through the analysis shown in this chapter shows the potentials of EEG to be used for biometric purposes, and the improvement that can be achieved employing a machine learning approach. Specifically the learning procedure allows to obtain a good accuracy reducing the time needed for the recognition procedure. These results are the subject of a current work carried out within a collaboration with the TAO team (Laboratoire de Recherche en Informatique, Gif-sur-Yvette, France).

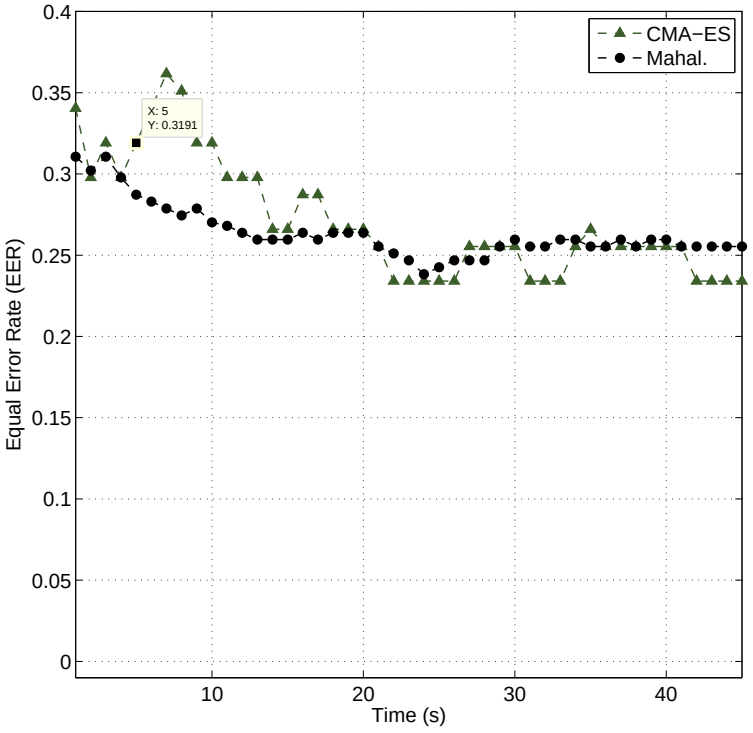

FIGURE 5.9: EER versus time obtained for a single representation of the data through the spectral coherence values. The shown result refers to channel pair $C_3 - C_z$ which gives better accuracy. Green markers refer to the CMA-ES optimization algorithm, while black markers refer to Mahalanobis-based classifier.

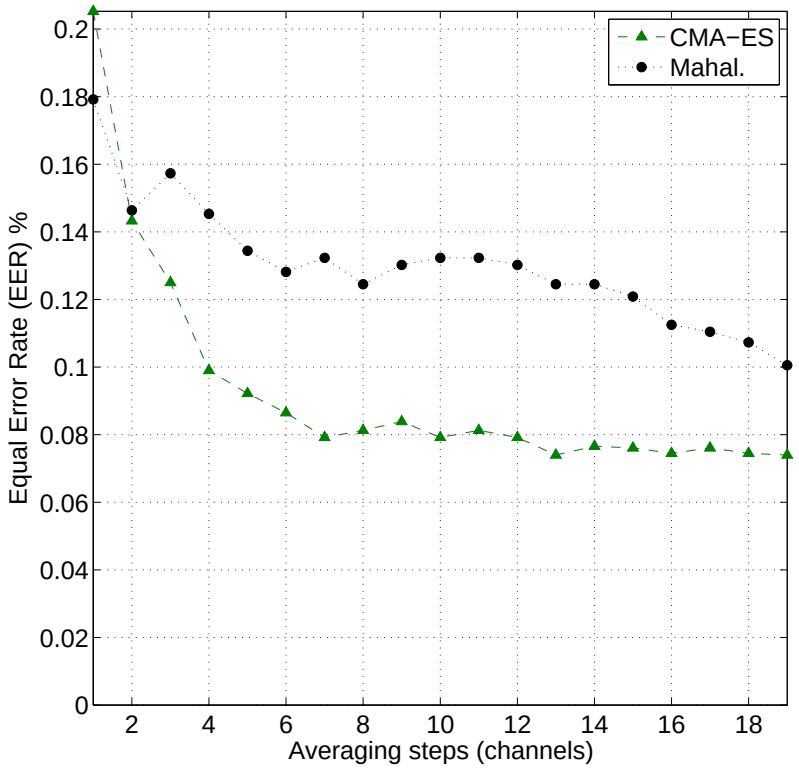

FIGURE 5.10: EER versus averaging steps obtained using AR features $\chi_{i,\tau}^{(I)}$. The shown accuracy refers to the averaging of the scores obtained considering different channels to represent the data, for $Q = 12$. Green markers refer to the CMA-ES optimization algorithm, while black markers refer to Mahalanobis-based classifier.

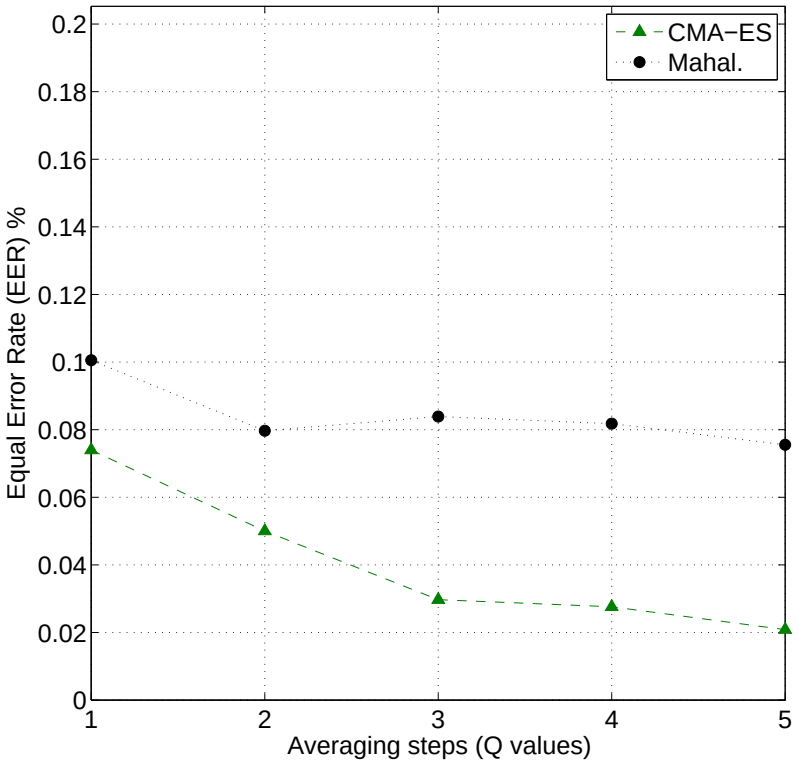

FIGURE 5.11: EER versus averaging steps using AR features $\chi_{i,\tau}^{(I)}$. The shown accuracy refers to the averaging of the scores obtained considering different channels and different Q values to represent the data. Green markers refer to the CMA-ES optimization algorithm, while black markers refer to Mahalanobis-based classifier.

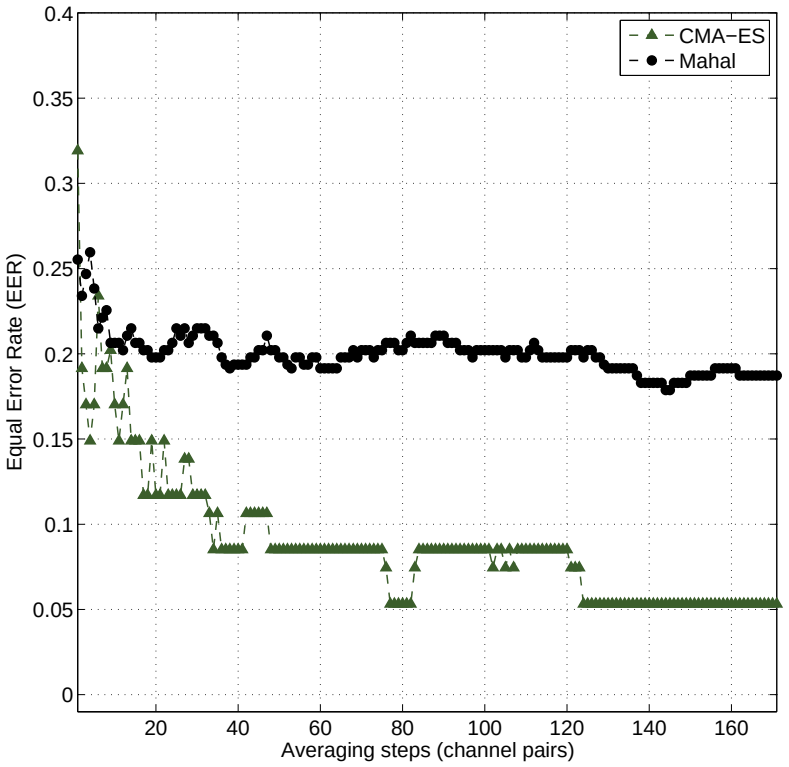

FIGURE 5.12: EER versus averaging steps using spectral coherence features $\chi_{i,\tau}^{(IV)}$. The shown accuracy refers to the averaging of the scores obtained considering different channel pairs to represent the data. Green markers refer to the CMA-ES optimization algorithm, while black markers refer to Mahalanobis-based classifier.

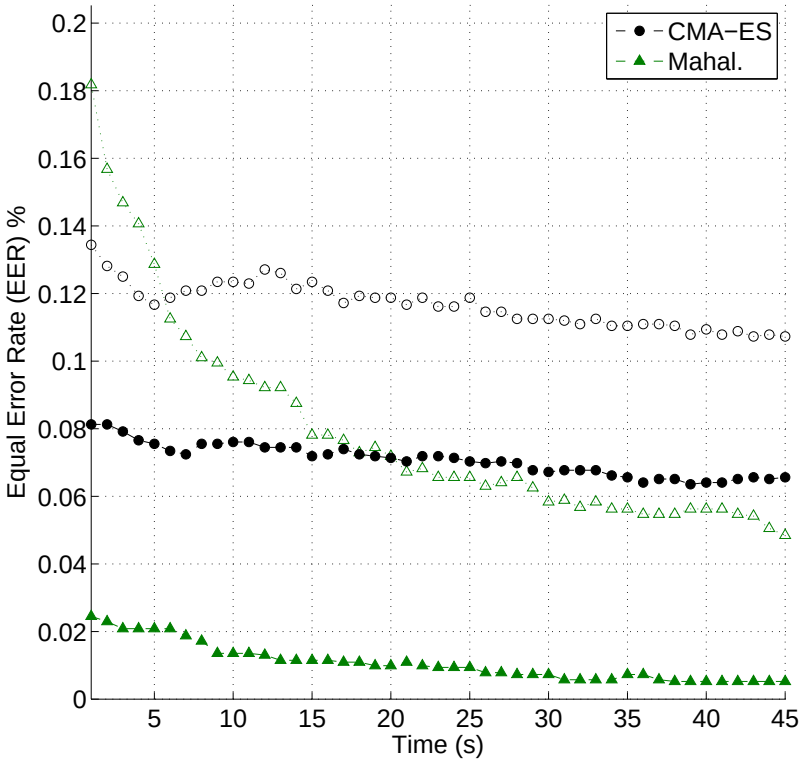

FIGURE 5.13: Solid lines: EER versus time using AR features $\chi_{i,\tau}^{(I)}$, for the averaging of the scores obtained considering different channels and different Q values to represent the data. Dashed lines: EER versus time, for a single representation of the data. The shown result refers to channel C_z and $Q = 12$. Green markers refer to the CMA-ES optimization algorithm, while black markers refer to Mahalanobis-based classifier.

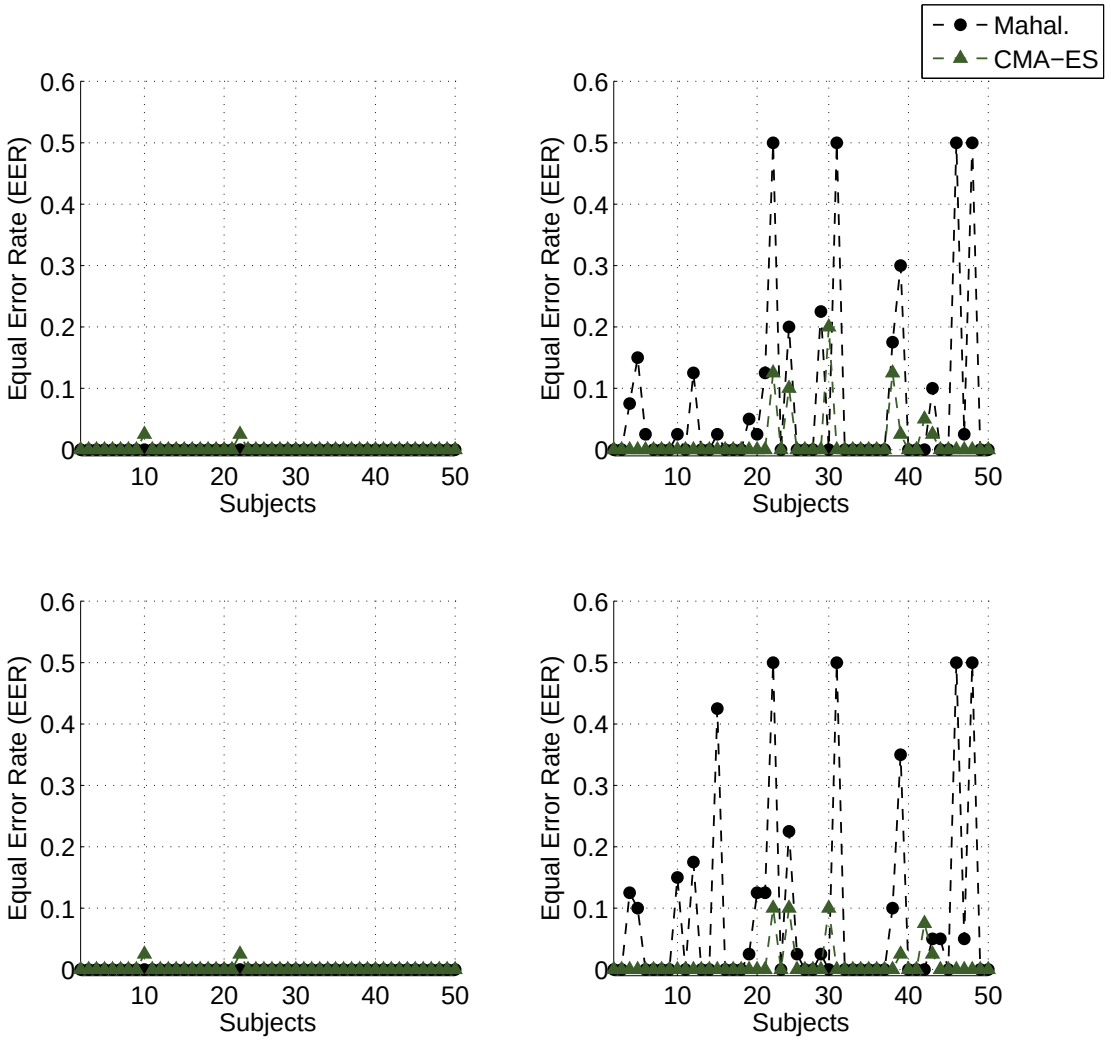

FIGURE 5.14: EER versus subjects using AR features $\chi_{i,\tau}^{(I)}$, for the averaging of the scores obtained considering different channels and different Q values to represent the data. The plots shown on the left hand side refer to training data from sessions S_1 and S_2, while the ones on the right refer to test data from session S_3. The plots on the top are obtained using all channels, while the results related to the channel selection are shown on the bottom. Green markers refer to the CMA-ES optimization algorithm, while black markers refer to Mahalanobis-based classifier.

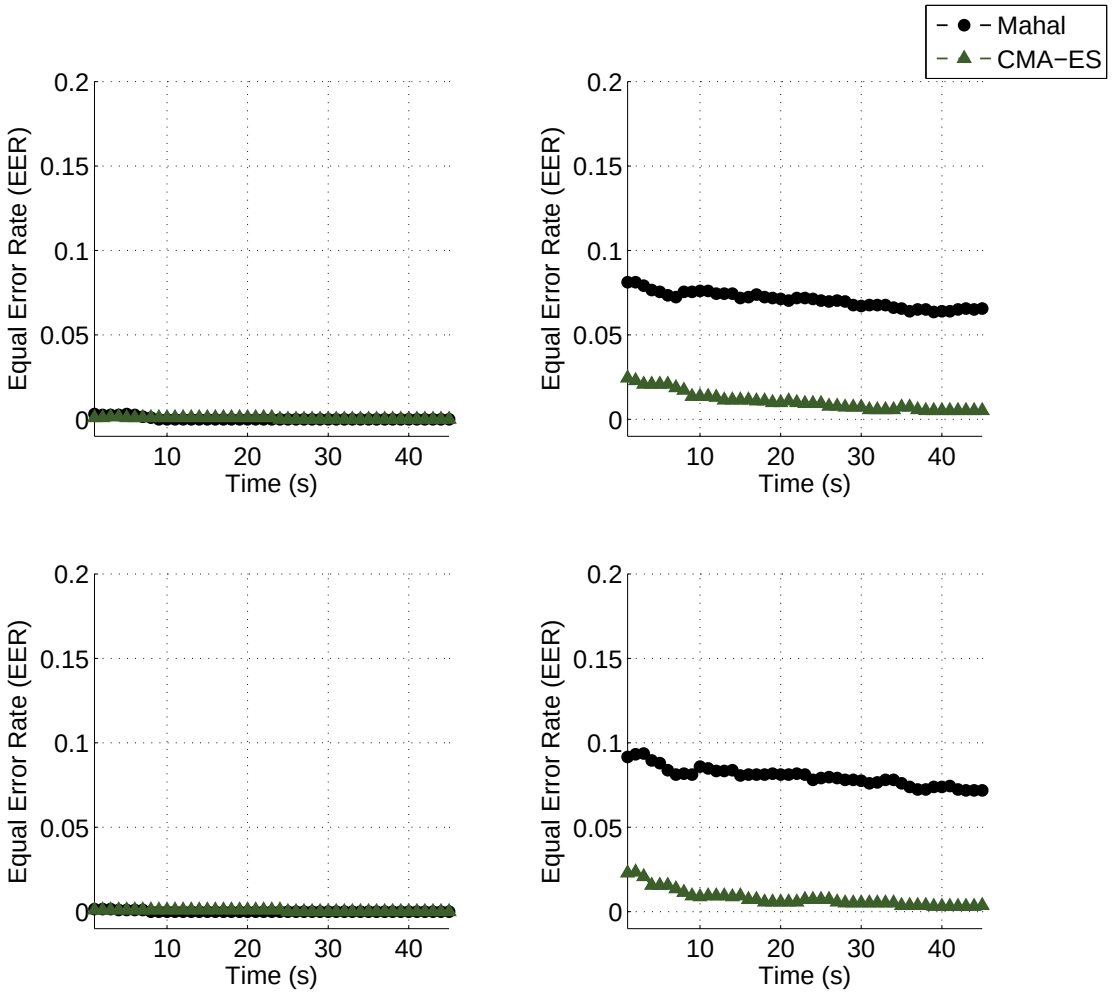

FIGURE 5.15: EER versus time using AR features $\chi_{i,\tau}^{(I)}$, for the averaging of the scores obtained considering different channels and different Q values to represent the data. The plots shown on the left hand side refer to training data from sessions S_1 and S_2, while the ones on the right refer to test data from session S_3. The plots on the top are obtained using all channels, while the results related to the channel selection are shown on the bottom. Green markers refer to the CMA-ES optimization algorithm, while black markers refer to Mahalanobis-based classifier.

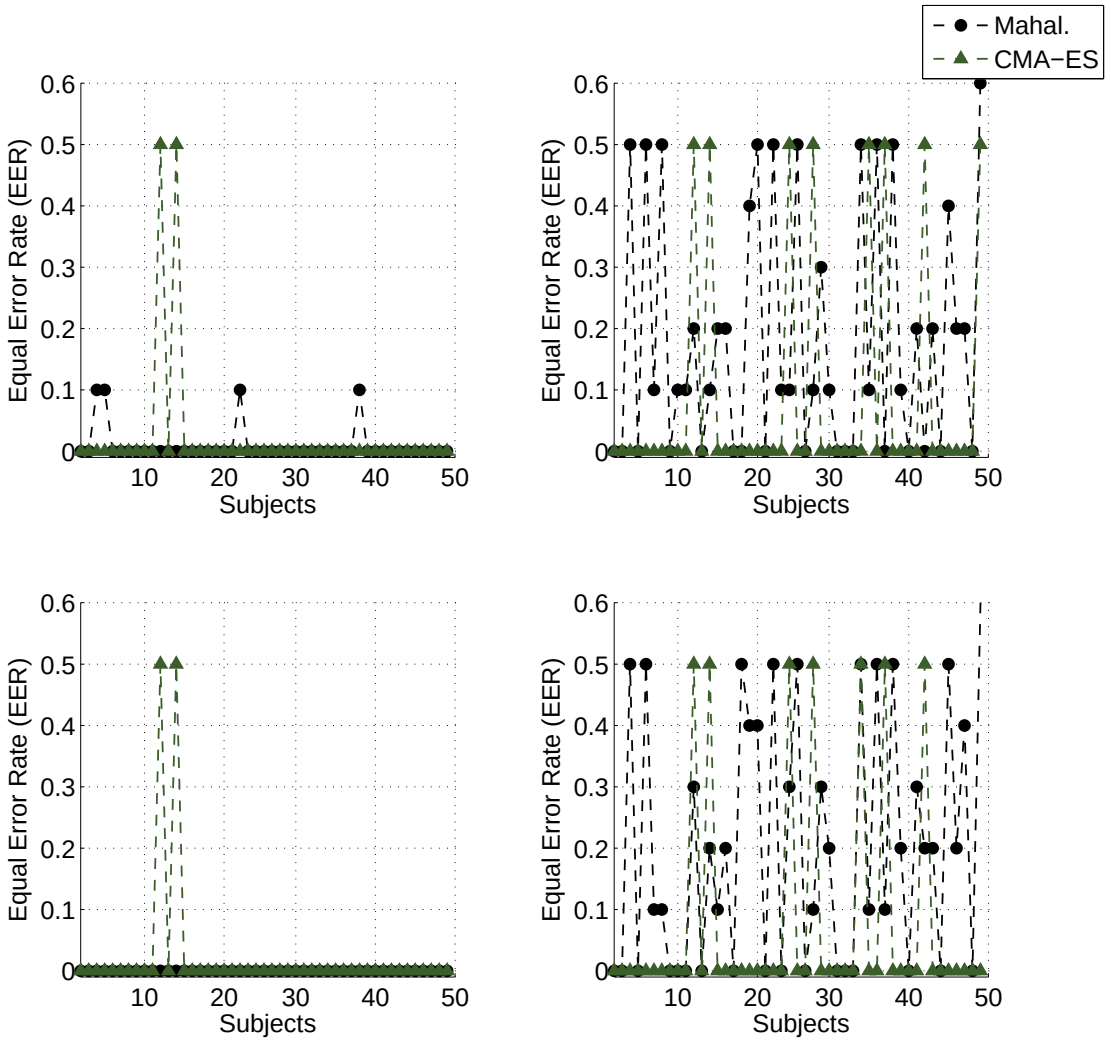

FIGURE 5.16: EER versus subjects using spectral coherence features $\chi_{i,\tau}^{(VI)}$, for the averaging of the scores obtained considering different channels and different Q values to represent the data. The plots shown on the left hand side refer to training data from sessions S_1 and S_2, while the ones on the right refer to test data from session S_3. The plots on the top are obtained using all channels, while the results related to the channel selection are shown on the bottom. Green markers refer to the CMA-ES optimization algorithm, while black markers refer to Mahalanobis-based classifier.

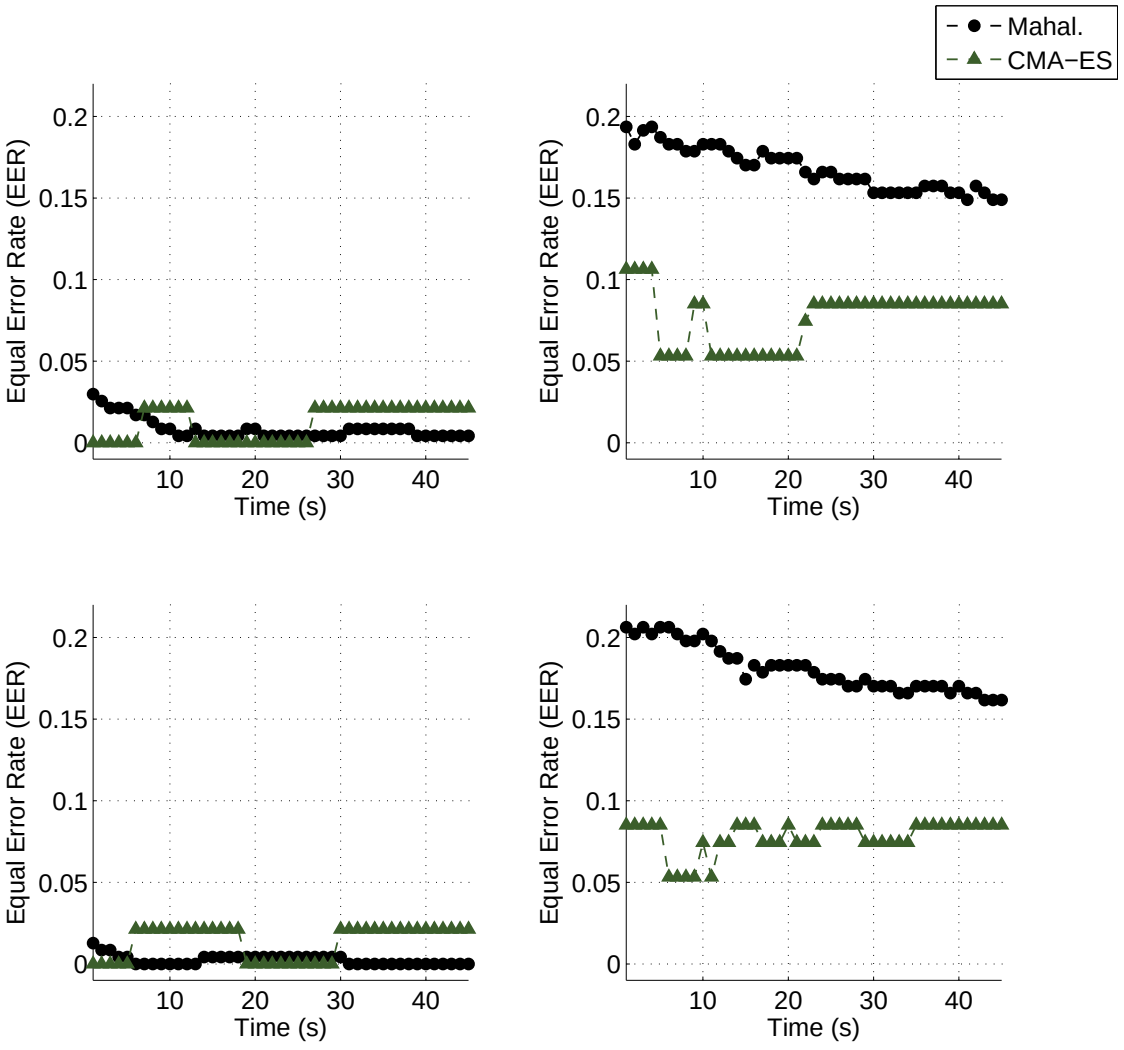

FIGURE 5.17: EER versus time using spectral coherence features $\chi_{i,\tau}^{(IV)}$, for the averaging of the scores obtained considering different channels and different Q values to represent the data. The plots shown on the left hand side refer to training data from sessions S_1 and S_2, while the ones on the right refer to test data from session S_3. The plots on the top are obtained using all channels, while the results related to the channel selection are shown on the bottom. Green markers refer to the CMA-ES optimization algorithm, while black markers refer to Mahalanobis-based classifier.

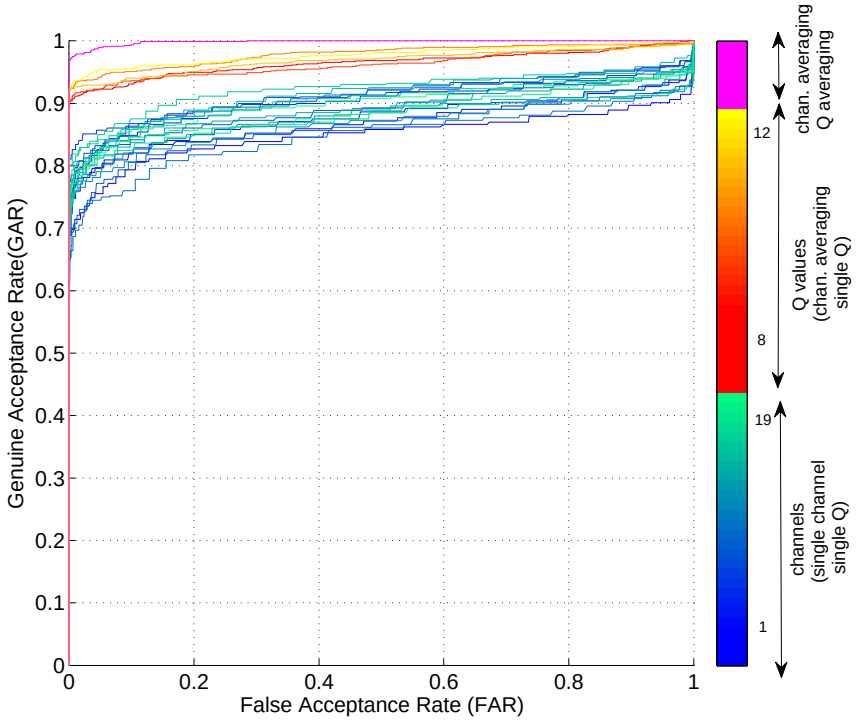

FIGURE 5.18: ROC curve for different averaging steps. The shown results refer to AR features $\chi_{i,\tau}^{(I)}$

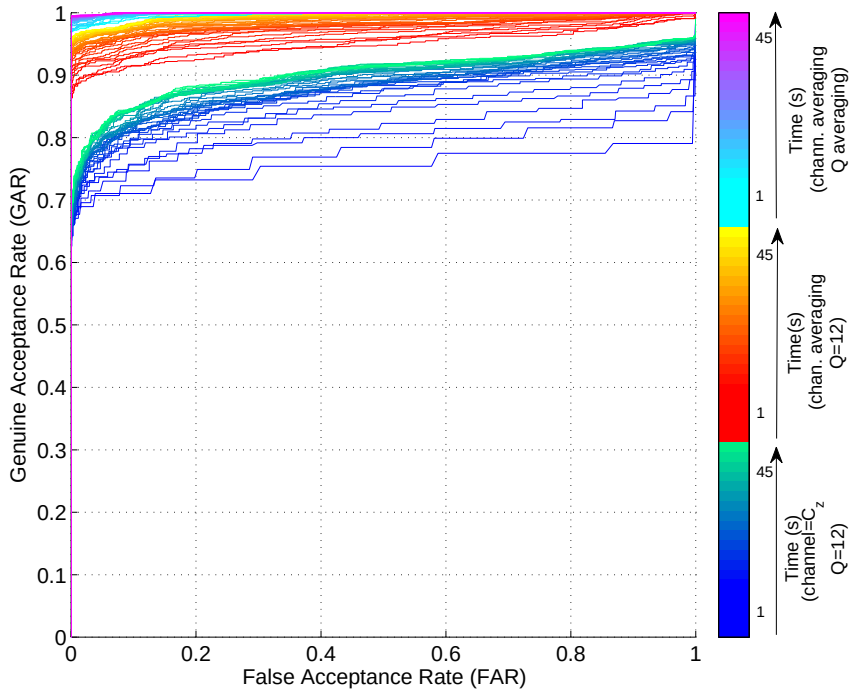

FIGURE 5.19: ROC curve for different lengths of tested EEG segments. The shown results refer to AR features $\chi_{i,\tau}^{(I)}$

Conclusion and Future Work

In the past few years there has been a growing interest in EEG-based biometric systems. Compared to other traits that are usually considered in biometrics (e.g. fingerprints, iris, voice, signatures), EEG activity presents two main advantages, among others: i) it's harder to steal and ii) it's a dynamic measure, thus allowing for constant recognition and mental state monitoring [6].

Despite such interest, classification performance decreases from maximum accuracy when the number of people to recognize becomes high, i.e. $N > 100$ [48], [79]. Possible causes rely on the methods that are commonly used to extract characteristic features from the EEG signals.

In the first part of the present work of doctoral thesis we give an extensive and critical review on the state of the art of EEG based automatic recognition systems. An overview of the neurophysiological basis which constitute the foundations on which EEG biometric systems can be built is also provided. The major obstacles towards the deployment of EEG based recognition systems in everyday life in the near future have been presented and the some challenging research lines for the interested researchers have been suggested.

In the second part different feature engineering approaches implemented within the present work are reported. Specifically parametric and non-parametric models are consider to perform feature extraction for biometric recognition purpose. The majority of the methods employed so far only consider the activity of a single brain region without taking into account its dynamic relationship with other regions. However, the human brain works as an interconnected system where different specialized areas continuously exchange information through stable synchronous connectivity patterns [18]. Among the non-parametric feature engineering approach we propose to exploit such synchronous "communication" between different EEG sensors, under the hypothesis that this information could exhibit stronger intra-class invariant properties, as supported by the obtained results.

A longitudinal dataset, acquired within this work in our laboratory, is also analyzed to address the repeatability of EEG distinctive traits. This is an important property of feasible biometric recognition systems. The obtained results show the potentials of EEG to be used for biometric

purposes, and the improvement that can be achieved employing a machine learning approach. Specifically the employed learning procedure allows to obtain a good accuracy reducing the time needed for the recognition procedure.

Appendix A

SINGLE ELEMENT RANKING AND FUSION ALGORITHM

SINGLE ELEMENT RANKING

- N number of subjects
- N_{runs} number of cross-validation runs
- N_{el} number of elements of the feature vector ($N_{el} = 56$ for χ^{III}, $N_{el} = 1540$ for χ^{IV})
- $\mathbf{M}$ misclassification matrix [108x108] representing the results of the identification test (columns) for all subjects (rows).

Input: $d_{k,m,r}(n)$ Mahalanobis distances for element k ($k = 1,\ldots,Nel$) between subject m and each class distribution n ($n = 1,\ldots,N$). r refers to the cross-validation run.

while $1 \leq \bar{k} \leq N_{el}$

```
    while 1 ≤ r̄ ≤ N_runs
        M ← null matrix
            while 1 ≤ m̄ ≤ N
                n̂ = min_n d_{k̄,m̄,r̄}(n);
                M(m̄, n̂) ←1
                m̄ ← m̄ + 1
            end
            CRR_{k̄,r̄} = (1/N) Σ_n M(n, n);
            r̄ ← r̄ + 1
    end
    k̄ ← k̄ + 1
end
mCRR_k = (1/N_runs) Σ rCRR_{k,r};
Next step consists in ranking elements sorting them in
descending order of CRR individually achieved.
```

- $mCRRval_h$ sorted values contained in $mCRR_k$
- $mCRRind_h$ elements corresponding to CRR values ranked in $mCRRval$

$mCRRind$ is used to define the steps s of the fusion, according to the ranking defined in $mCRRind$.

FUSION ALGORITHM

- N number of subjects
- N_{runs} number of cross-validation runs
- N_{el} number of elements of the feature vector ($N_{el} = 56$ for χ^{III}, $N_{el} = 1540$ for χ^{IV})

Inizialization

$fusionElements \leftarrow mCRRind_1$

$CRRsteps_1 \leftarrow mCRRval_1$

$cs = 1$ current fusion elements

while $2 \leq \bar{s} \leq N_{el}$

```
        select subsequent elements sorted in descending order of
        CRR individually achieved.
        h̄ = mCRRind(s̄);
        E ← fusionElements;
        E_{cs+1} ← h̄;
            while 1 ≤ r̄ ≤ N_runs
                    M ← null matrix
                    CRR related to step s is computed in similarly
                    as described above.
                        while 1 ≤ m̄ ≤ N
                                Score_m̄(n) = Σ_{fe∈E} 1 / d_{f,m̄,r̄}
                                n̂ = max_n Score_m̄(n)
                                M(m̄, n̂) ← 1
                                m̄ ← m̄ + 1
                        end
                        CRR_r̄ = (1/N) Σ_n M(n, n);
                        r̄ ← r̄ + 1
            end
            mCRR = (1/N_runs) Σ rCRR_r;
            If mCRR, related to elements newfusionElements,
            > mCRR related to elements fusionElements then element
            mCRRind(s) is selected for the fusion.
                if mCCR > CRRsteps_cs
                        fusionElement ← E;
                        cs ← cs + 1
                        CRRsteps_cs ← mCCR;
                end
                s̄ ← s̄ + 1
end
```

Appendix B

CONNECTIVITY PATTERN FOR THE WHOLE HEAD

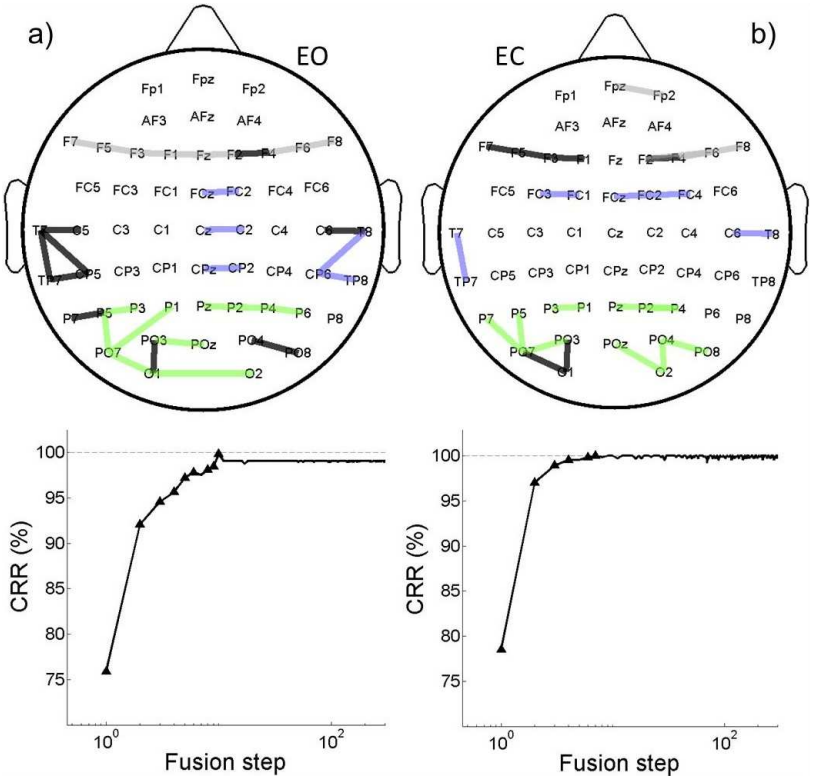

FIGURE B.1: Distinctive functional connectivity patterns for the whole head (on the top) and related steps for the match score fusion selection (on the bottom). Results for the EO and EC two conditions are reported in a) and b) respectively. On the top: black links indicate the channel pair selected by the fusion algorithm when considering the connectivity within and between all the cerebral zones. On the bottom: Symbol markers highlight the fusion steps that increased the overall CRR accuracy. X-axes are put into logarithmic scales for the sake of representation. It should be noticed that the best distinctive connectivity patterns are a subset of the results obtained when restricting the fusion within single cerebral zones, i.e. gray, blue and green are the colors used for specific zones (F, C and P respectively) tested separately.

Appendix C

REAL AND IMAGINARY COHERENCE

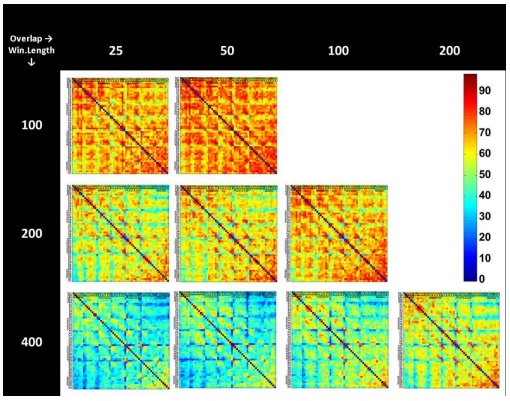

(a)

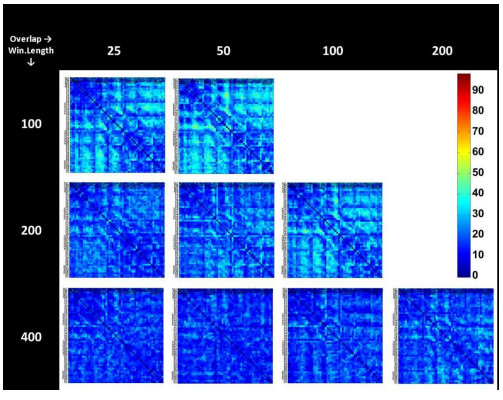

(b)

FIGURE C.1: CRR results obtained with single-element classification of spectral coherence (a) and imaginary coherence (b) in a group of N=20 subjects during the eyes-open EO resting state condition. Results are reported for different configurations of Hanning window lengths (rows in each panel) and overlapping data points (columns in each panel).

Appendix D

VARIABILITY OF SPECTRAL FEATURES

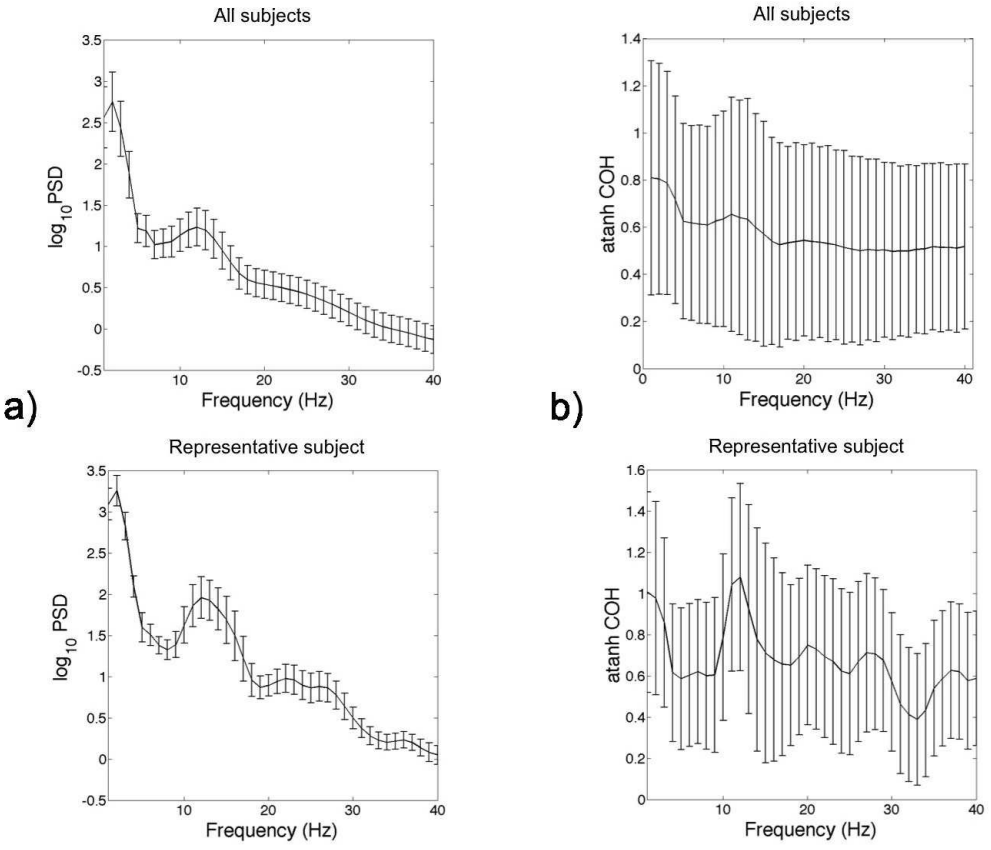

FIGURE D.1: Variability of power spectrum PSD (a) and spectral coherence COH (b) features across EEG sensors. In the upper panels solid lines represent the grand average (across all the subjects $N = 108$) of the mean profile of the feature vector across all the considered EEG sensors ($N_{ch} = 56$). Vertical bars indicate the grand average of the standard deviation of the feature vector across sensors. In the lower panels solid lines represent the mean profile of the feature vector across all the considered EEG sensors for a representative subject. Vertical bars indicate the standard deviation of the feature vector across sensors.

Bibliography

[1] E. Başar. *Brain Function and Oscillations: Integrative brain function. Neurophysiology and cognitive processes*. Springer series in synergetics. Springer, 1999. ISBN 9783540643456.

[2] G. Dornhege, J. del R. Millán, T. Hinterberger, D.J. McFarland, and K.-R. Móller, editors. *Towards Brain-Computing Interfacing*. MIT Press, Cambridge, MA, 2007.

[3] Jonathan R. Wolpaw and Elizabeth Winter Wolpaw, editors. *Event-Related Brain Potentials: Methods, Theory, and Applications*. Wiley, Oxford Univ. Press.

[4] J. M. Carmena. Becoming bionic. *IEEE Spectrum*, 49(3):24–29, 2012.

[5] H. H. Stassen. Computerized recognition of persons by EEG spectral patterns. *Electroen Clin Neuro*, 49:190–194, 1980.

[6] P. Campisi, D. La Rocca, and G. Scarano. EEG for automatic person recognition. *Computer*, 45(7):87–89, 2012.

[7] Patrizio Campisi and Daria La Rocca. Eeg biometrics. In Stan Z. Li and Anil K. Jain, editors, *Encyclopedia of Biometrics*, pages 1–11. Springer US, 2014. doi: 10.1007/978-3-642-27733-7_9145-2. URL http://dx.doi.org/10.1007/978-3-642-27733-7_9145-2.

[8] J Berkhout and D. O. Walter. Temporal stability and individual differences in the human EEG: An analysis of variance of spectral values. *IEEE Trans. Biomed. Eng.*, 15(3):165–168, 1968.

[9] H Van Dis, M Corner, R Dapper, G Hanewald, and Kok H. Individual differences in the human electroencephalogram during quiet wakefulness. *Electroen Clin Neuro*, 47:87–94, 1979.

[10] Gennady G. Knyazev. Motivation, emotion, and their inhibitory control mirrored in brain oscillations. *Neuroscience and Biobehavioral Reviews*, 31(3):377–395, 2007.

[11] E. Niedermeyer and F.H.L. Da Silva. *Electroencephalography: Basic Principles, Clinical Applications, and Related Fields*. Doody's all reviewed collection. Lippincott Williams & Wilkins, 2005.

[12] Erol Başar, Canan Başar-Eroglu, Sirel Karakaş, and Martin Schürmann. Gamma, alpha, delta, and theta oscillations govern cognitive processes. *Int. Journal of Psychophysiology*, 39(2-3):241 – 248, 2001. ISSN 0167-8760. doi: 10.1016/S0167-8760(00)00145-8.

[13] T. Harmony, T. Fernández, J. Silva, J. Bernal, L. Díaz Comas, A. Reyes, E. Marosi, Mario Rodríguez, and Miguel Rodríguez. EEG delta activity: an indicator of attention to internal processing during performance of mental tasks. *International Journal of Psychophysiology*, 24(1):161171, 1996.

[14] W Klimesch, M Doppelmayr, H Russegger, and Th Pachinger. Theta band power in the human scalp eeg and the encoding of new information. *Neuroreport*, 7(7):1235–1240, 1996.

[15] R.J. Barry, A.R. Clarke, S.J. Johnstone, C.A. Magee, and J.A. Rushby. EEG differences between eyes-closed and eyes-open resting conditions. *Clinical Neurophysiology*, 118: 2765–2773, 2007.

[16] W Klimesch, M Doppelmayr, T Pachinger, and H Russegger. Event-related desynchronization in the alpha band and the processing of semantic information. *Cognitive Brain Research*, 6(2):83–94, 1997.

[17] K. J. Meador, P. G. Ray, J. R. Echauz, D. W. Loring, and G. J. Vachtsevanos. Gamma coherence and conscious perception. *Neurology*, 59(6):847–854, 2002.

[18] Francisco Varela, Jean-Philippe Lachaux, Eugenio Rodriguez, and Jacques Martinerie. The brainweb: phase synchronization and large-scale integration. *Nature reviews neuroscience*, 2(4):229–239, 2001.

[19] E. Donchin, W. Ritter, and W. C. Mccallum. Cognitive psychophysiology: The endogenous components of ERP. *Event-related brain potentials in man. Academic Press*, pages 349–411, 1978.

[20] S. L. Bressler. Event-related potentials of the cerebral cortex. In R. P. Vertes and R. W. Stackman, editors, *Electrophysiological Recording Techniques*, volume 54 of *Neuromethods*, pages 169–190. 2011.

[21] Sidney J. Segalowitz and Kerry L. Barnes. The reliability of ERP components in the auditory oddball paradigm. *Psychophysiology*, 30(5):451–459, 1993.

[22] Niels Birbaumer. Slow cortical potentials: Plasticity, operant control, and behavioral effects. *Neuroscientist*, 5(2):74–78, March 1999.

[23] Yu. Boytsova and S. Danko. EEG differences between resting states with eyes open and closed in darkness. *Human Physiology*, 36(3):367–369, 2010. doi: doi:10.1134/S0362119710030199.

[24] D.A. Gusnard and M.E. Raichle. Searching for a baseline: functional imaging and the resting human brain. *Nature Reviews Neuroscience*, (3):685–694, 2001.

[25] T. Fernández, T. Harmony, M. Rodriguez, J. Bernal, J. Silva, A. Reyes, and E. Marosi. EEG activation patterns during the performance of tasks involving different components of mental calculation. *Electroencephalography and Clinical Neurophysiology*, 94(3): 175–182, 1995.

[26] John Polich. Neuropsychology of P300. *The Oxford Handbook of Event-Related Potential Components*, 2008.

[27] John Polich. Updating P300: an integrative theory of p3a and p3b. *Clinical neurophysiology*, 118(10):2128–2148, 2007.

[28] L. A. Farwell and E. Donchin. Talking off the top of your head: toward a mental prosthesis utilizing event-related brain potentials. *Electroen Clin Neuro*, 70:510–523, 1988. doi: 10.1016/0013-4694(88)90149-6.

[29] J. V. Odom, M. Bach, C. Barber, M. Brigell, M. F. Marmor, A. P. Tormene, G. E. Holder, and Vaegan. Visual evoked potentials standard (2004). *Documenta ophthalmologica. Advances in ophthalmology*, 108(2):115–123, 2004.

[30] D. J. McFarland, L. A. Miner, T. M. Vaughan, and J. R. Wolpaw. Mu and beta rhythm topographies during motor imagery and actual movements. *Brain topography*, 12(3): 177–186, 2000.

[31] Charles S. DaSalla, Hiroyuki Kambara, Makoto Sato, and Yasuharu Koike. Single-trial classification of vowel speech imagery using common spatial patterns. *Neural Networks*, 22(9):1334–1339, 2009.

[32] Thilo Hinterberger, Stefan Schmidt, Nicola Neumann, Jurgen Mellinger, Benjamin Blankertz, Gabriel Curio, and Niels Birbaumer. Brain-computer communication and slow cortical potentials. *IEEE Trans. Biomed. Eng.*, 51(6):1011–1018, 2004.

[33] M. Murugappan, M. Rizon, R. Nagarajan, and S. Yaacob. EEG feature extraction for classifying emotions using fcm and fkm. In *Proceedings of the 7th WSEAS International Conference on Applied Computer and Applied Computational Science*, ACACOS'08, pages 299–304, Stevens Point, Wisconsin, USA, 2008. World Scientific and Engineering Academy and Society (WSEAS).

[34] P.C. Petrantonakis and L.J. Hadjileontiadis. Emotion recognition from EEG using higher order crossings. *Information Technology in Biomedicine, IEEE Transactions on*, 14(2): 186–197, march 2010.

[35] Giacomo Rizzolatti and Laila Craighero. The mirror-neuron system. *Annu. Rev. Neurosci.*, 27:169–192, 2004.

[36] Michael Tangermann, Guido Dornhege, Matthias Krauledat, Gabriel Curio, and Benjamin Blankertz. Machine learning for real-time single-trial EEG-analysis: From brain-computer interfacing to mental state monitoring. *Journal of neuroscience methods*, 167 (1):82–90, 2008.

[37] Dean J Krusienski, Eric W Sellers, François Cabestaing, Sabri Bayoudh, Dennis J McFarland, Theresa M Vaughan, and Jonathan R Wolpaw. A comparison of classification techniques for the P300 speller. *Journal of neural engineering*, 3(4):299, 2006.

[38] Simon P Kelly, Edmund C Lalor, Ciarán Finucane, Gary McDarby, and Richard B Reilly. Visual spatial attention control in an independent brain-computer interface. *IEEE Trans. Biomed. Eng.*, 52(9):1588–1596, 2005.

[39] C. E. Henry. Electroencephalographic individual differences and their constancy: I. during sleep. *Journal of Experimental Psychology*, 29(2):117–132, 1941.

[40] C. E. Henry. Electroencephalographic individual differences and their constancy: II. during waking. *Journal of Experimental Psychology*, 29(2):236–247, 1941.

[41] M.A. Kennard and A.E. Schwartzman. A longitudinal study of electroencephalographic frequency patterns in mental hospital patients and normal controls. *Electroen Clin Neuro*, 9(2):263–274, 1957.

[42] T Gasser, P Bacher, and H Steinberg. Test-retest reliability of spectral parameters of the EEG. *Electroen Clin Neuro*, 60:312–319, 1985.

[43] M.C. Salinsky, B.S. Oken, and L. Morehead. Test-retest reliability in EEG frequency analysis. *Electroen Clin Neuro*, 79(5):382–392, 1991.

[44] András Kondacs and Mihály Szabó. Long-term intra-individual variability of the background EEG in normals. *Clinical Neurophysiology*, 110(10):1708–1716.

[45] Markus N*ä*pflin, Marc Wildi, and Johannes Sarnthein. Test-retest reliability of resting EEG spectra validates a statistical signature of persons. *Clinical Neurophysiology*, 118 (11):2519–2524, 2007.

[46] L.K McEvoy, M.E Smith, and A Gevins. Test-retest reliability of cognitive EEG. *Clinical Neurophysiology*, 111(3):457–463, 2000.

[47] M N$\ddot{a}pflin$, M Wildi, and Sarnthein J. Test-retest reliability of EEG spectra during a working memory task. *Neuroimage*, 43:687–693, 2008.

[48] K. Brigham and B.V.K. Vijaya Kumar. Subject identification from electroencephalogram (EEG) signals during imagined speech. In *Proceedings of the IEEE Fourth International Conference on Biometrics: Theory, Applications and Systems (BTAS'10)*, 2010.

[49] D. La Rocca, P. Campisi, and G. Scarano. On the repeatability of EEG features in a biometric recognition framework using a resting state protocol. In *BIOSIGNALS 2013*, 2013.

[50] E. Maiorana, G.E. Hine, D. La Rocca, and P. Campisi. On the vulnerability of an eeg-based biometric system to hill-climbing attacks algorithms' comparison and possible countermeasures. In *Biometrics: Theory, Applications and Systems (BTAS), 2013 IEEE Sixth International Conference on*, pages 1–6, Sept 2013.

[51] F. Vogel. The genetic basis of the normal human electroencephalogram (EEG). *Humangenetik*, 10(2):91–114, 1970.

[52] G.C. Lairy, editor. *Handbook of Electroencephalography and Clinical Neurophysiology. Vol.6. The Normal EEG Throughout Life*. Elsevier, 1976.

[53] L.C. Johnson and G.A. Ulett. Quantitative study of pattern and stability of resting electroencephalographic activity in a young adult group. *Electroen Clin Neuro*, 11:233–249, 1959.

[54] J. Lynch, D.A. Paskewitz, and M.T. Orne. Intersession stability of human alpha rhythm densities. *Electroen Clin Neuro*, 36:538–540, 1974.

[55] F. Vogel and E. Schalt. The electroencephalogram (EEG) as a research tool in human behavior genetics: Psychological examinations in healthy males with various inherited EEG variants. *Human Genetics*, 47:81–111, 1979. ISSN 0340-6717. doi: 10.1007/BF00295571.

[56] J.L. Varner, R.A. Potter, and J.W. Rohrbaugh. A procedure for automatic classification of EEG genetic variants. In *Annual Int. Conf. of the IEEE Eng. in Medicine and Biology Society*, volume 13, pages 451–452, 1991.

[57] C.E. van Beijsterveldt, P.C. Molenaar, E.J. de Geus, and D.I. Boomsma. Heritability of human brain functioning as assessed by electroencephalography (EEG). *American Journal of Human Genetics*, 58:562–573, 1996.

[58] Common and specific genetic influences on EEG power bands delta, theta, alpha, and beta. *Biological Psychology*, 75(2):154–164, 2007.

[59] John Polich and Albert Kok. Cognitive and biological determinants of P300: an integrative review. *Biological Psychology*, 41(2):103–146, 1995.

[60] Margaret J. Wright, Narelle K. Hansell, Gina M. Geffen, Laurie B. Geffen, Glen A. Smith, and Nicholas G. Martin. Genetic influence on the variance in P3 amplitude and latency. *Behavior Genetics*, 31(6), 2001.

[61] Andrey P. Anokhin, G.C.M. van Baal, C.E.M. van Beijsterveldt, E.J.C. de Geus, J. Grant, and D.I. Boomsma. Genetic correlation between the P300 event-related brain potential and the EEG power spectrum. *Behavior Genetics*, 31:545–554, 2001.

[62] Georg Stenberg. Personality and the EEG: Arousal and emotional arousability. *Personality and Individual Differences*, 13(10):1097–1113, 1992.

[63] Jeffrey A Gray. The psychophysiological basis of introversion-extraversion: A modification of eysenck's theory. *The biological bases of individual behavior*, pages 182–205, 1972.

[64] Richard J Davidson. Anterior cerebral asymmetry and the nature of emotion. *Brain and cognition*, 20(1):125–151, 1992.

[65] Stanislaw S Sobotka, Richard J Davidson, and Joseph A Senulis. Anterior brain electrical asymmetries in response to reward and punishment. *Electroen Clin Neuro*, 83(4):236–247, 1992.

[66] Andrew J Tomarken, Richard J Davidson, Robert E Wheeler, and Linda Kinney. Psychometric properties of resting anterior EEG asymmetry: Temporal stability and internal consistency. *Psychophysiology*, 29(5):576–592, 1992.

[67] Gennady G Knyazev. Antero-posterior EEG spectral power gradient as a correlate of extraversion and behavioral inhibition. *The open neuroimaging journal*, 4:114, 2010.

[68] D Lehmann, H Ozaki, and I Pal. EEG alpha map series: brain micro-states by space-oriented adaptive segmentation. *Electroen Clin Neuro*, 67(3):271–288, 1987.

[69] Felix Schlegel, Dietrich Lehmann, Pascal L Faber, Patricia Milz, and Lorena RR Gianotti. EEG microstates during resting represent personality differences. *Brain topography*, 25 (1):20–26, 2012.

[70] M Poulos, M Rangoussi, and N Alexandris. Neural network based person identification using EEG features. In *IEEE Int. Conf. on Acoustics, Speech, and Signal Processing*, volume 2, pages 1117–1120, 1999.

[71] M. Poulos, M. Rangoussi, V. Chrissikopoulos, and A. Evangelou. Person identification based on parametric processing of the EEG. In *The 6th IEEE Int. Conf. on Elec., Circ. and Systems*, pages 283–286, 1999.

[72] A. Riera, A. Soria-Frisch, M. Caparrini, C. Grau, and G. Ruffini. Unobtrusive biometric system based on electroencephalogram analysis. *EURASIP J. Adv. Signal Process*, 2008.

[73] Fei Su, Huangling Zhou, Zhiyin Feng, and Junshui Ma. A biometric-based covert warning system using EEG. In *Biometrics (ICB), 2012 5th IAPR International Conference on*, pages 342–347, 2012.

[74] P. Campisi, G. Scarano, F. Babiloni, F. De Vico Fallani, S. Colonnese, E. Maiorana, and Forastiere L. Brain waves based user recognition using the.

[75] D. La Rocca, Patrizio Campisi, and Gaetano Scarano. EEG biometrics for individual recognition in resting state with closed eyes. In *Proceedings of the International Conference of the Biometrics Special Interest Group (BIOSIG)*, pages 1–12, 2012.

[76] M.K. Abdullah, K.S. Subari, J.L.C. Loong, and N.N. Ahmad. Analysis of effective channel placement for an EEG-based biometric system. In *Biomedical Engineering and Sciences (IECBES), 2010 IEEE EMBS Conference on*, pages 303–306, 30 2010-dec. 2 2010.

[77] R.B. Paranjape, J. Mahovsky, L. Benedicenti, and Z. Koles. The electroencephalogram as a biometric. In *Canadian Conference on Electrical and Computer Engineering*, pages 1363–1366, 2001.

[78] Koel Das, Sheng Zhang, Barry Giesbrecht, and Miguel P Eckstein. Using rapid visually evoked EEG activity for person identification. In *Conf Proc IEEE Eng Med Biol Soc.*, pages 2490–2493. IEEE, 2009.

[79] R. Palaniappan and D.P. Mandic. Biometrics from brain electrical activity: A machine learning approach. *IEEE Transactions on Pattern Analysis and Machine Intelligence*, 29 (4):738–742, 2007.

[80] R. Palaniappan. Method of identifying individuals using vep signals and neural network. *Science, Measurement and Technology, IEE Proceedings*, 151(1):16–20, jan. 2004.

[81] Ramaswamy Palaniappan. Two-stage biometric authentication method using thought activity brain waves. *International Journal of Neural Systems*, 18(01):59–66, 2008.

[82] S. Marcel and J. del R. Millan. Person authentication using brainwaves (EEG) and maximum a posteriori model adaptation. *IEEE Trans. on Pattern Analysis and Machine Intell.*, 29(4):743–748, 2006.

[83] C. He and Z. Jane Wang. An independent component analysis (ICA) based approach for EEG person authentication. In *3rd International Conference on Bioinformatics and Biomedical Engineering, (ICBBE'09)*, 2010.

[84] Therese O'Donoghue, Derek W. Morris, Ciara Fahey, Andreia Da Costa, John J. Foxe, Doreen Hoerold, Daniela Tropea, Michael Gill, Aiden Corvin, and Gary Donohoe. A NOS1 variant implicated in cognitive performance influences evoked neural responses during a high density EEG study of early visual perception. *Human Brain Mapping*, 33 (5):1202–1211, 2012. ISSN 1097-0193. doi: 10.1002/hbm.21281.

[85] Daria La Rocca, Patrizio Campisi, and Gaetano Scarano. Stable eeg features for biometric recognition in resting state conditions. In Mireya Fernández-Chimeno, Pedro L. Fernandes, Sergio Alvarez, Deborah Stacey, Jordi Solé-Casals, Ana Fred, and Hugo Gamboa, editors, *Biomedical Engineering Systems and Technologies*, volume 452 of *Communications in Computer and Information Science*, pages 313–330. Springer Berlin Heidelberg, 2014. ISBN 978-3-662-44484-9. doi: 10.1007/978-3-662-44485-6_22. URL http://dx.doi.org/10.1007/978-3-662-44485-6_22.

[86] M. Fernandes, N.S. Dias, J.S. Nunes, M. El Tahchi, S. Lanceros-Mendez, J.H. Correia, and P.M. Mendes. Wearable brain cap with contactless electroencephalogram measurement for brain-computer interface applications. In *Proceedings of the 4th International IEEE EMBS Conference on Neural Engineering*, pages 387–390, Apri-May 2009.

[87] Stefan Debener, Falk Minow, Reiner Emkes, Katharina Gandras, and Maarten de Vos. How about taking a low-cost, small, and wireless EEG for a walk? *Psychophysiology*, 49 (11):1617–1621, 2012.

[88] J. Klonovs, C.K. Petersen, H. Olesen, and A. Hammershoj. ID proof on the go: Development of a mobile EEG-based biometric authentication system. *IEEE Vehicular Tech. Mag.*, 8(1):81–89, 2013.

[89] P. Campisi and D. La Rocca. Brain waves for automatic biometric-based user recognition. *Information Forensics and Security, IEEE Transactions on*, 9(5):782–800, May 2014.

[90] D. La Rocca, P. Campisi, B. Vegso, P. Cserti, G. Kozmann, F. Babiloni, and F. De Vico Fallani. Human brain distinctiveness based on eeg spectral coherence connectivity. *Biomedical Engineering, IEEE Transactions on*, 61(9):2406–2412, Sept 2014.

[91] M.S. Schwartz and F. Andrasik. *Biofeedback: A Practitioner's Guide*. Guilford Press, 2003. ISBN 9781572308459.

[92] D. McFarland, L. McCane, S. David, and J. Wolpaw. Spatial filter selection for EEG-based communication. *Electroencephalography and Clinical Neurophysiology*, 103(3): 386–394, September 1997.

[93] P. Stoica and R. Moses. *Spectral Analysis of Signals*. Prentice-Hall, 2005.

[94] S.M. Kay. *Modern Spectral Estimation. Theory and Applications*. Prentice-Hall, 1988.

[95] J.P. Burg. *Maximum entropy spectral analysis*. Stanford Exploration project. Stanford University, 1975. URL http://books.google.it/books?id=Xug_AAAAIAAJ.

[96] Shinn-Yih Tseng, Rong-Chi Chen, Fok-Ching Chong, and Te-Son Kuo. Evaluation of parametric methods in eeg signal analysis. *Medical engineering & physics*, 17(1):71–78, 1995.

[97] J. Schurmann. *Pattern Classification: A Unified View Of Statistical And Neural Approaches*. Wiley, 1996.

[98] François B Vialatte, Claire Martin, Rémi Dubois, Joëlle Haddad, Brigitte Quenet, Rémi Gervais, and Gérard Dreyfus. A machine learning approach to the analysis of time–frequency maps, and its application to neural dynamics. *Neural networks*, 20(2):194–209, 2007.

[99] William H Press, Saul A Teukolsky, William T Vetterling, and Brian P Flannery. Numerical recipies in fortran 77. *CUP,*, 1992.

[100] Grossmann A. Kronland-Martinet R., Morlet J. The wavelet transform. In C.H. Chen, editor, *Proceedings of IEEE Workshop on Expert Systems and Pattern Analysis*, pages 97–126. World Scientific, 1987.

[101] François Vialatte, Jordi Solé-Casals, Justin Dauwels, Monique Maurice, and Andrzej Cichocki. Bump time-frequency toolbox: a toolbox for time-frequency oscillatory bursts extraction in electrophysiological signals. *BMC neuroscience*, 10(1):46, 2009.

[102] D. La Rocca, P. Campisi, and J. Sole-Casals. Eeg based user recognition using bump modelling. In *Biometrics Special Interest Group (BIOSIG), 2013 International Conference of the*, pages 1–12, Sept 2013.

[103] M Poulos, M Rangoussi, N Alexandris, A Evangelou, et al. Person identification from the eeg using nonlinear signal classification. *Methods Inf Med*, 41(1):64–75, 2002.

[104] Andrew A Fingelkurts and Alexander A Fingelkurts. Making complexity simpler: multivariability and metastability in the brain. *Int. J. Neurosci.*, 114(7):843–862, 2004.

[105] ns. Database physionet bci, . URL http://www.physionet.org/pn4/eegmmidb/.

[106] F. De Vico Fallani, G. Vecchiato, J. Toppi, L. Astolfi, and F. Babiloni. Subject identification through standard eeg signals during resting states. In *Proc. IEEE Int. Conf. Eng. Med. Biol. Soc.*, pages 2331–2333, 2011.

[107] Sereina Bodenmann, Thomas Rusterholz, Roland Dürr, Claudia Stoll, Valérie Bachmann, Eva Geissler, Karin Jaggi-Schwarz, and Hans-Peter Landolt. The functional val158met polymorphism of comt predicts interindividual differences in brain α oscillations in young men. *J. Neurosci.*, 29(35):10855–10862, 2009.

[108] Rebecca Saxe and Nancy Kanwisher. People thinking about thinking people: the role of the temporo-parietal junction in "theory of mind". *Neuroimage*, 19(4):1835–1842, 2003.

[109] Guido Nolte, Ou Bai, Lewis Wheaton, Zoltan Mari, Sherry Vorbach, and Mark Hallett. Identifying true brain interaction from eeg data using the imaginary part of coherency. *Clin. Neurophysiol.*, 115(10):2292–2307, 2004.

[110] Wallace Chafe. Discourse, consciousness, and time. *Chicago: The*, 1994.

[111] E. Lombardi Vallauri. *La struttura informativa: forma e funzione negli enunciati linguistici*. Lingue e letterature Carocci. Carocci, 2009. ISBN 9788843052158.

[112] Emanuela Cresti. *Corpus di italiano parlato*. Accademia della Crusca, 2000.

[113] Edoardo Lombardi Vallauri. *Dati empirici e teorie linguistiche, Atti del XXXIII Congresso della Società di Linguistica Italiana (Napoli, 28-30 ottobre 1999)*, chapter La teoria come separatrice di fatti di livello diverso: l'esempio della struttura informativa dell'enunciato, pages 151–173. Bulzoni, Roma, 2001.

[114] John Langshaw Austin. *How to do things with words*, volume 367. Oxford university press, 1975.

[115] Petr Sgall. Topic, focus and generative semantics. 1973.

[116] D. La Rocca, E. Maiorana, P. Campisi, E. Lombardi-Vallauri, and V. Masia. Brain response to information structure misalignments in linguistic contexts. *Neuroinformatics*, submitted.

[117] G Pfurtscheller. Functional brain imaging based on erd/ers. *Vision research*, 41(10): 1257–1260, 2001.

[118] Douglas J Davidson and Peter Indefrey. An inverse relation between event-related and time-frequency violation responses in sentence processing. *Brain research*, 1158:81–92, 2007.

[119] Y Luo, Y Zhang, X Feng, and X Zhou. Electroencephalogram oscillations differentiate semantic and prosodic processes during sentence reading. *Neuroscience*, 169(2):654–664, 2010.

[120] Lin Wang, Ole Jensen, Danielle Van den Brink, Nienke Weder, Jan-Mathijs Schoffelen, Lilla Magyari, Peter Hagoort, and Marcel Bastiaansen. Beta oscillations relate to the n400m during language comprehension. *Human brain mapping*, 33(12):2898–2912, 2012.

[121] Sabine Weiss and Horst M Mueller. "too many betas do not spoil the broth": the role of beta brain oscillations in language processing. *Frontiers in psychology*, 3, 2012.

[122] Wolfgang Klimesch. Eeg alpha and theta oscillations reflect cognitive and memory performance: a review and analysis. *Brain research reviews*, 29(2):169–195, 1999.

[123] Marcel CM Bastiaansen, Marieke Van Der Linden, Mariken Ter Keurs, Ton Dijkstra, and Peter Hagoort. Theta responses are involved in lexical—semantic retrieval during language processing. *Journal of cognitive neuroscience*, 17(3):530–541, 2005.

[124] Sabine Weiss and Horst M Mueller. The contribution of eeg coherence to the investigation of language. *Brain and language*, 85(2):325–343, 2003.

[125] Sabine Weiss, Horst M Mueller, Baerbel Schack, Jonathan W King, Martha Kutas, and Peter Rappelsberger. Increased neuronal communication accompanying sentence comprehension. *International Journal of Psychophysiology*, 57(2):129–141, 2005.

[126] Sabine Weiss and Peter Rappelsberger. Long-range eeg synchronization during word encoding correlates with successful memory performance. *Cognitive Brain Research*, 9 (3):299–312, 2000.

[127] ns. Bci2000 system, . URL http://www.bci2000.org.